AN ULTRASONIC IMAGE-FORMING SYSTEM FOR IONOSPHERIC STUDIES

by

N.E. Holmes

A Thesis
presented for the degree of

DOCTOR OF PHILOSOPHY

at the

UNIVERSITY OF ADELAIDE
(Physics Department)

January 1974

FRONTISPIECE - A view of the receiving array of transducer holders showing the layout of the holders and the stainless steel plate in which they are held. The emitting or focussing array is of similar design. (Note, at the time the photograph was taken, the transducers were not in position).

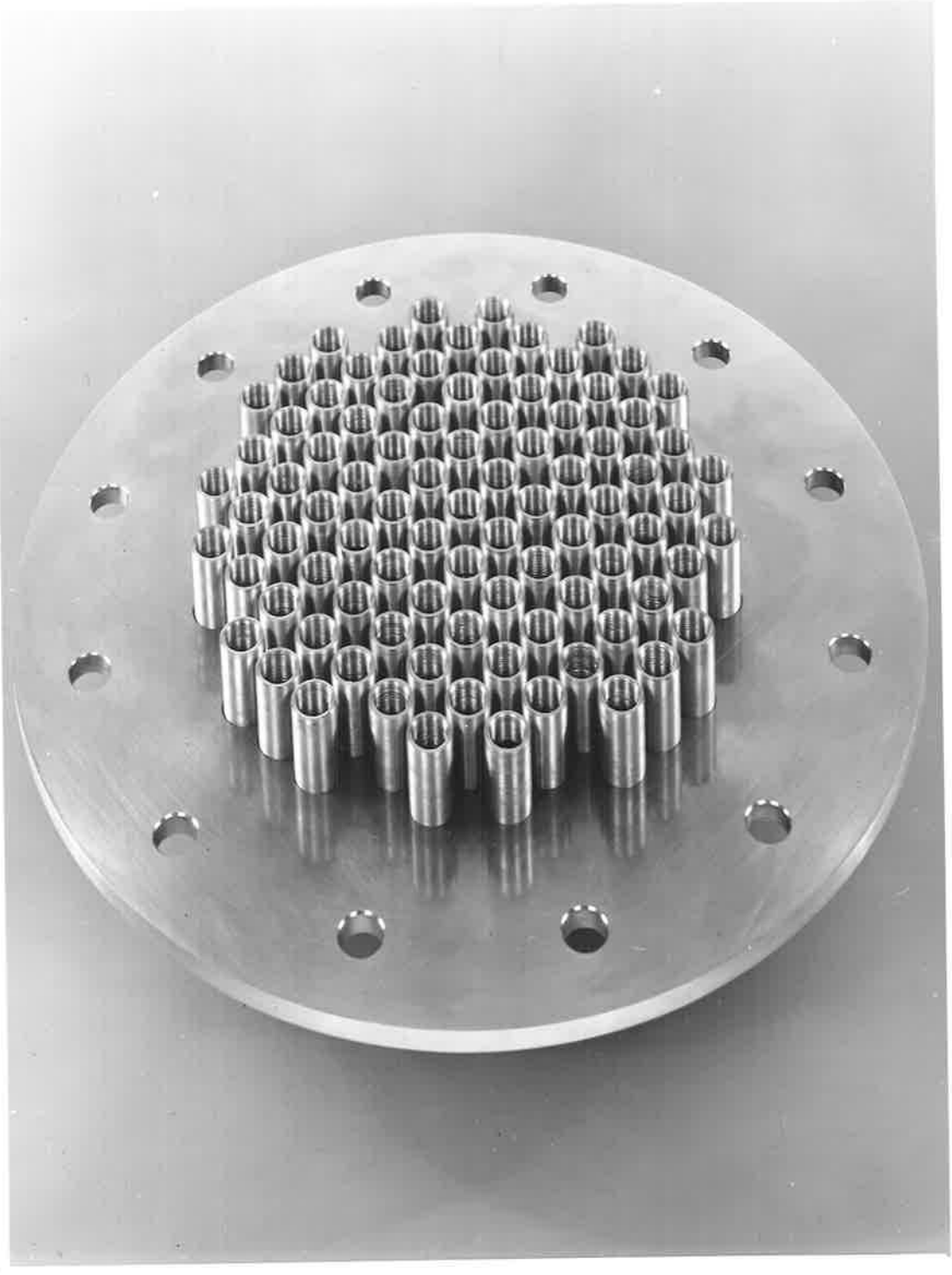

CONTENTS

AN ULTRASONIC IMAGE-FORMING SYSTEM FOR IONOSPHERIC STUDIES

SUMMARY

The first part of this thesis is of an introductory nature and is concerned with briefly outlining the history of the way in which radio techniques have been used to study the ionosphere. Also presented is a brief discussion of some theory which establishes the relationship between the complex function describing the phase and amplitude of an ionospherically reflected radio wave and its angular spectrum.

Chapter 2 consists of a review of the various techniques that have been or might be used to measure the angular spectrum of radio waves incident on an antenna array. The methods considered range from conventional scanning systems to more recent developments such as Electro-Optical and acoustic array processors.

Chapter 3 contains a detailed description of an image-forming system (acoustic array processor) which has been designed for use with the large antenna array at Buckland Park (near Adelaide). This instrument, which uses an ultrasonic technique, is capable of measuring the two dimensional angular spectrum of radio waves reflected from the ionosphere.

Chapter 4 is concerned with describing the procedure used to adjust the system so that it operates in the desired way and chapter 5 is concerned mainly with discussing the performance of the system and comparing it with the "ideal performance" as determined from a

computer model which simulates the principle of operation.

In chapters 6 and 7 some preliminary measurements of the angular spectra of radio waves reflected from the E, E_s and F layers of the ionosphere are presented. The different types of spectra observed are classified and their relative frequency of occurrence is determined.

Finally, in chapter 8 the major conclusions of the preceding chapters are summarised and some experiments which may be undertaken in the future are suggested.

PREFACE

To the best of the author's knowledge this thesis contains no material previously published or written by another person, except where due reference is made in the text. It contains no material which has been submitted or accepted for the award of any other degree or diploma in any University.

(N.E. Holmes)

University of Adelaide
18-12-73

ACKNOWLEDGEMENTS AND BACKGROUND FOR THE PROJECT

The work described in this thesis was undertaken in the Department of Physics at the University of Adelaide under the supervision of Dr B.H. Briggs. The author is grateful to Dr Briggs for suggesting the project and for his help and encouragement during the course of the work.

Construction of the Buckland Park antenna array commenced in 1965 and work on the image-forming system (described in this thesis) began in April 1970. The author is indebted to those who preceded him and constructed the antenna array, the transmitting system, and installed the magnetic tape recording facilities.

One of the first experiments in which the whole array was used was undertaken by Dr D.G. Felgate. In this experiment the 89 antennas in the array were connected to 89 radio receivers and this system was used to sample the radio diffraction pattern formed by waves reflected from the ionosphere. The output of each receiver was then used to drive a lamp so that its brightness was related to the amplitude of the received signal. By arranging the lamps in the same layout as the antennas it was possible to convert the diffraction pattern into a visible image. This project, which preceded the image-forming experiment, resulted in the development of equipment and techniques which have been further developed in the present work.

On a more specific level the author would like to thank the following for their help; Mr P. Schebella for his advice on the mechanical aspects of the project; Mr T. Spurr who did most of the work in construc-

ting the transducer focussing and receiving arrays (see frontispiece); Mr J.W. Smith for designing the camera drive unit and for his help in designing the amplifying and detecting circuits, as well as for advice on the many problems in electronics which arose from time to time; Mr D. Creighton who suggested the PIN diode attenuators; Dr D.G. Felgate who designed the post detector amplifiers and who was responsible for the basic receiver design of the earlier project referred to above; Mr A.W. Robertson who helped with the assembly of over 350 printed circuit cards which make up the system and Mr L.A. Hettner who is responsible for maintaining the field station.

The author would also like to acknowledge the help received from Mr N. Wild and Mr D.N. Hart who gave help of a general nature. Mr Hart joined the project in its final year and will be continuing with some of the work discussed in chapter 8.

Finally thanks are due to Dr R.A. Vincent for several helpful discussions relating to internal atmospheric gravity waves.

Finance for this project was provided by the Australian Research Grants Committee, the Radio Research Board (Australia) and the University of Adelaide. The author is also indebted to the University of Adelaide for the award of a University Research Grant postgraduate scholarship.

CHAPTER 1

INTRODUCTION

For the past half century radio techniques have been used to study the ionosphere. The earliest experiments of this type were undertaken in America by Briet and Tuve (1925,1926) and in England by Appleton and Barnett (1925). From these experiments it was possible not only to show that an ionised layer existed in the upper atmosphere but also to estimate its approximate height. In subsequent years these experiments were extended and modified and it was noticed that radio waves reflected from the ionosphere exhibited short period fluctuations in signal strength, called fading. Fading was found to persist even when special precautions were taken to ensure that there was no interference between the ground wave and the reflected wave or between multiply-reflected waves. Care was also taken to ensure that there was no magnetoionic fading. In 1933 Ratcliffe and Pawsey suggested that this phenomenon was caused by the diffractive reflection of the radio waves from ionospheric irregularities. This would result in the formation of an irregular radio diffraction pattern on the ground. These workers also studied the spatial structure of the pattern using what they called a "spaced receiver" experiment. They found that the fading observed by two antennas separated by more than one wavelength was usually uncorrelated. Later experiments carried out by Pawsey (1935), showed that on some occasions the fading at two neighbouring points on the ground was similar but displaced in time. This type of observation was explained by assuming

that the ionosphere contained irregularities of ionisation which drifted horizontally. Using diffraction theory it is possible to show that the velocity of the moving radio pattern is twice that of the irregularities at the reflection level, provided the irregularities do not change with time. This technique for measuring ionospheric movements was further developed by several workers including Mitra (1949) and Krautkrämer (1950).

In 1950 Briggs *et al.* introduced what is known as "full correlation" analysis which allowed estimates of the drift velocity to be made even when the form of the irregularities was changing. This analysis was later extended and made more general by Phillips and Spencer (1955). However both these methods of analysis made assumptions about the temporal and spatial properties of the diffraction pattern which needed to be tested. Partly for this purpose, several large antenna arrays were built which sampled the diffraction pattern at many points on the ground (see for example, Kelleher, 1966; MacDougall, 1966; and Haubert and Doyen, 1966). Unfortunately these arrays were rather small and it was found that features in the diffraction pattern were usually of the same size or larger than the array. In 1969 a larger array (1 km in diameter) was built at Buckland Park near Adelaide, South Australia. This array was used by Briggs *et al.* (1969) to investigate the properties of the diffraction pattern. One technique used in these experiments was to convert the diffraction pattern into a visible form by using the signals from the antennas in the array to drive an array of lamps which were arranged in the same layout as the antennas. These

experiments showed that on some occasions the application of full correlation analysis could give misleading results; but more importantly (for this thesis) it was shown that on many occasions the diffraction pattern structure was periodic, being composed of sets of fringes or crossing fringes. These had been observed previously by Haubert and Doyen (1966) as well as several others and it had been suggested that the fringe structures were formed by the interference of two or more rays which had been specularly reflected from the ionosphere. The resulting interference pattern would give rise to periodic structures in the diffraction pattern, similar to Young's interference fringes, which are familiar in optics.

Although it was known that on occasions the ionospheric reflecting layer was smooth enough to reflect radio waves specularly, it had been implicitly assumed by many workers (e.g. Booker *et al.*, 1950 and Ratcliffe, 1956) that the diffraction pattern was the result of the interference between rays diffractively reflected or scattered from the irregular ionosphere, and having a continuous distribution in their directions of arrival. A third model for the formation of the diffraction pattern, suggested by Monro (1962) and Pfister (1971), considers that there may be a discrete number of reflection points, each of which returns a continuous filled in cone of energy. Thus this model is a combination of the two already discussed. These models, for the formation of the diffraction pattern are of course related, but nevertheless it is interesting to find out which is more appropriate. To do this it is necessary to have an instrument capable of measuring the angles of arrival of the reflected

signals. In addition the instrument must be capable of making these measurements even when signals are arriving from several directions simultaneously.

This problem is in fact common to many investigations in radio physics. The quantity that is measured (the distribution of energy with angle) has come to be known as the angular power spectrum. The related term angular spectrum (see Booker and Clemmow 1950 and Booker *et al.* 1950) is a complex function describing both the phase and the amplitude of the signals as a function of the direction of arrival. At this point it is appropriate to discuss this concept in a little more detail.

If a transmitter is used to illuminate a limited, two-dimensional region of the ionosphere with radio waves, then the totally reflected electromagnetic field will have a phase modulation imposed upon it by the variations in the reflection height over the illuminated region. The field at the reflecting height, or indeed in any plane parallel to the mean reflecting layer, can be represented in terms of an angular spectrum of plane waves which should be imagined as a set of waves whose amplitudes and relative phases vary with direction. The quantity is usually represented by the symbol $\underline{P}\ (s_1, s_2)$ which is a complex function because both phase and amplitude have to be specified. If the variables s_1 and s_2 are direction cosines then the function $\underline{P}\ (s_1, s_2)$ is related, by a Fourier transform, to the complex function, $\underline{F}\ (x, y)$, which specifies the phase and amplitude of the electromagnetic wave over the horizontal (x, y) plane. This relation is expressed mathematically by the following

equation:

$$\underline{P}(s_1 , s_2) = \int_{-\infty}^{\infty}\int_{-\infty}^{\infty} \underline{F}(x ,y) \exp \left\{ -2\pi i(s_1 x + s_2 y) \right\} dxdy \qquad 1.1$$

which is valid provided the spatial coordinates x and y are measured in units of λ (the wave length of the radio waves). Since the relationship is a Fourier transform then the inverse transformation may be used to calculate $\underline{F}(x ,y)$ from a known angular spectrum $\underline{P}(s_1 , s_2)$ i.e. we can write,

$$\underline{F}(x , y) = \int_{-\infty}^{\infty}\int_{-\infty}^{\infty} \underline{P}\ (s_1 , s_2) \exp \left\{ + 2\pi i(s_1 x + s_2 x) \right\} ds_1\ ds_2 \qquad 1.2$$

It is important to note that although the integrals are calculated over an infinite domain, in practice the function $\underline{F}(x , y)$ is only defined or measured over a finite area. Similarly, for the problems considered here, the angular spectrum will only be non zero in directions close to the normal of the diffracting surface. Evanescent contributions to the spectrum are ignored. The angular power spectrum is obtained by calculating the square of the modulus of the angular spectrum, $|\underline{P}(s_1 , s_2)|^2$.

Equation 1.1 shows that the angular spectrum of a wave can be calculated provided the complex function representing the wave field is known over any horizontal plane. However in the past this method has generally not been used and the measurement has been made using a variety of techniques ranging from the use of two element interferometers to complicated scanning systems which use delay or shifting networks to steer the beams of large antenna arrays across the sky.

This thesis describes a new approach to the problem that makes use of the relationship expressed in equation 1.1. Equipment has been constructed in which the electromagnetic field is sampled by a large array and converted, using an array of piezo-electric transducers, to an acoustic field which has the same variations of phase and amplitude. Using a focussing system an image can be formed. Now it is a well known result in optics that the light distribution in the image plane of a focussing system is related to the light distribution in the object plane by a two dimensional Fourier transform. The same result applies for the formation of an acoustic image and thus a focussing or image-forming system may be considered as an analogue Fourier transform computer. The image can be made visible by sampling at a large number of points with another array of transducers each of which drives a light emitting diode. The visible image is equivalent to the modulus of a desired angular spectrum. For convenience, this quantity will be referred to, in this thesis, as the angular spectrum. Whether this refers to $\underline{P}(s_1,s_2)$ or $|P(s_1,s_2)|$ will be clear from the context. The angle of arrival is easily determined because radio waves arriving from a given direction will give rise to acoustic signals at a given point in the image plane. Further, the amplitude of the signals in the acoustic image will be related to the amplitude of the incoming radio signal. Although the acoustic image does in fact contain information about the phase as well as the amplitude of the angular spectrum, with the present equipment the phase information is not used.

The work described in this thesis shows that the technique is feasible, and in addition some preliminary results showing the angular spectrum of radio waves reflected from the ionosphere under different conditions are presented. This type of data is useful insofar as it provides information about the structure of ionospheric irregularities, and with this knowledge it is possible to test theories about their origin.

Although the equipment described here has been designed with ionospheric investigations in mind, the application of the technique to many problems in radio physics is obvious. It is hoped that the system that has been built will also prove useful for low frequency (6 MHz) radio astronomical observations.

CHAPTER 2

SURVEY

2.1 INTRODUCTION

The purpose of this chapter is to review the various methods that may be used to process the outputs from multi-element antenna arrays. The particular type of processors that will be considered are those which provide information about the direction of arrival of signals received by an array.

The methods to be examined may be divided into five categories.

(1) Scanning methods.

(2) Electro-Optical methods

(3) Acoustic methods.

(4) Computing methods.

(5) Holographic methods.

2.2 BASIC THEORY OF SCANNING METHODS

One of the most direct methods of measuring the angle of arrival of radio waves, which are confined to a known plane, is illustrated in fig. 2.1. The magnitude and sense of the phase difference α, between signals received on antennas A_1 and A_2, which are separated by a distance Δd, is measured and the angle of arrival θ can be calculated from the equation,

$$\theta = \arcsin \left\{\frac{\alpha\lambda}{\Delta d}\right\} \qquad 2.1$$

where λ = wavelength of the radio waves being used.

This equation has only two solutions provided that the condition $\Delta d < \frac{\lambda}{2}$ is satisfied. However it is usually possible to determine θ unambiguously because in practical cases the direction of arrival is confined

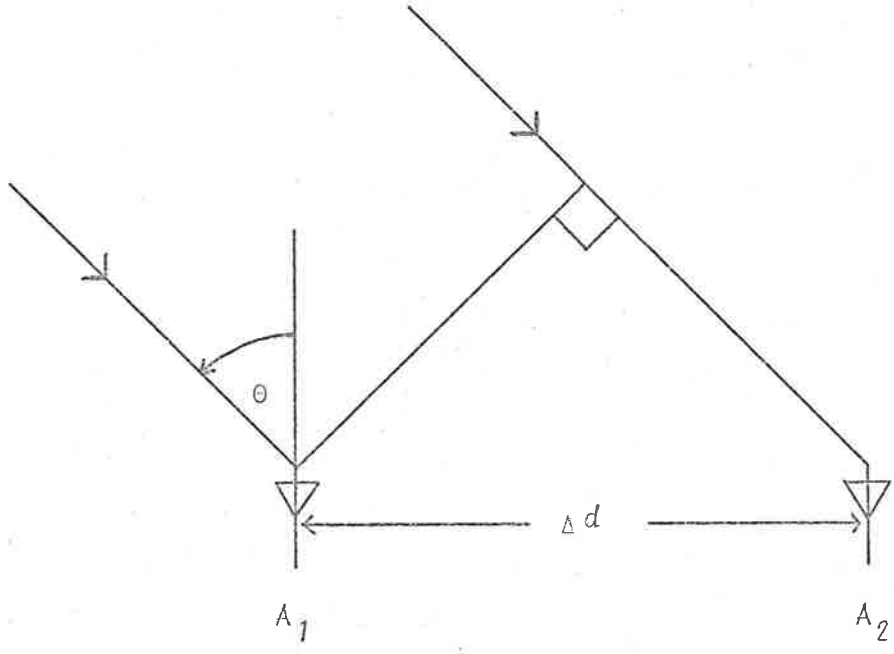

Fig. 2.1

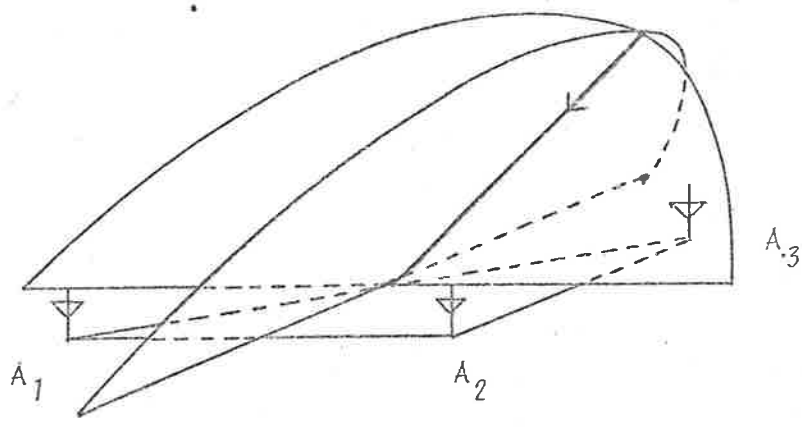

Fig. 2.2

to the visible half space.

The addition of a third antenna A_3, as shown in fig. 2.2 permits the measurement of both the elevation and the azimuth of the incident wave. Each pair of antennas determines a plane in which the direction of incidence must lie, and the intersection of these planes uniquely determines the direction of arrival.

It is important to notice that equation 2.1 is invalid when signals are arriving from more than one direction simultaneously.

A true scanning system avoids this difficulty. Fig. 2.3 illustrates how such a system (in its one dimensional form) operates. The elements $A_1 \ldots\ldots\ldots A_n$, are assumed to be antennas with equal gains and isotropic beam patterns. The beam pattern of this system, $A(\theta)$, (a function describing the way in which the output of an array varies with the angle of arrival of the incident signals) can be easily calculated. This is done as follows. The phase difference between the signals received by adjacent elements is equal to

$$\frac{2\pi\Delta d.\ \sin\theta}{\lambda}$$

where θ is the angle of arrival of the incoming signal (see fig. 2.3). The output of the array, when connected up as a broadside array, is found by summing the signals from each element (taking proper account of phase) and is thus given by the expression

$$A(\theta) = \sum_{i=1}^{n} \sin \left\{ \omega t + \frac{2\pi\Delta d.\ \sin\theta(i-1)}{\lambda} \right\} \qquad 2.2$$

where ω = the angular frequency of the signals being received,

λ = the wavelength of the signals,

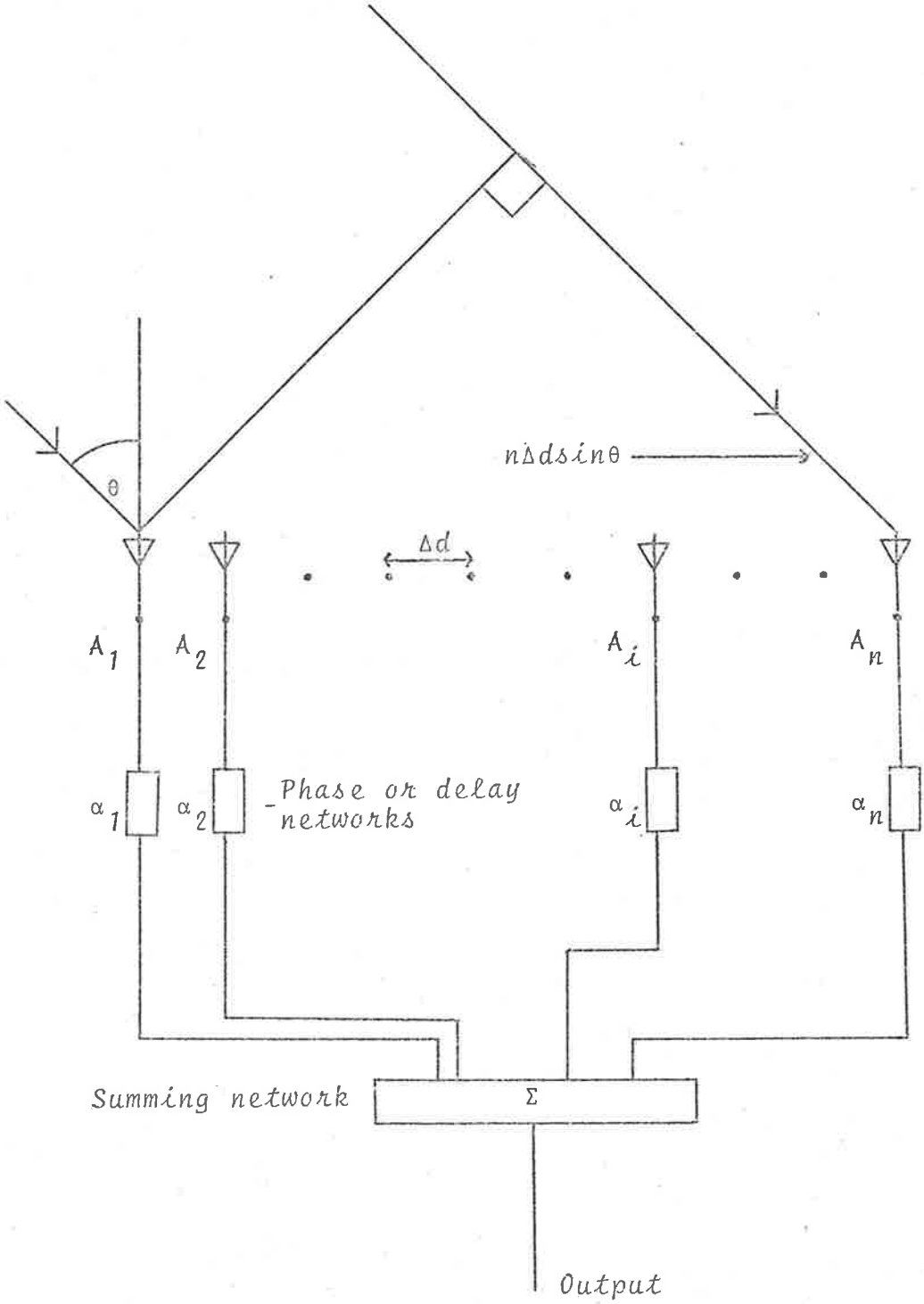
θ
nΔdsinθ
Δd
A1
A2
Ai
An
α1
α2
Phase or delay networks
αi
αn
Summing network
Σ
Output
n
= Σ sin{ωt+(i-1)α}
i=1

Fig. 2.3

t = time,

Δd = the distance between array elements.

By expressing the sine in its complex form and summing the series it can be shown that,

$$A(\theta) = \sin\left\{ \omega t + \frac{(n-1)\pi\Delta d.\sin\theta}{\lambda} \right\} \frac{\sin(\sin\theta n\pi\Delta d/\lambda)}{\sin(\sin\theta\pi\Delta d/\lambda)} \qquad 2.3$$

The first term is a sine wave with angular frequency ω and phase shift $\frac{(n-1)\pi\Delta d.\sin\theta}{\lambda}$, while the second is an amplitude factor of the form

$$\frac{\sin(\sin\theta n\pi\Delta d/\lambda)}{\sin(\sin\theta\pi\Delta d/\lambda)} \qquad 2.4$$

If a series of n-individual variable delay (or phasing) circuits are used to delay the signals before the summation is performed (see fig. 2.3), then it is possible to steer the array beam. Let the i^{th} phasing network introduce a phase shift of $(i-1)\alpha$ into the signal from the i^{th} antenna. This produces a new beam pattern $A_1(\theta)$ which is related to $A(\theta)$ by the following equation.

$$A_1(\theta) = A(\theta - \theta_o) \qquad 2.5$$

where

$$(\theta_o) = \arcsin\left\{ \frac{\alpha\lambda}{\Delta d.2\pi} \right\} \qquad 2.6$$

Clearly the effect of the phase shifting networks is to point the beam to a new direction θ_o.

It should be noted, that as the array beam is steered to off vertical angles (θ_o) the beam pattern becomes broader by a factor approximately equal to $\sec(\theta_o)$ (Skolnik 1962). This point will not be pursued in this discussion.

It can be seen, from the arguments above, that for each direction θ_o into which the beam is to be pointed, n-phase shifting networks are required. For a two dimensional array, with n-rows and n-columns, n^2 such networks are required for each direction. If a beam is to be steered across some two dimensional region of the sky, then the number of independent directions into which the beam must be directed, depends upon the resolving power (array beam width) and the field of view. For practical situations the number of independent phase shifting networks is extremely large. For example consider the case in which a planar two dimensional array, containing 10 rows and 10 columns with an inter-element separation of half a wavelength, is required to scan (without loss of information) a region of the sky defined by a cone with a semi-angle of 30°. The number of phase shifting networks needed to do this is approximately 5,700. If the scanning is only required in one plane then the elements can be connected in rows and the problem is much less formidable.

This type of beam swinging technique is quite practicable for arrays which are required to scan in one plane only, e.g. Cottony and Wilson (1960), Vogt (1962), Burtynk (1964) and Hamilton (1968). Many different methods are used to introduce the necessary phase shifts but the principle of operation of the systems described by these workers is the same as that outlined above. However, the approach is unsuitable for use with filled in planar arrays containing many elements.

2.3 PRACTICAL SCANNING SYSTEMS

Despite the difficulties referred to in section 2.2, useful two-dimensional scanning systems have been constructed; Morris *et al.* (1963), Wild (1967), Large and Frater (1969) and Brownlie *et al.* (1973a)

A common approach used by these workers in their solutions to the problem, has been to use a dilute instead of a filled in array. In this way it is possible to achieve high resolution with an instrument using a relatively small number of phasing or delay networks.

The earliest instruments of this type (used in radio astronomy) were cross-type antennas (Mills and Little 1953, Mills 1963). The system described by Mills consisted of two orthogonal rows of antennas, see fig. 2.4, each row producing a fan beam, whose width in the direction perpendicular to the row depends on the directivity functions of the individual elements. If the signals from the two rows are added together with an appropriate phase shift introduced between signals from different elements then the resultant antenna response pattern is as shown in fig. 2.4. Although the beam has an enhanced response in the direction of the intersection of the two fans, it can be seen that the side lobes will be large and the beam shape is therefore not ideal. However, the beam pattern can be considerably improved if the voltage polar diagrams of the two arms are multiplied together instead of added. Mills (1963) describes a method of processing the received signals which results in the desired multiplication. Essentially the processing is performed by firstly connecting the two arms so that their signals add in phase and then reversing the phase of the signal from one arm before the addition. If the difference in the two signals, formed by this procedure, is amplified and detected with a square law detector then the effective antenna polar diagram is the same as that obtained by multiplying the voltage polar diagrams of the two arms. However the side lobe levels are still unacceptably high in the directions in which either one of the

Cross type radio telescope

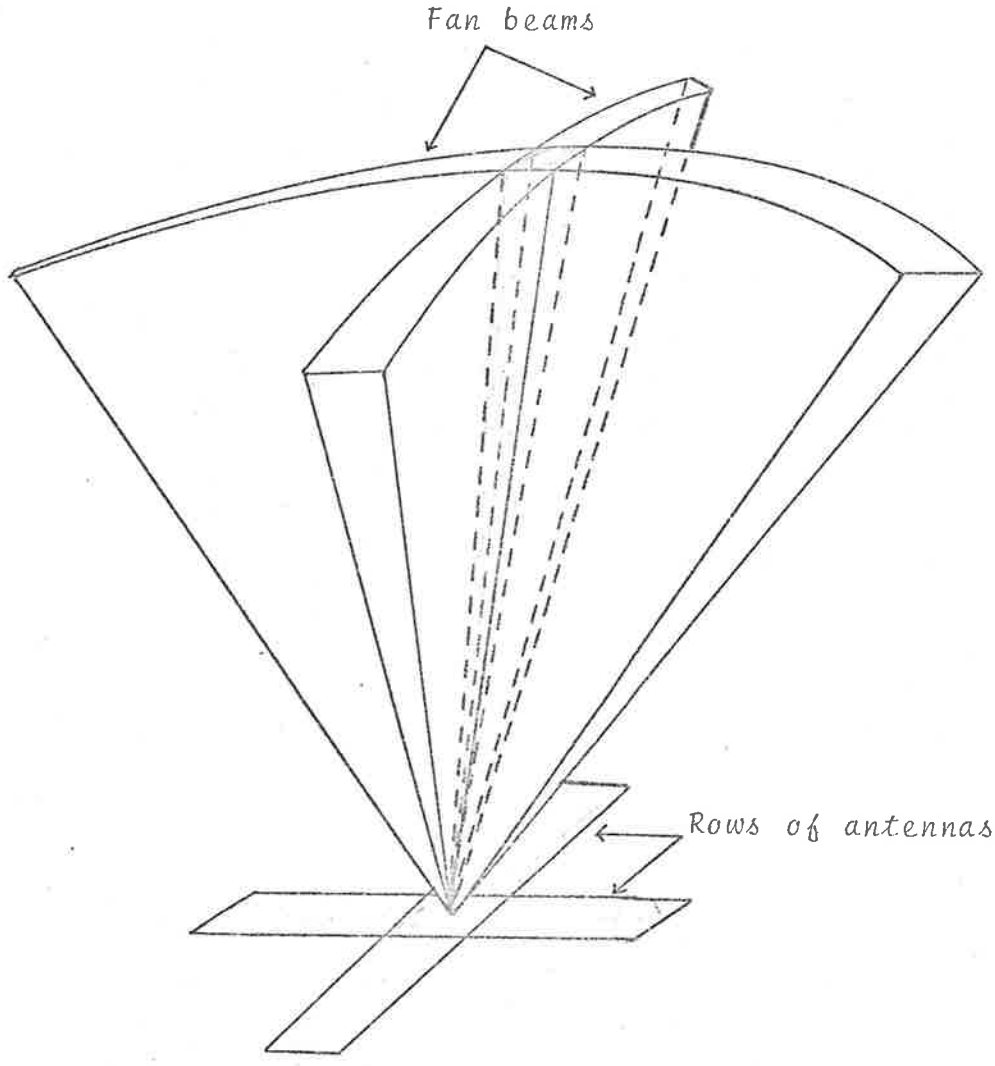

Fig.2.4

arms has a wide angle of reception. This problem can be overcome, and the sidelobes eliminated if a Gaussian taper is applied to the signals from the elements in the two array arms. This simply means that the elements at the extreme ends of the arms will contribute less to the polar diagram than those nearer the centre. This results in a reduction of sidelobe level and, unfortunately, a broadening of the main lobe. In practice to retain the same resolving power the array size must be increased by 50 per cent.

The reduction in the number of elements obtained by using a cross instead of a filled in array reduces costs and makes electronic beam steering a practical proposition. However there are disadvantages and these are outlined below:

(1) There is an increase in the complexity of the signal processing procedure.

(2) There is a degradation in the resolving power.

(3) There is a reduction in the allowable signal phase errors (for the same performance, see Large and Frater 1969). This arises because a filled in array has a certain amount of redundancy which has been removed by diluting the array.

(4) There is a decrease in the sensitivity caused by the reduced collecting area.

Even with these disadvantages, cross type radio-telescopes have proved to be very powerful and popular tools particularly in radio astronomy and more recently in ionospheric physics. Arrays of this basic design have been constructed by many workers including Mills (1953), Bracewell (1961a),

Braccesi and Cecarelli (1962), Christiansen *et al.* (1963) and Kalachov (1963).

Another cross type array, which has been designed specifically for ionospheric investigations, has been built at Bribie Island near Brisbane (Brownlie *et al.* 1973a). This system consists of two orthogonal one kilometer arms each containing 10 elements. A novel feature of this system is that one arm is used to transmit while the other is used for reception. The result is a pencil beam radar system (beam width of 4° at 4 MHz) which may be scanned in a raster pattern by using a computer to introduce suitable phase shifts between the array elements. The instrument is thus able to measure the angular spectra of radio waves reflected from the ionosphere within its field of view, which is ± 20° from the zenith.

Annular arrays have also been used to form the pencil beams required for scanning radio telescopes. Probably the most sophisticated instrument of this type is"The Culgoora Radioheliograph" (Wild 1967). This array consists of 96 steerable paraboloid antennas arranged regularly on the circumference of a circle 3 km in diameter. The pencil beam is formed using the so-called "J^2-synthesis". This consists of adding to the beam formed by the in phase addition of the signals (from the array elements), other weighted beam patterns, which are formed by introducing progressive phase shifts into the signal from each antenna channel. The phase shifts are made to increase uniformly around the array starting at zero from an arbitrary antenna.

Using this technique it is possible to form a beam with a shape that gives equal weighting to all the spatial Fourier components in the image

up to the resolution limit of the instrument.

The half power beam width of the Culgoora system is 3.55' at zenith. The field of view of the array is limited by the appearance of grating sidelobes which occur approximately 2° away from the central beam. The position of the grating sidelobes depends on the inter-element spacing of the array. Since the instrument has been designed primarily for solar observations, this small field of view is acceptable. Pictures of a radio sources are constructed by scanning 48 simultaneously formed beams across the field of view. The final picture consists of 60 x 48 samples, each sample being separated by 2.1' of arc. Using 48 beams the time taken to construct a picture is approximately half a second.

Conceptually, the simplest method of forming a picture of the radio sky is to steer a parabolic dish mechanically,so that its beam sweeps over the region of interest. Mechanical considerations at the present time, place an upper limit of about 100 metres on the diameter of steerable dishes and since the beam width of a given array is proportional to the wavelength at which it is being used this restricts the use of steerable dishes to wavelengths of less than a few metres. An additional disadvantage is that the scanning rate is slow and rapid changes in the picture cannot be followed. Non steerable parabolic dishes may be much larger e.g., Arecibo (Sky and Telescope, 1961) which is approximately 300 meters in diameter. Beam steering with this type of antenna can be achieved by moving the primary feed radially in the focal plane (Jasik 1961). However, the field of view is confined to within a few beam widths of the boresight. Phase errors result in excessive beam deterioration for large off boresight directions, although Rudge and Withers (1971) have described a fairly complicated feed

device which allows the beam to be steered in the range ± 15 beam widths with "negligible" distortion of the direction pattern.

However the scanning rate remains slow when compared with electronically steered beams and even the largest dishes built do not have useful resolving powers at frequencies in the medium wave band.

2.4 ELECTRO-OPTICAL IMAGE-FORMING METHODS.

Extensive theoretical and experimental investigations on Electro-Optical array processors have been made in recent years; see for example Lambert and Arm (1963), Aimette *et.al.* (1963., 1964(a),(b),(c), 1966), Arm *et al.* (1964, 1965(a),(b), 1966(a),(b)), Lambert (1965(a),(b)), Lambert *et al.* (1965), Chinnick (1972).

The basic unit in an Electro-Optical array processor is the Debye-Sears light modulator, a full description of the contruction and principle of operation of which may be found in a number of texts, including Born and Wolf (1959). However for completeness a brief description is included here.

The discussion which follows will be made with reference to fig. 2.5. Sound travelling through a transparent medium (usually water) modifies the refractive index. If the travelling sound wave is produced by an electrical signal V(t) which is driving a piezo-electric transducer then the spatial variation of the refractive index can be represented by n(z) where,

$$n(z) = n_o + n_m . V(\frac{z}{s}) \qquad 2.7$$

where n_o = ambient refractive index of the fluid,

n_m = proportionality constant which depends on the efficiency of the transducer and the way in which the refractive index of the fluid varies with pressure,

Debye-Sears light modulator

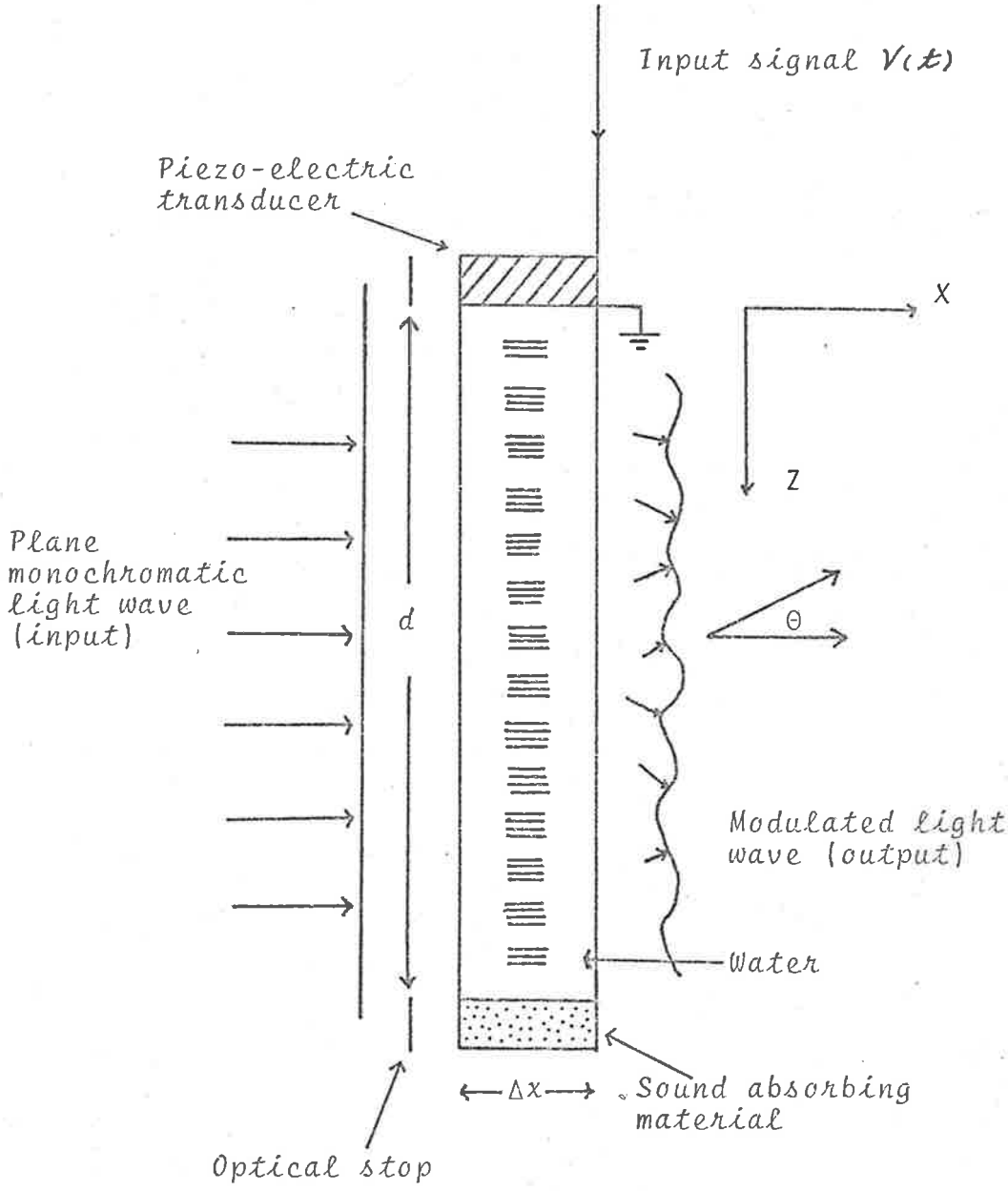

Fig. 2.5

s = velocity of sound in the fluid,

z = distance, see fig. 2.5.

(Here it has been assumed that the signal begins at time t = o and that the transducer is at z = o). The change in the refractive index of water has been shown to be proportional to the change in pressure (Willard 1949) which in turn is proportional to the voltage applied to the transducer (Hueter and Bolt 1955).

Thus an electrical signal applied to the transducer will produce a similar pressure signal in the light modulator and if the signal V(t) has a duration τ such that,

$$\tau = \frac{d}{s} \qquad 2.8$$

where d = length of the cell,

then there will be an instant of time when the signal completely fills the cell.

If the cell is now illuminated with a plane wave, produced by a coherent monochromatic source of light travelling along the x-axis, then the non-uniform refractive index of the medium in the cell will distort the plane wave fronts of the incident light. The cell acts as a phase modulating screen; the modulation depending on the signal V(t).

The phase modulation impressed on a plane polarised light wave passing through the cell can be represented by ψ (z) where,

$$\psi(z) = \frac{2\pi}{\lambda_L} \left\{ n(z) - n_o \right\} \Delta x \qquad 2.9$$

$$= \frac{2\pi}{\lambda_L} n_m V(\tfrac{z}{s}) \Delta x \qquad 2.10$$

where λ_L = the wavelength of the light being used.

If $V(\frac{z}{s})$ is a pulse modulated cosine wave of duration τ which just fills the cell at time $t = \tau$ then,

$$\psi(z) = \Delta x . \frac{2\pi}{\lambda_L} n_m V_o \cos(k_s z + \phi_o) \qquad 2.11$$

where V_o = amplitude of driving signal,

$k_s = \frac{2\pi}{\lambda_s}$,

λ_s = wavelength of sound in the cell,

ϕ_o = phase (the significance of which will be discussed later).

A plane polarised monochromatic light wave travelling in the x-direction can be represented by,

$$A \exp i(\omega t + k_L x + \phi_1) ,$$

where $k_L = \frac{2\pi}{\lambda_L}$,

λ_L = wavelength of the light being used,

ω = angular frequency of the light wave,

ϕ_1 = an arbitrary phase term,

A = constant related to the amplitude of the wave.

If we consider the situation at a fixed time τ we can ignore the time dependent part of the equation and represent the wave by,

$$A \exp i(k_L x + \phi_2) ,$$

where $\phi_2 = \phi_1 + \omega\tau$ 2.12

This plane wave has its wave fronts distorted as it passes through the light modulator and is now represented by f(x,z) where

$$f(x,z) = A \exp i \left\{k_L x + \phi_2 + \psi(z)\right\}$$

$$= A \exp i \left\{k_L x + \phi_2 + m\cos\ (k_s z + \phi_o)\right\}$$

$$\text{where } m = \frac{\Delta x\ 2\pi\ n_m\ V_o}{\lambda_L} \qquad \text{(see equation 2.11)}$$

The cell acts as a phase diffraction screen and the phase and amplitude of the various diffraction orders may be calculated. This is the same as calculating the frequency spectrum of the modulating wave and the calculation can be accomplished by taking the Fourier transform of f(0,z); (Ratcliffe 1956). If we make the approximation that $m.\cos(k_s z + \phi_o) \ll 1$ then the Fourier transform F(s) is given by,

$$F(s) = C\left\{\frac{\sin \pi d s}{\pi d s} + \frac{im}{2}\left(\frac{\sin \pi d(s-k_s)}{\pi d(s-k_s)} e^{i\phi_o} + \frac{\sin \pi d(s+k_s)}{\pi d(s+k_s)} e^{-i\phi_o}\right)\right\} \qquad \text{..... 2.13}$$

where s = $\sin\theta$ (see fig. 2.5)

d = length of cell.

The first term represents the zeroth order and the second and third terms represent the two first order components on opposite sides of the zeroth order. An important point to notice is that the phases of the last two terms depend on ϕ_o (see equation 2.11).

If V(t) (the signal applied to the transducer) is the signal received by an antenna in an array then the phase of light diffracted into the first order is related to the phase of the received signal.

If we now use an array consisting of a row of antennas each feeding a light modulating cell, the arrangement of antennas and cells being as shown in fig. 2.6, then the relative phase differences between the signals received by each antenna (which is a measure of the angle of arrival of the signals incident on the array) will be the same as the relative phase differences between the light, diffracted into the first order from each cell.

If there is a linear phase progression across the array then there will be a linear phase progression in the light diffracted into the first order from each cell. This light after passing through a lens (see fig. 2.6) will converge to a point in the image plane and the position of the point will depend on the phase differences between the light from adjacent cells. If signals are incident from k different directions simultaneously then it can be shown that the diffracted light will converge to k points in the image plane, the positions of the points being determined by the directions of arrival of the incident signals. The system can thus form simultaneously and as a continuum, all the beams that the receiving array is capable of forming.

The arrangement described is only capable of processing signals from a one dimensional array. However this processing capability may extend to a planar, or two dimensional array, by making use of a time multiplexing technique which is used in conjunction with the so-called spatial multiplexing

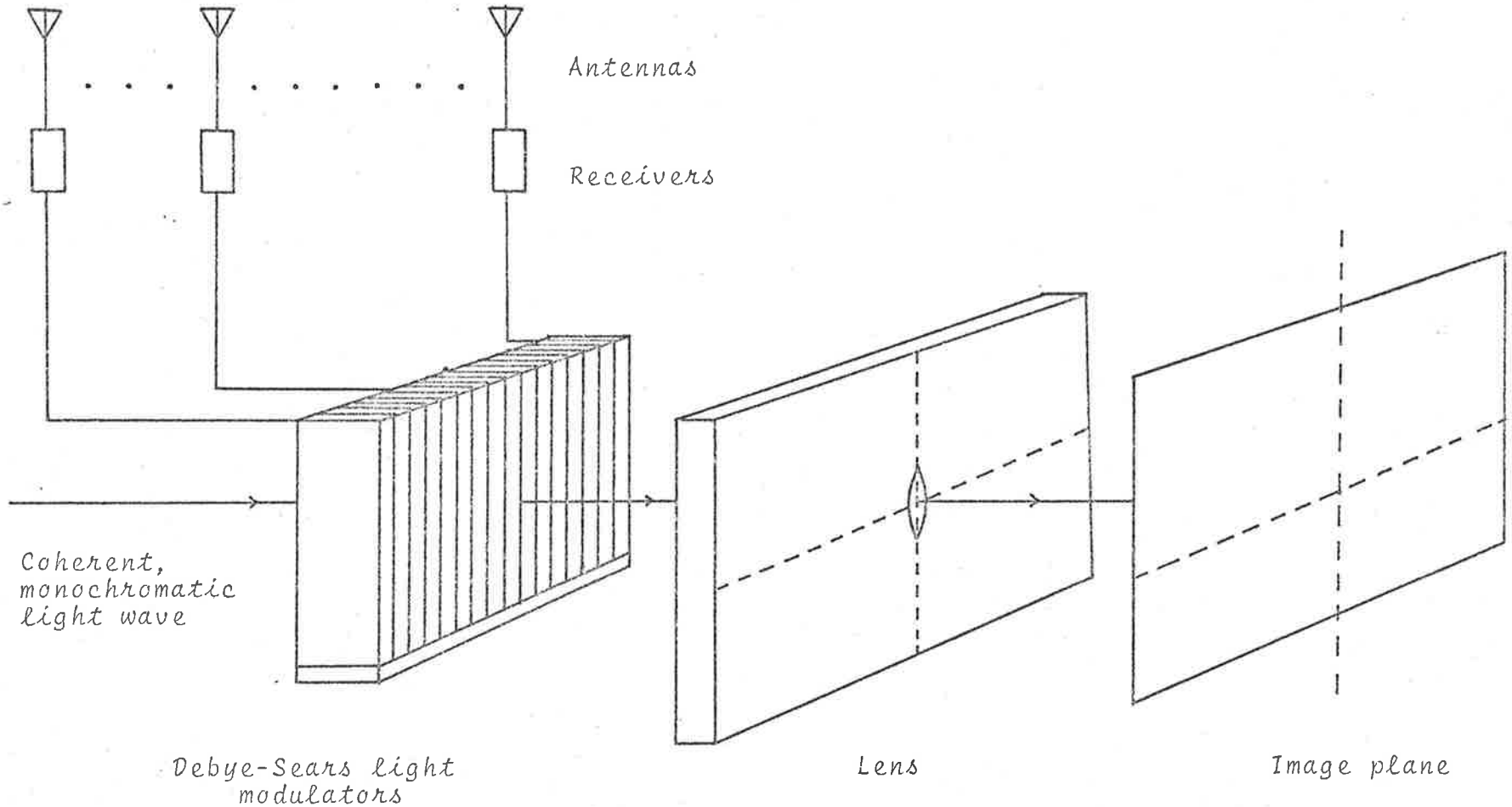

Fig.2.6

Schematic representation of a one dimensional array and an Electro-Optical array processor (see Lambert 1965b)

technique described above. The signals from a planar array consisting of n^2 elements (n-rows and n-columns) can be processed by sequentially feeding the signals from the n-elements in the first column of the array into a single light modulating cell. To do this the signals from each element in the column must be delayed by a time equal to the duration of the signals (see fig. 2.7).

The light cell is then filled with n separate acoustic signals which are similar in phase and amplitude to the signals received by the array. The delays must of course be chosen so that the phase relationship between the pulses is preserved. The signals from the other (n-1) rows of the array are processed by (n-1) separate light modulators which are adjacent to one another. The system described is now capable of processing the signals from a two-dimensional array.

Electro-Optical array processors of the type described above have been built at Columbia University (Lambert *et.al.* 1965) and also at Queen's University in Ontario (Chinnick 1970).

The systems have been thoroughly investigated from both theoretical and experimental points of view and the following are the conclusions reached by Lambert (1965a) after investigating this type of system with a view to radar applications.

"These processors produce output signals such that all beam angles within the visible half-space of the antenna are obtained (1) simultaneously, (2) as a continuum, (3) without ambiguities, (4) with nearly ideal side lobe envelopes that can be suppressed, (5) with nearly ideal angle resolutions".

Two dimensional Electro-Optical

array processor

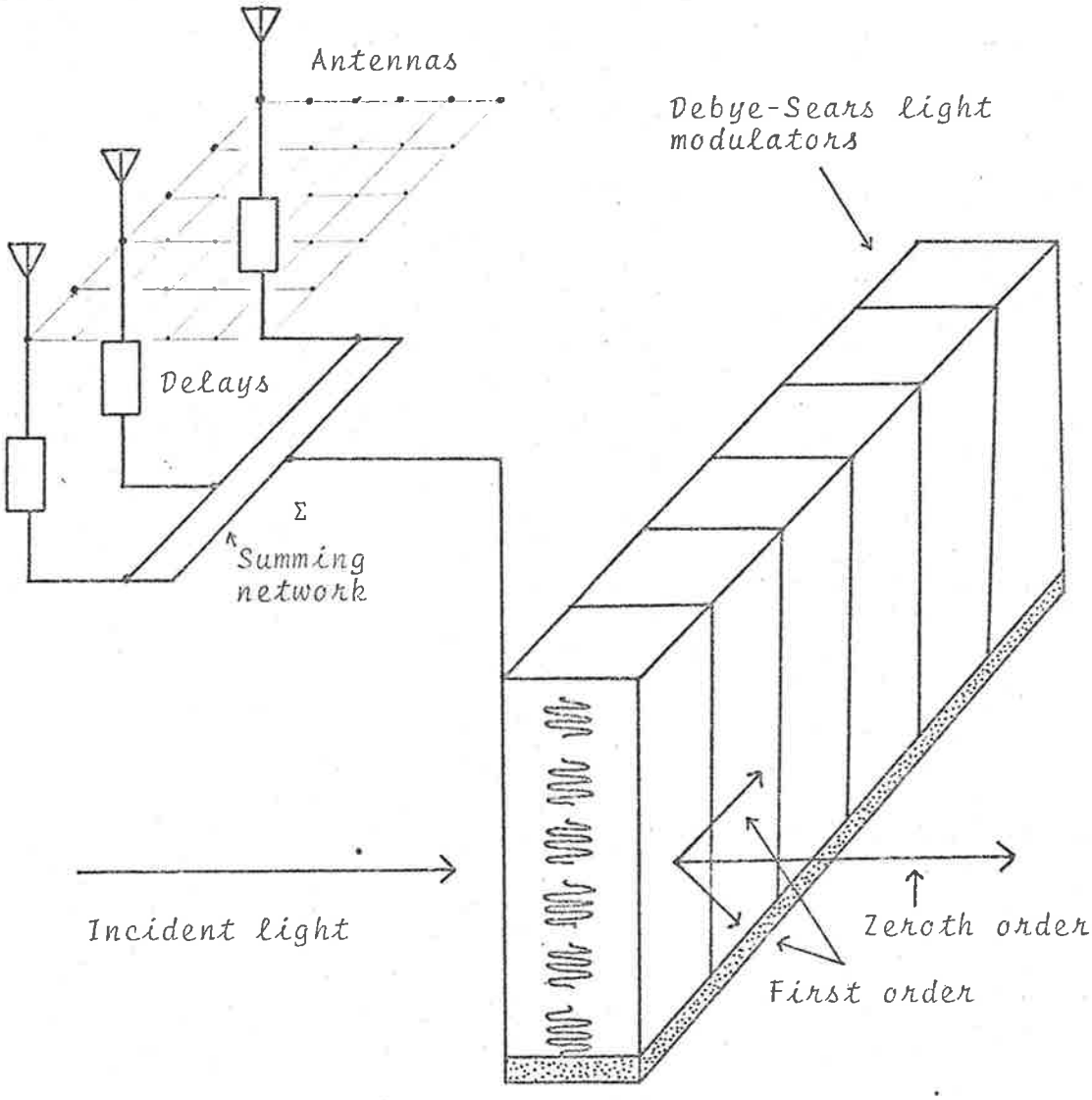

(see Lambert 1965b)

Fig. 2.7

The above conclusions were reached after using an Electro-Optical processor in conjunction with a specially designed signal simulator. Although some consideration has been given to the design of an Electro-Optical processor for use with the Culgoora Radioheliograph (McLean and Wild 1961, McLean *et.al.* 1967, McLean 1967) there do not appear to be any arrays actually using this technique. The reasons for this are not clear but the method is technically fairly difficult because of the severe mechanical tolerances involved in the construction of the Debye-Sears light modulators.

2.5 ACOUSTIC METHODS

Acoustic processors, although simpler in construction than Electro-Optical processors, essentially belong to the same class in that they have the capability of simultaneously forming as a continuum all the beams that an array is capable of forming.

Investigations into the design of ultrasonic cameras have been made since the 1930's. Much of this early work was carried out in the U.S.S.R. by Sokolov. The principle of operation of an ultrasound camera is similar to that of a conventional camera. A field is illuminated with ultrasound and the scattered or reflected sound is brought to a focus using an acoustic lens. The acoustic image is then made visible using one of a number of techniques which will be discussed later. Because the attenuation of ultrasound in air is high, the object to be viewed, the lens, and the detecting device are usually immersed in a liquid, e.g. water. Even so, attenuation restricts the useful range of frequencies to less than 10 MHz, (corresponding to a wavelength in water of 0.014 cm). In general these devices are used

for medical and engineering purposes, but they can be adapted to process signals from antenna arrays. The feature which makes the camera useful as a signal processor is that the two complex functions which describe the phases and amplitudes of the focussed acoustic image and the wave field in the corresponding object plane are a Fourier transform pair, (provided we ignore the effect of the aperture). Thus the camera may be thought of as an analogue Fourier transform computer. This is exactly what is required for an array signal processor which has as its output information about the angular spectrum of signals incident on an array.

McLean and Wild (1961) describe an acoustic image forming device intended for use in radio astronomy. Fig. 2.8 illustrates its mode of operation. The design as shown is for an annular array, however the extension to other configurations is obvious. The signals from each array element after amplification and coherent frequency changing, are used to drive piezoelectric transducers, each of which produces an acoustic signal of the same phase and proportional in amplitude to the driving signal. An acoustic image can be formed by using an acoustic lens (Smythe *et.al.* 1963, Harrold 1969) or, more simply by tilting the transducers towards the centre of the image plane.

An acoustic image-forming system which is under construction in Alaska has been described by Parthasarathy (1971, 1972). The method is similar to that suggested by McLean and Wild and is also similar to the method described in chapter 3 of this thesis. The signals received by the antennas in a linear array (later to be extended to a two-dimensional

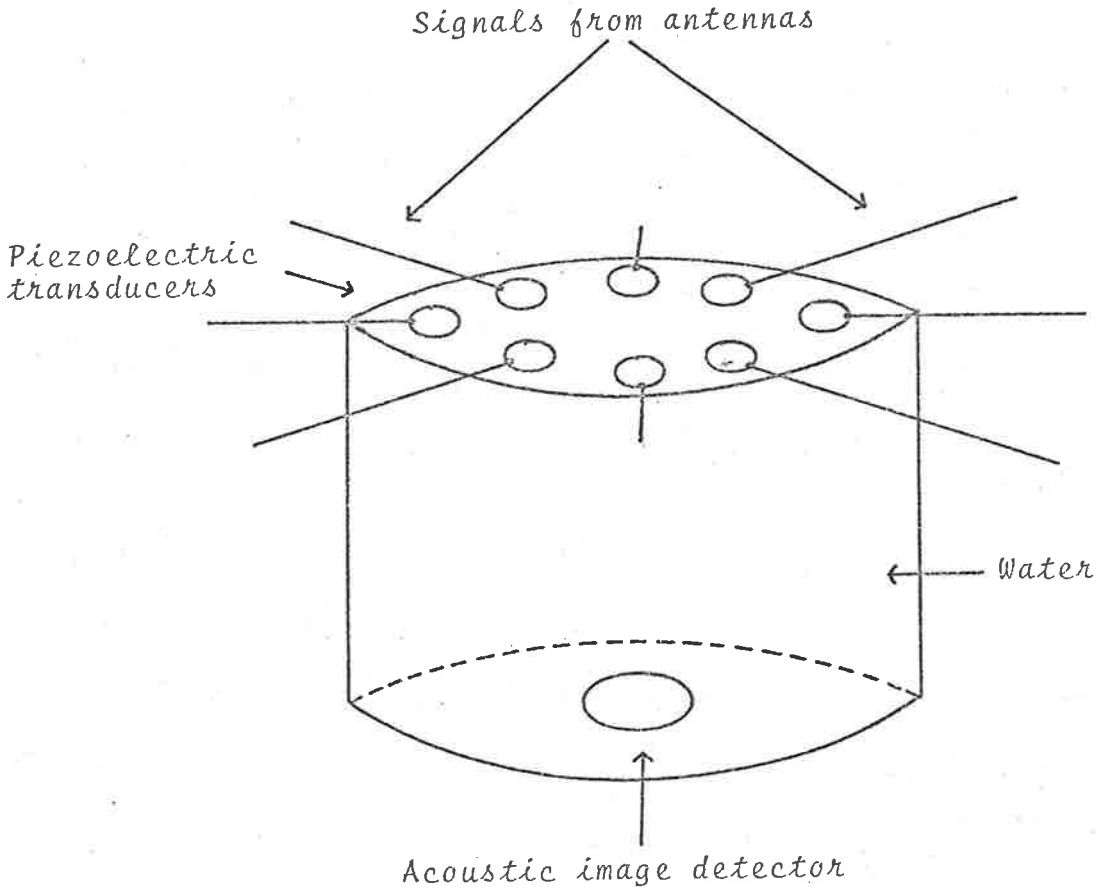

(see McLean and Wild 1961)

Fig.2.8

planar array) are to be used to drive a focussing array of piezo-electric transducers. The focussed acoustic image that will be produced is then (approximately) the Fourier transform of the signal distribution in the antenna array.

The problem of detecting the acoustic image and displaying it in a useful form remains. It is an important problem affecting the usefulness of all acoustic image-forming systems and it will be discussed in a little detail here.

A number of display techniques suggest themselves, the simplest of which is to sample the acoustic image at a number of points with an array of piezo-electric transducers lying in the image plane. The spacing of the transducers should be chosen so that no information contained in the image is lost.

There are variations of this method. For example Harrold (1969) and Cook (1972) used a single large piezo-electric transducer as a detector. In the equipment described by Harrold the detecting transducer was a lead zirconate disk approximately 8 cm in diameter and silvered on both faces. The face which was not in contact with the water was cut by a grid of horizontal and perpendicular lines. The signal on each of the squares formed by the grid was proportional to the amplitude of the acoustic signal in the region directly opposite. Coupling between adjacent sensor elements presents a difficulty. However coupling levels as low as -25 db. can be achieved. This problem does not occur when an array of separate transducers is used although for mechanical reasons the separation of the individual sensors is comparatively large.

A more sophisticated display technique, which allows a much larger number of image points to be sampled, is based on a design patented by Sokoloff. This method again depends on the fact that the charge pattern produced by an extended piezo-electric plate, which is subjected at one point to an impinging ultrasonic field, is confined to the irradiated point. This occurs because most piezo-electric materials are very poor electrical conductors. Fig. 2.9 shows schematically the principle of operation of a commercial ultrasound image converter tube based on the Sokoloff patent (Jacobs 1968a and 1968b). A rapidly scanning electron beam holds the surface of the piezo-electric plate at approximately 3 volts positive relative to the mesh (see figure). The scanning beam produces secondary electrons. The number depends on the piezo-electrically induced potential which depends, in turn, on the intensity distribution of the acoustic image. The secondary electrons are then attracted towards the multiplier by the accelerating mesh and the video signal that results can then be displayed on a television screen.

The minimum resolvable detail of this type of system, when used in the most sensitive mode, is approximately equal to the thickness of the transducer layer. The maximum sensitivity is achieved when the transducer is used at its fundamental frequency (thickness mode). A general formula for this minimum resolvable diameter is given by Jacobs (1968a).

$$\text{Minimum resolvable diameter} = \frac{2.86}{\text{freq. in MHz}} \quad \text{mm}$$

$$= \frac{5.72}{\sout{11.44}} \text{ mm at 500 kHz.}$$

Ultrasound image converter tube

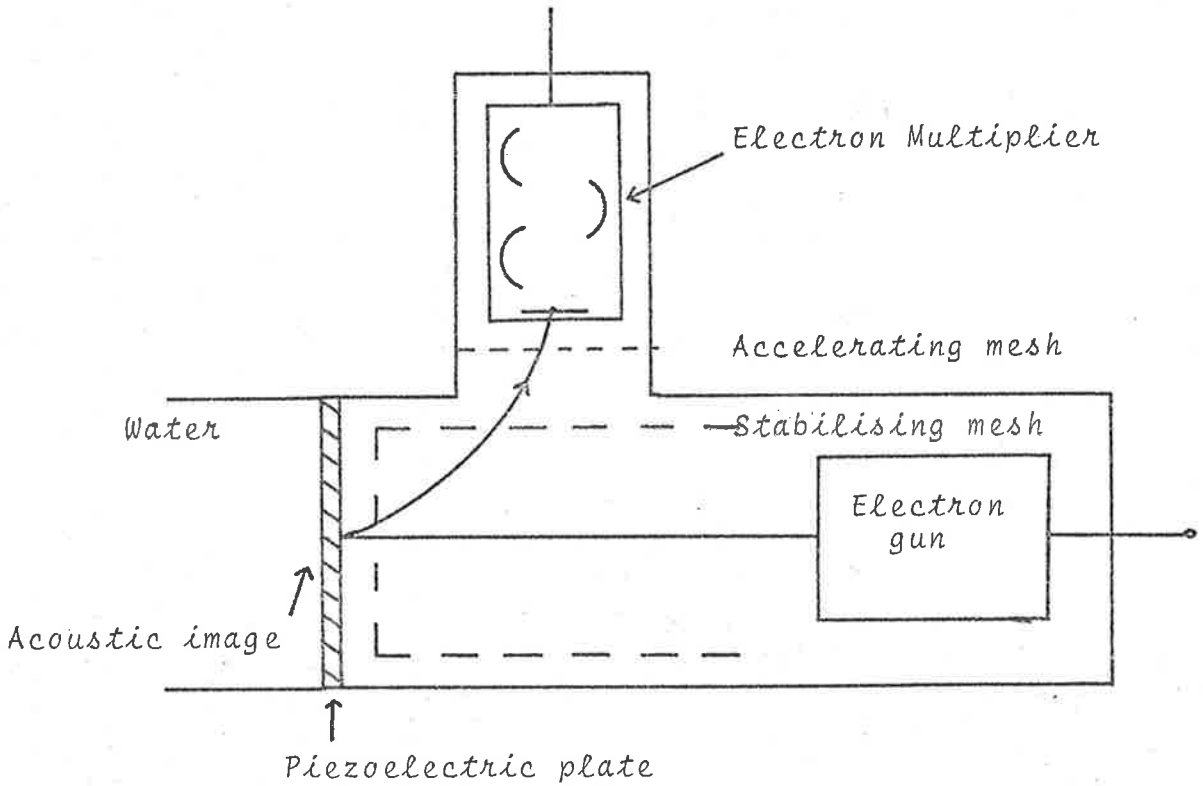

(see Jacobs 1968(a), (b))

Fig.2.9

Both Jacobs (1968a) and Smythe *et.al.* (1963) claim sensitivities such that an acoustic power input of the order of 10^{-7} watts cm^{-2} gives rise to a detectable signal from the system.

One of the disadvantages of this type of image converter is the limitation in the area of the detecting transducer which arises because one side of the transducer is at atmospheric pressure while the other is at a very low pressure ($\sim 10^{-5}$ torr). Unfortunately the thickness and the mechanical strength of the transducer are not design variables. Smythe *et al.* (1963) describe an attachment that fits over the transducer face and prevents it from being stressed by atmospheric pressure. This device should allow the transducer area to be increased from ~ 3 cm^2 to ~ 80 cm^2.

A further review of ultrasonic image converter tubes has been made by Haslett (1966) but the essential principles of operation and performance characteristics are similar to those described above.

Another method of converting acoustic images to visible images is to make use of the properties of liquid crystals which are materials which exhibit reversible colour changes if their temperatures are made to vary over a narrow range ($\sim 3°C$). This technique has been used by Cook and Werchan (1971). A cholesteric liquid crystal, in sheet form, was placed in the plane of an acoustic image, which, in this case lay at an air-water interface By controlling the water temperature the colour of the crystal could be made uniform over its entire area (~ 18 cm^2). Irradiating the crystal with ultrasound causes local heating in the regions of high acoustic intensity which produces a visible colour change. Removal of the ultrasound allows the crystal to revert to its original uniform colour which depends on the ambient

water temperature. There are two major difficulties incurred with this type of display.

(1) Relatively large amounts of acoustic power are required to produce detectable colour changes; the threshold intensity being about 0.03 W cm^{-2}.

(2) It takes 3-5 second for the sound field to establish thermal equilibrium which lasts only a few seconds before lateral heat flow destroys the mapped image.

Clearly the technique is unsuitable for making visible rapidly changing acoustic images.

Small aspherical particles (filings of magnesium or aluminium) when placed in an ultrasonic field experience a turning moment (Pohlman 1937), which causes them to align themselves in a direction that depends on the intensity of the ultrasonic field. This property may be exploited to make acoustic images visible. Although the method is sensitive, requiring only 10^{-7}watts cm^{-2}, the time required for the particles to reach their equilibrium orientation is of the order of minutes.

Photographic material may also be used to visualise acoustic images. A uniformly exposed photographic plate when placed in the plane of an ultrasonic image, which exists in a weak solution of developer, will develop most rapidly in the regions where the intensity of the acoustic image is greatest. Workers in Alaska (Parthasarathy 1971,1972) intend to use this method to make visible an acoustic image produced by a "Radio Wave Camera" (see above). Once again the technique is slow and not particularly sensitive requiring intensities of the order of 1 watt cm^{-2} over periods of minutes or hours.

An alternative method which may be used by Parthasarathy is to make use of the effect of ultrasound on an excited phosphorescent screen (Rosenberg 1955). The luminescence of a glowing screen is quenched within 6-12 seconds when the screen is placed in an ultrasonic field, the quenching being more rapid in regions of high acoustic intensity. Again, the power required to produce a detectable effect is large, e.g. 0.1-0.5 watts cm^{-2} at a frequency of 4.47 MHz.

From the above discussion it can be seen that the major difficulty in using acoustic image forming devices is the difficulty of converting the acoustic image into a visible one. A satisfactory solution has been reached for the equipment described in this thesis but the general problem remains.

2.6 COMPUTING METHODS

Computing methods for calculating the angular distribution of radio waves received by an array are based on the fundamental relationship (already encountered in chapter 1)which connects, via a Fourier transformation, the complex function describing the wave field over the array with the corresponding function representing the angular spectrum.

Thus a digital computer can be used in conjunction with an antenna array to form an image of the radio sky. To actually construct the image, the array would be used to sample the phase and amplitude of the wave field and suitable circuitry would be used to amplify and record this information in digital form. A digital computer could then be used to perform a two-dimensional Fourier transform on this data, and finally the output would be displayed in suitable form.

This approach is quite feasible for linear arrays or dilute planar arrays containing a small number of elements. However the rate at which data must be handled for the real time processing of the information from a filled in planar array containing say, 100 elements, precludes the use of this technique for real time processing (McLean and Wild 1961). For example a CDC 6400 takes 0.775 seconds of central processor time to calculate the Fourier transform of a two dimensional complex function defined at 100 points on a 10 x 10 grid, using the fast Fourier transform program developed by Singleton (1969).

2.7 HOLOGRAPHIC METHODS

A radio wave hologram can be formed using the same principles as are used in the formation of an optical hologram. Fig. 2.10 illustrates how a one dimensional hologram could be produced using a radar system. A transmitter is used to illuminate the targets and the reflected waves are sampled by an array. The sampled signals are added to a reference signal derived from the transmitter and the resulting signals are then used to drive an array of light sources, the brightness of each source being proportional to the amplitude of the sum of the received and reference signals. The radio wave hologram has now been converted into a visible form which can be photographically reduced. The light diffracted into the first order, when the reduced photograph is illuminated with a coherent monochromatic light source, would be similar to the radio wave front incident on the array. This wave could then be made to form an image using a conventional lens.

The major technical problem with this approach is to obtain the reduction in size. For example, to maintain the same scale, an array, 10 radio

Method of recording a radio hologram

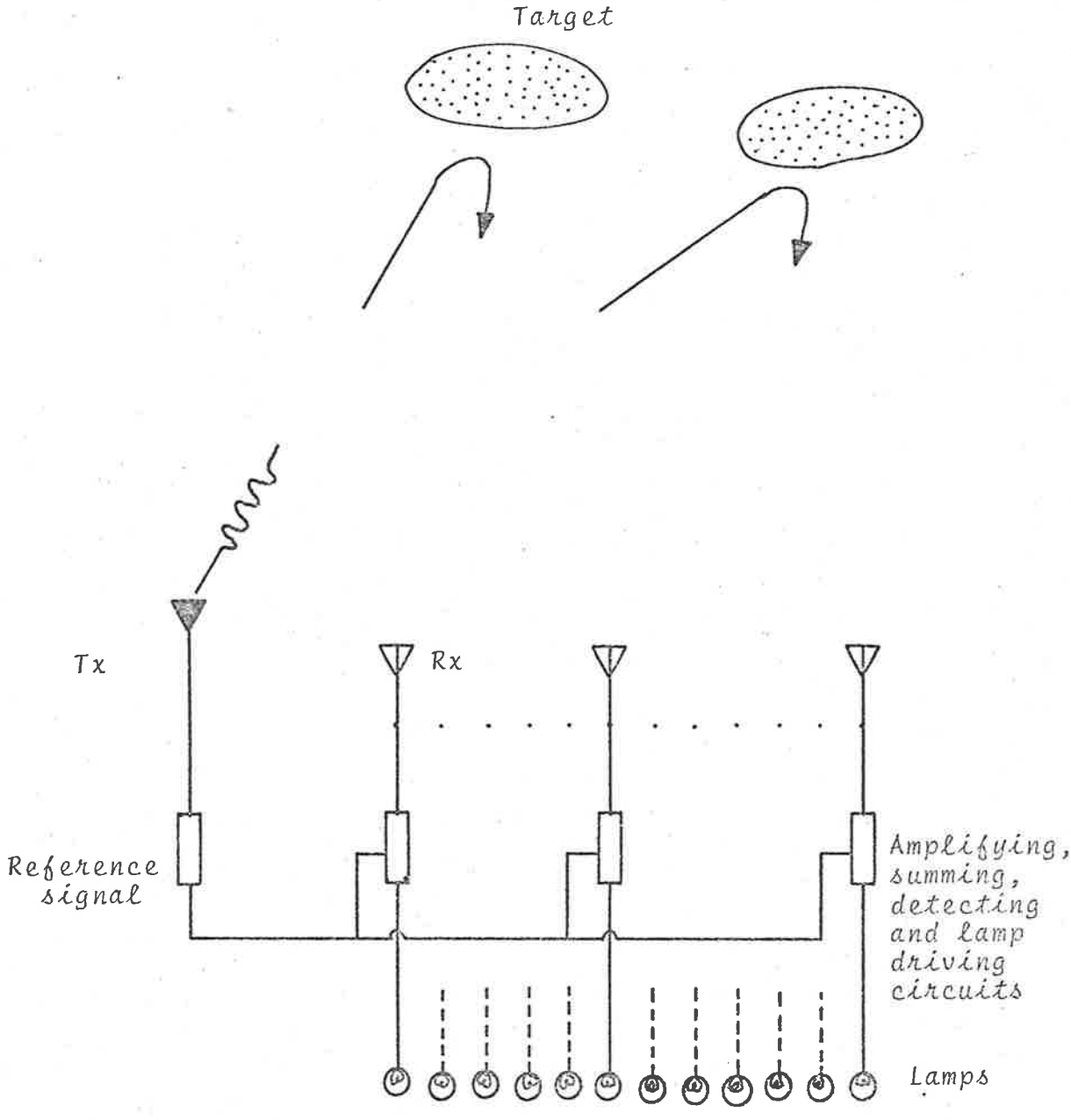

Fig.2.10

wave lengths in diameter, would have to produce a hologram 10 wave lengths of visible light in diameter. Thus the image on the reduced hologram would have to be about 7 μm in diameter (for red light). This is only slightly larger than the grain size of normal photographic emulsions. Thus the technique is only applicable for arrays with diameters which are very large when compared with the operating wave length and in any case it is not a suitable method for real time processing.

2.8 CONCLUSION AND SUMMARY

Five different methods of processing the signals from antenna arrays have been considered. The objective of the processing is to obtain information about the angular spectrum of waves collected by the array which is equivalent to the formation of an image of the radio sources producing the incident radiation.

From the above discussions the following conclusions, relating to the different methods, may be drawn.

(1) Scanning methods have been and are currently being successfully used in radio astronomy and ionospheric physics (Mills 1963, Wild 1967 and Brownlie *et al.* 1973a). These operating systems use dilute arrays. The scanning approach is not suitable for processing signals from filled in arrays containing many elements.

(2) Electro-Optical techniques appear to be very promising and they offer a practical solution to the problem of real time signal processors for filled in arrays. To date however there appear to be no arrays which actually use this method (except possibly some secret military radar systems) and these conclusions are based on the successes achieved with simulated inputs.

(3) Acoustic methods have been shown to be useful for large filled arrays containing many elements (Briggs and Holmes 1973); the method is relatively simple and cheap. The approach awaits the development of the acoustic equivalent of the photographic plate before the method can be applied to arrays with high resolutions and large fields of view.

(4) Normal computing techniques are precluded from the real time processing of signals from filled in arrays because they are unable to handle data sufficiently rapidly. Specially designed computers could of course be made much faster. Presumably even when sufficiently fast digital computers are available their cost will prevent their use as on line processors, at least in the near future. The major advantage of the computing technique would be its versatility. In principle a computer could be programmed to handle the input in any way desired. This would allow optimum use to be made of an array's beam forming capabilities and in addition both the phase and amplitude of the processed data would be readily available.

(5) The holographic technique described above is only suitable for arrays which are many wave lengths in diameter and is not useful for real time processing.

CHAPTER 3

THE EQUIPMENT

3.1 INTRODUCTION

The first part of this chapter will be devoted to an overall description of the ultrasonic image-forming system and an explanation of its principle of operation. The remaining sections will contain a more detailed description of the characteristics and performance of the important parts of the instrument.

3.2 GENERAL DESCRIPTION

The objective of the system is to measure the angular spectrum of radio waves reflected from the ionosphere. To do this, a large, 89 element antenna array (described by Briggs *et al.* 1969) is used to sample the phase and amplitude of the diffraction pattern formed over the ground when the ionosphere is illuminated from below with radio waves transmitted from a nearby pulse transmitter. The elements of the array are arranged on a square grid inside a circle 1 km in diameter, and the signals that are induced in each antenna are carried by buried coaxial cables to a central laboratory. By making the coaxial cables an integral number of wavelengths long, and using transformers to change the phases of the signals by 180° when necessary, it is possible to ensure that the signals available in the central laboratory have the correct phases and amplitudes. These 89 sampled signals then provide the inputs to 89 superheterodyne radio receivers. The required ionospheric echo is selected by a gating system. The receivers have a common local

oscillator and consequently the relative phases of the signals are preserved. As is shown in fig. 3.1 the outputs from the receivers at the intermediate frequency of 455 kHz are used to drive 89 piezo-electric transducers, which are arranged inside a circle 18 cm in diameter and in the same configuration as the dipoles in the array. An acoustic wavefront is produced in water, and the amplitude and phase of this wavefront match the amplitude and phase of the radio wave over the ground. A focussed acoustic image is obtained by adjusting the positions of the transducers so that they lie on part of the surface of a sphere, the centre of curvature of which lies in the image plane. By using another similar array of piezo-electric transducers, lying in the image plane, the focussed acoustic image is sampled, and the voltages derived, are, after suitable processing, used to drive an array of light emitting diodes, once again arranged in the same configuration as the antennas. In this way a visible representation of the required angular spectrum is obtained. At the same time the detected outputs of the 89 receivers are peak rectified and the resulting voltages are used to drive another array of light emitting diodes which produce a visible representation of the modulus of the amplitude variations in the diffraction pattern. The two displays are positioned side by side so that they may be photographed by a single ciné camera. Data are also recorded in digital form on a magnetic tape. A complete block diagram of the system is shown in fig. 3.2,and an overall view of the equipment is shown in fig. 3.3.

ULTRASONIC IMAGE FORMING SYSTEM

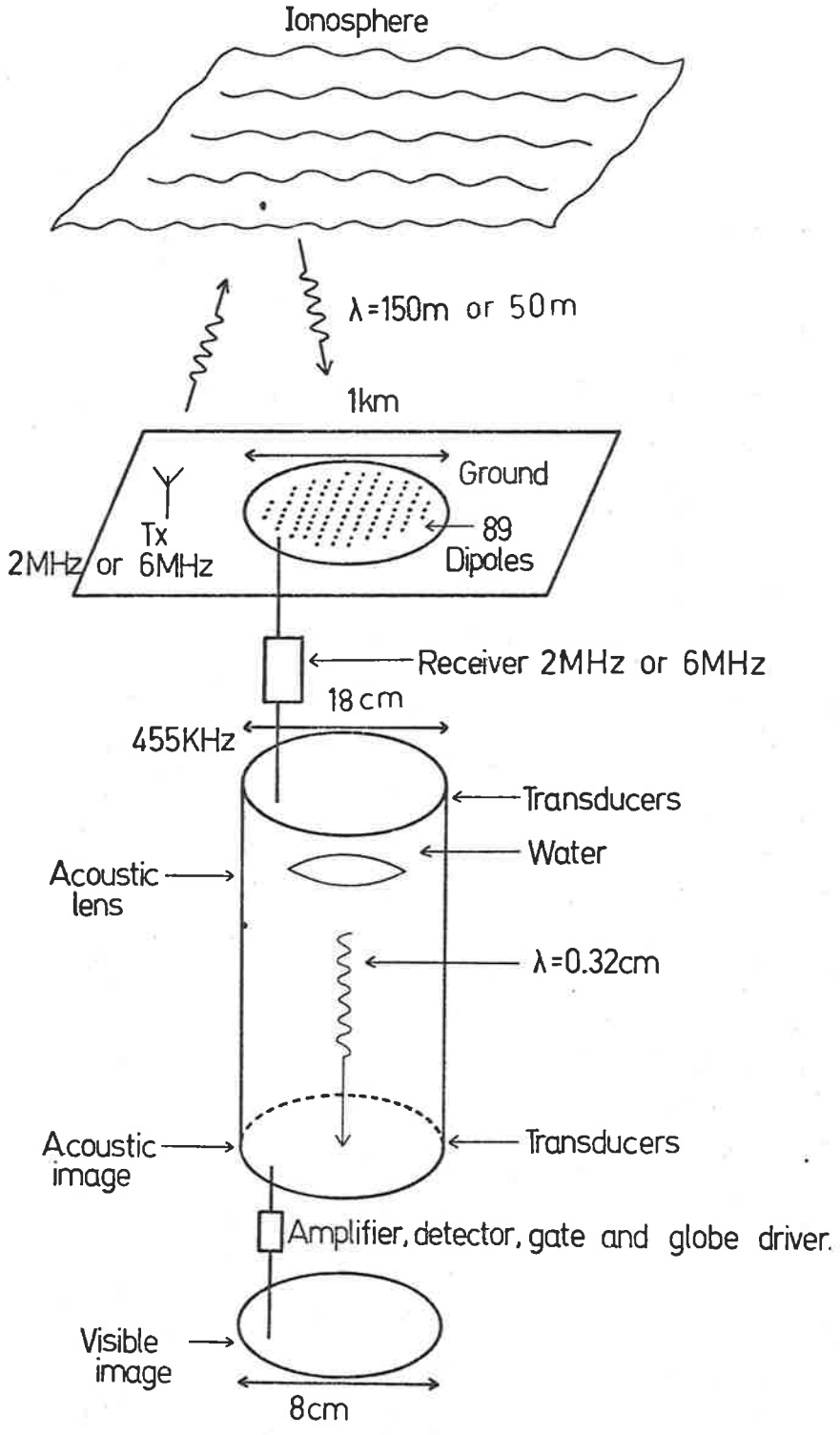

Fig. 3.1

Detailed block diagram of image-forming system

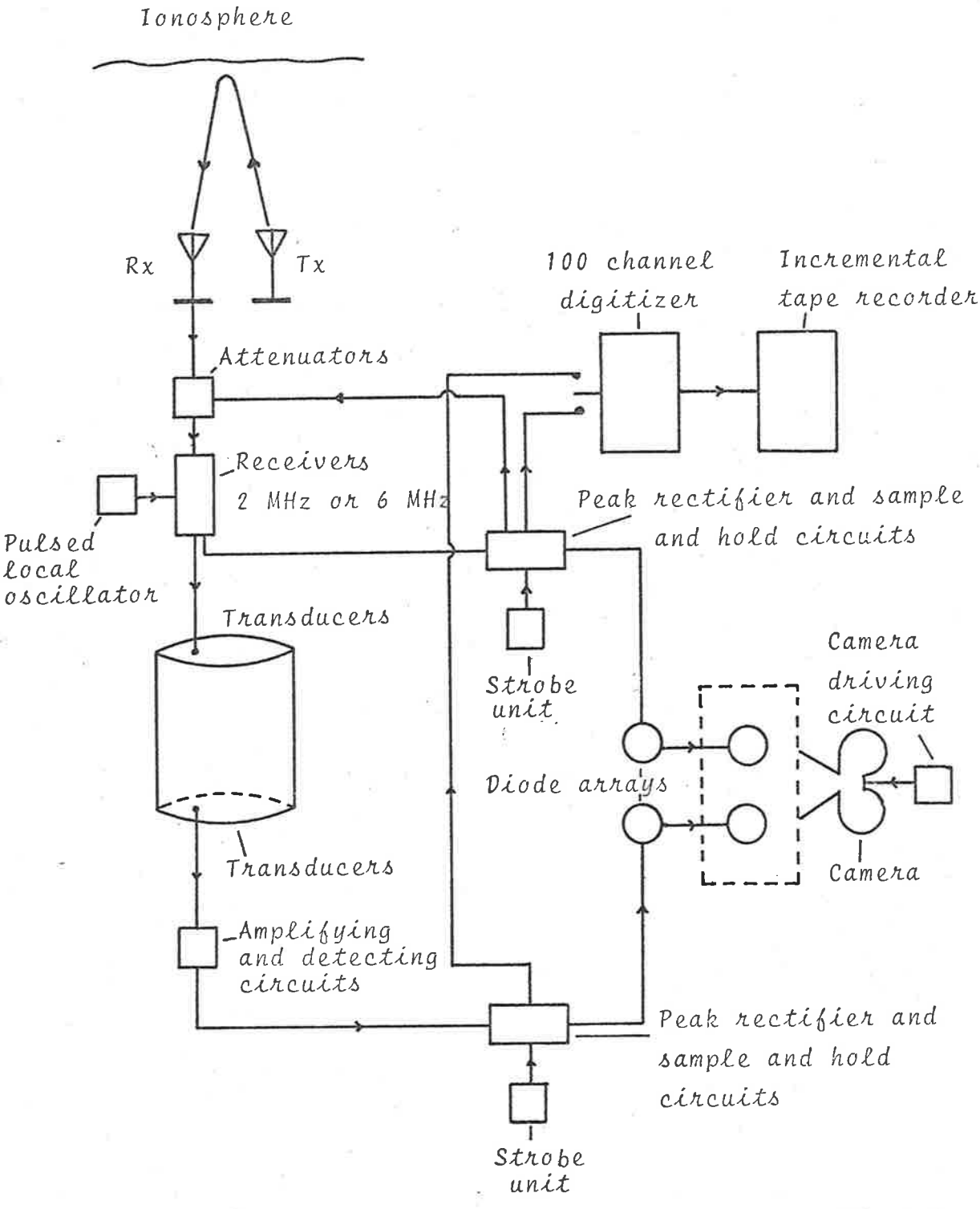

Fig. 3.2

An overall view of the equipment

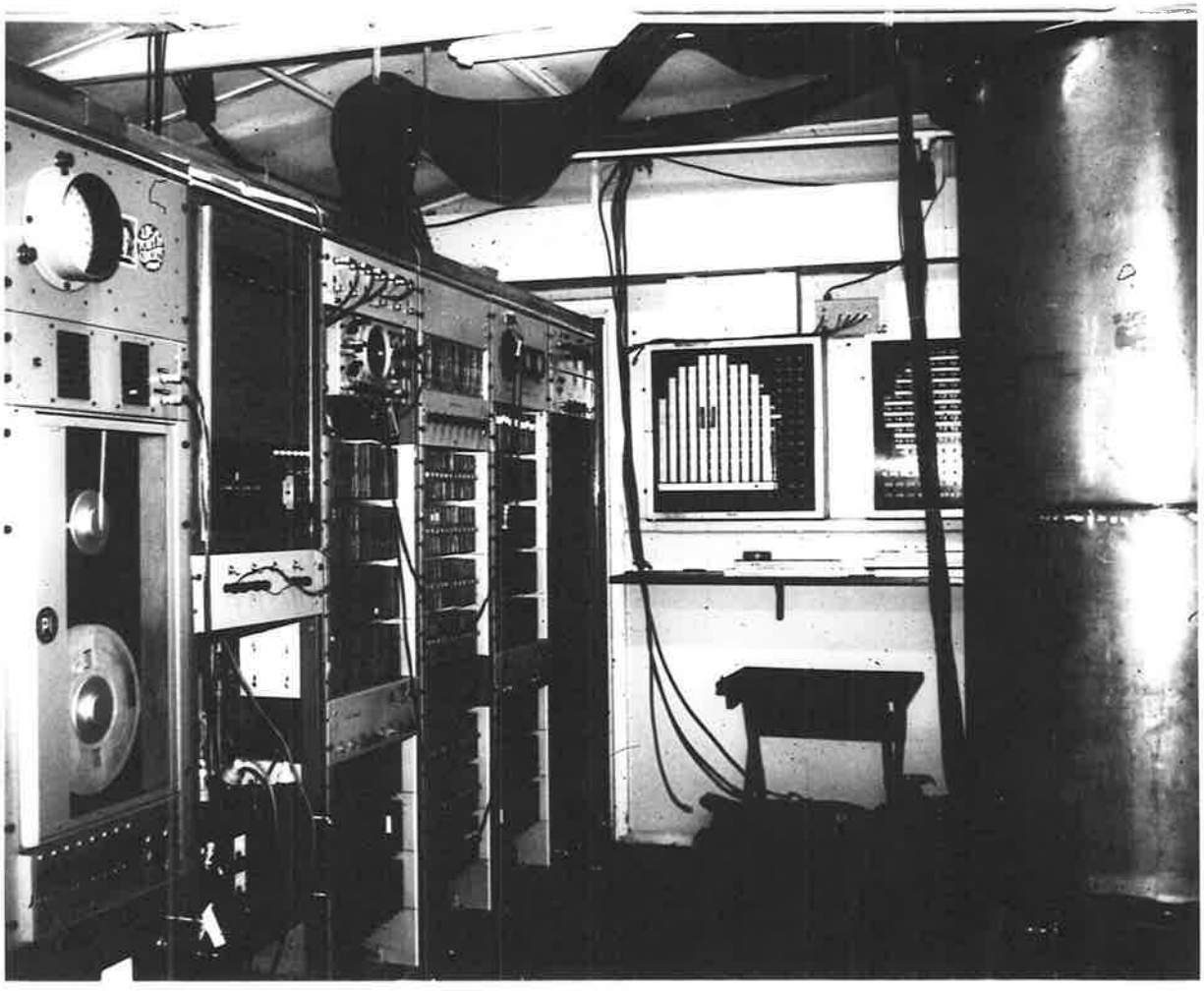

The major features, described from the left, are as follows;
Rack no.1: The magnetic tape recorder and a lamp display which is not part of the present equipment.
Rack no.2: The 100 channel digitiser and power supplies.
Rack no.3: A monitor oscilloscope, one set of 89 post detector receiver cards and a gate pulse generator for selecting the ionospheric echo.
Rack no.4: The 89 attenuators, 89 receivers (r.f. stage), the 89 transducer drivers and the local oscillator.
Rack no.5: Two light emitting diode displays, 89 amplifying and detecting circuits and the second set of 89 post detector receiving cards. Also contained in this rack is the second gate pulse generator for selecting the appropriate acoustic echo.
Rack no.6: The camera drive unit and the camera (not visible).
On the right of the photograph is the tank and also visible are the 178 input and output coaxial cables.

Fig. 3.3

3.3 THE TRANSMITTER AND TRANSMITTING ARRAY

The transmitter is situated close to the receiving array which has been built on a flat coastal plain at Buckland Park (34°38'23" south latitude and 138°27'45" east longitude) about 36 km north of Adelaide. Pulses at 1.98 MHz (which will be referred to as 2 MHz) with a peak power of up to 100 kW can be transmitted. The pulse repetition frequency may be set at 200, 100, 50, 25, 2 or 1 Hz depending on the experiment, the most commonly selected repetition rate in the experiments described here being 50 Hz. The pulse length was continuously variable from about 20-200 μseconds, and in order to reduce interference with other radio users the pulses were shaped so that they had an approximately Gaussian envelope. The triggers for the transmitter pulses were derived either from the mains or alternatively from the count down of a 100 kHz crystal oscillator which was also used to control the recording facilities (100 channel digitiser and magnetic tape recorder).

The r.f. pulses from the transmitter were fed via a tuning/impedance matching network and an open wire feeder system to an array of four half wavelength (71.8 metres) folded dipoles, each with an impedance of 400 ohms. The four antennas were arranged so that they formed the sides of a square suspended approximately 29.8 metres above the ground. The transmission polar diagram of this arrangement of antennas is approximately 50° wide at the half power points.

Circularly polarised radio waves were transmitted by feeding one pair of parallel antennas with signals which were in quadrature

with the signals feeding the other perpendicular pair. The required polarisation, ordinary or extraordinary, was selected by using vacuum relays to switch the r.f. signal through appropriate lengths of phasing cables. In addition it was possible to select (using a control in the central laboratory) twelve levels of transmitted power. In this way the strength of the received signal could be chosen so that it approximately matched the dynamic range of the receiving equipment. This modification to the transmitter proved necessary because, as will be seen in Section 3.5, the dynamic range of the receiving equipment is small and not able to cope with the large range of signal amplitudes received under different ionospheric conditions.

Also available is a much lower powered (4 kW peak power) 5.94 MHz (which will be referred to as 6 MHz) pulse transmitter with which, at the present time, it is only possible to transmit linearly polarised signals. This transmitter has not been used in the experiments described in this thesis, but will be used in the near future to extend the use of the image-former to 6 MHz as well as 2 MHz.

3.4 THE ARRAY AND ANTENNAS

The receiving array consists of two sets of 89 half-wave dipoles which are suspended approximately 10.6 metres above ground level by 121 timber poles. The wires for one set of dipoles run in a north-south direction while the other set are oriented in an east-west direction. The layout of the antennas is shown in fig. 3.4. The signals from the 178 antennas are carried by separate 75 ohm coaxial cables, which

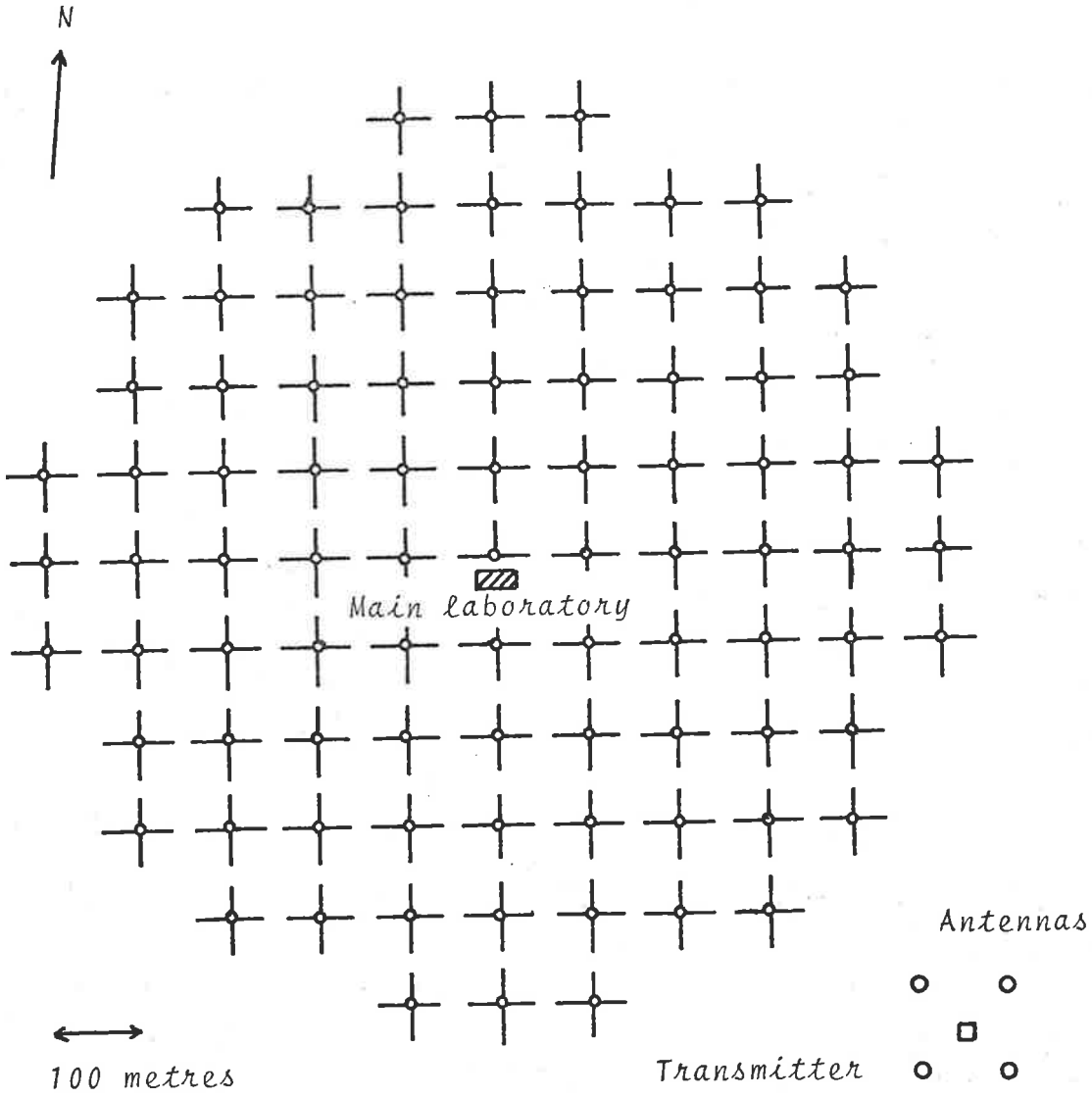

Diagram showing the layout of the receiving array. Each cross represents a pair of dipoles. The transmitting array is positioned 700 metres to the south-east of the array centre.

Fig. 3.4

are buried in a network of shallow trenches, to the central laboratory where they are then terminated on two 89 pole 3 position switches. The 89 antennas used in the image-forming experiment are aligned north-south and these may be switched into either the image-forming system or to a set of Belling-Lee sockets where they may be used for other experiments. The third switch position is not used at present.

As has been explained before the electrical lengths of the feeder cables have been made equal to an integral number of half wave lengths at 2 MHz, transformers being used to introduce a further 180° phase shift where necessary. In this way it is possible to preserve the phases of not only the 2 MHz signals but also of the signals at the third harmonic, 6 MHz.

The type of cable used for the feeders was chosen for its low attenuation, good shielding, and durability in wet conditions; even so the attenuation of signals from the most distant antennas is approximately 6 db. Often when antennas are connected up as broadside arrays the signals from the outer elements are deliberately attenuated so that they contribute less to the final output than those nearer the centre. The effect of this on the polar diagram is to reduce the side lobe level and increase the width of the main beam (see Kraus 1966). The attenuation caused by the feeder cables provides the Buckland Park array with a natural grading of this type. However in the present experiment use is not made of this and the effective receiver gains have been adjusted to compensate for any signal losses. Cross talk between the cables is at least 80 db below the signal and consequently is probably considerably

less than the coupling between the antennas.

The impedances of the dipoles used in the array (measured directly at the given height above ground) were 20 ohm at 2 MHz and 97 ohm at 6 MHz. The circuit shown in fig 3.5 was used to match each dipole to the 75 ohm cable. Fig. 3.6 shows the way in which the impedance, as measured in the central hut, varied with frequency (in the range 1.98 MHz ± 14 kHz) for a typical dipole. Ground conditions were found to have little effect on the impedances except at times when water was actually lying on the surface. Under these conditions the resistive component becomes large, of the order of 100 ohms, while the reactive component remains unchanged.

If the ground is assumed to be perfectly conducting then the beam width (to the half power points) of the individual receiving dipoles is greater than 30° (Trott 1966). Trott has also calculated the polar diagram of the array when one set of dipoles is connected as a broadside array. This calculation, which is illustrated by fig. 3.7, takes into account the beam shapes of the individual dipoles. However some simplifying assumptions have been made. The most important of these are that the ground is a perfect conductor, that coupling between individual dipoles can be ignored and that there is no signal loss in the feeder cables. In fact figure 3.7 shows only the intersection of the beam pattern with a plane which is parallel to the set of dipoles and perpendicular to the plane of the array. The beam pattern in an orthogonal plane is very similar (Trott 1966).

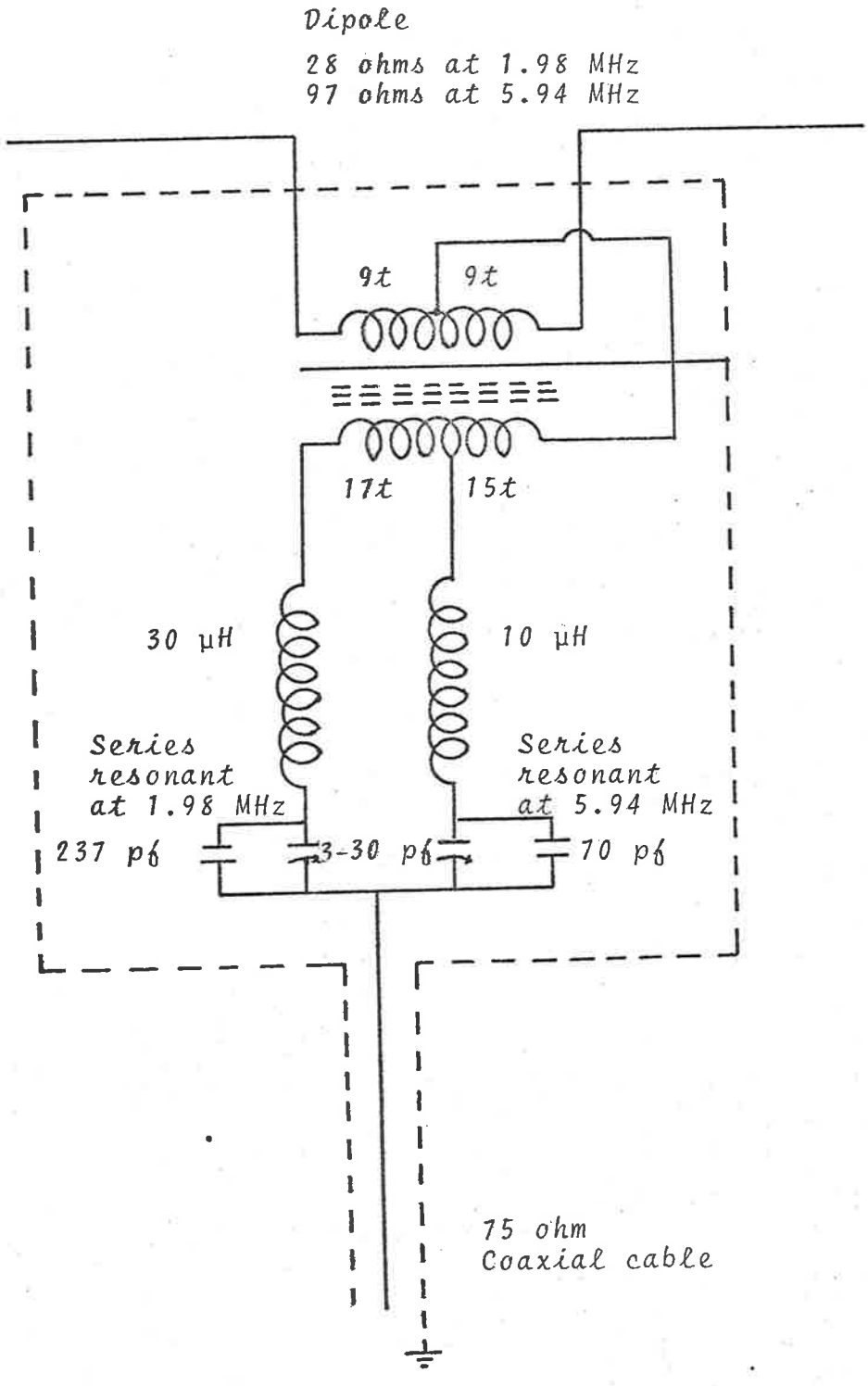

Circuit diagram of the receiving antenna matching network

Fig. 3.5

The impedance of a dipole, as measured from the central laboratory, at frequencies close to 2 MHz.

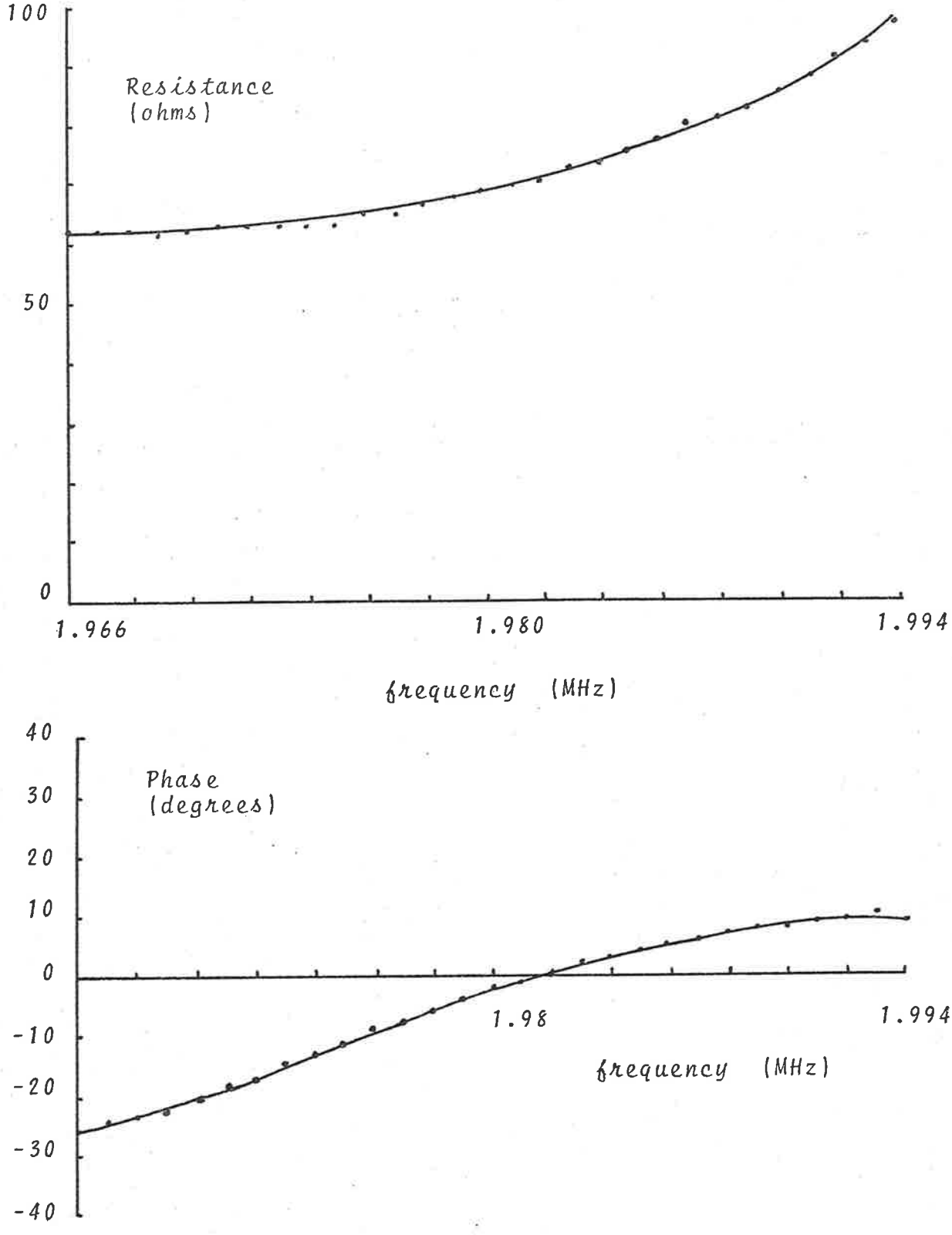

Fig. 3.6

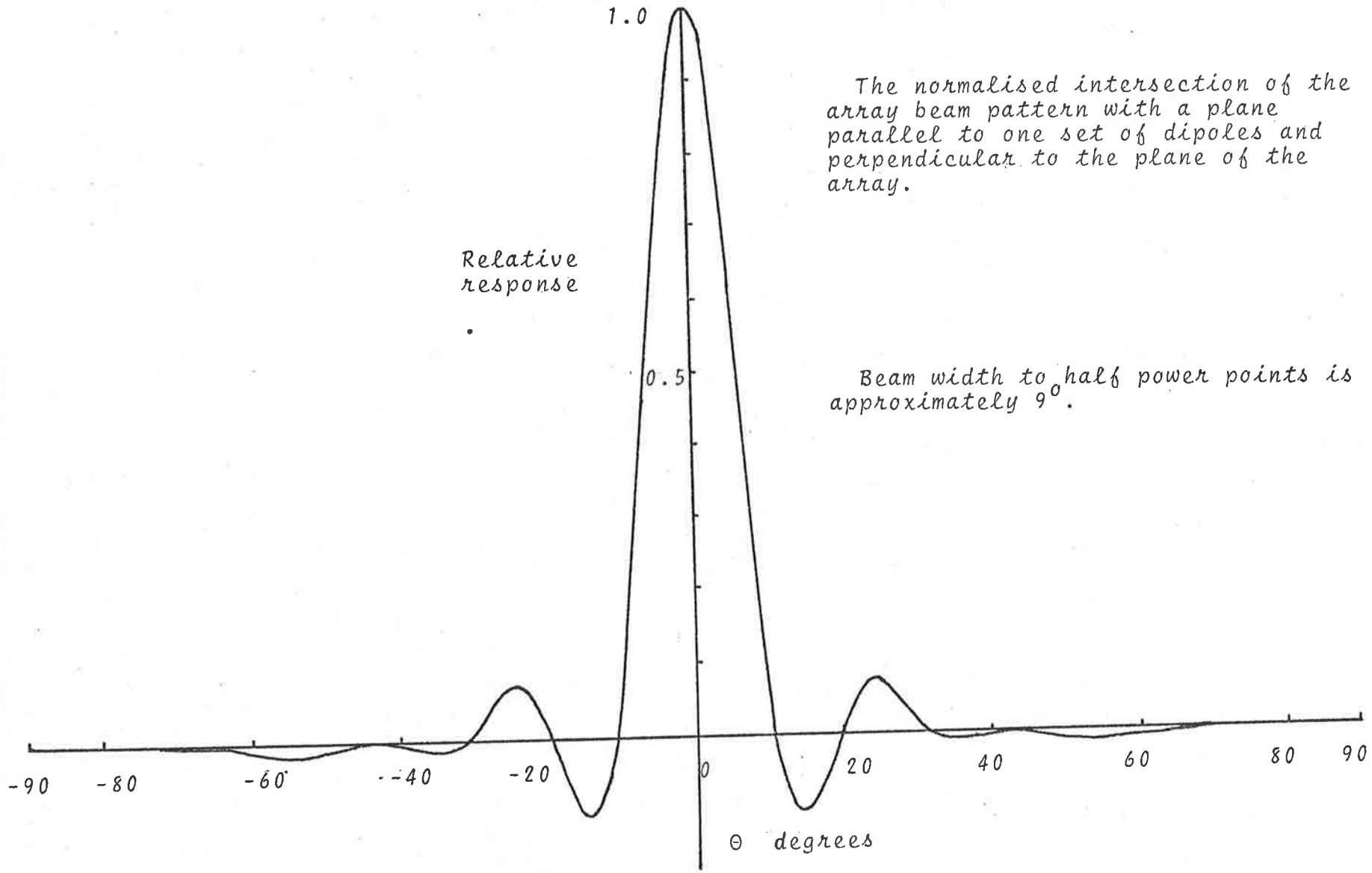

The normalised intersection of the array beam pattern with a plane parallel to one set of dipoles and perpendicular to the plane of the array.

Beam width to half power points is approximately 9°.

The array beam pattern (after Trott, 1966)

Fig. 3.7

3.5 THE ATTENUATORS

Reference to fig. 3.2 shows that the signal from each antenna passes through a voltage controlled attenuator before being applied to the receiver input. These attenuators (developed for the image-forming system from a basic design appearing in a Hewlett-Packard application note, No. 912) were used to provide the receiving system with an automatic gain control (A.G.C.). This was necessary because the amplitude of signals reflected from the ionosphere varies over a wide range; depending mainly on D region absorption. A useful receiving system must be designed with this point in mind.

A set of 89 receivers with sufficient dynamic range had been built and used in earlier experiments reported by Briggs *et al.* (1969) and Felgate and Golley (1971). These receivers use a conventional automatic gain control which operates on the intermediate frequency amplifier and provides the receivers with a dynamic range of approximately 75 db. Unfortunately, with this type of system, the phase of the signal being amplified changes as the receiver gain is varied. Had these receivers been used in their A.G.C. mode then phase errors as large as 50° would have been introduced into the system, and errors of this magnitude would have resulted in an unacceptable deterioration of the focussed acoustic image (see chapter 5 for discussion of the effects of phase errors on the acoustic image). However it was found that if the receivers were operated at a fixed gain then the phase errors, although still large, were stable and could be compensated for by adjusting the position of the relevant transducers in the focussing

array (see chapter 4).

Operating the receivers in this way solves the problem of obtaining signals with the correct phase but now the dynamic range of the system is small. By using the continuously variable attenuators the effective dynamic range could be increased. A circuit diagram and a brief description of the mode of operation of the attenuators can be found in appendix 1. In brief the circuit behaves as a voltage controlled constant impedance attenuator which is continuously variable in the range -1 to -36 db. The voltage which controls the attenuators is derived from the receiver output and is applied so that the strong signals are attenuated more than weak signals.

This approach has the obvious disadvantage of decreasing the signal to noise ratio. However as external noise rather than receiver noise is usually the limiting factor, this effect is not important. Some phase errors are introduced by the attenuators but in practice these are small (less than 5°).

The dynamic range of approximately 35 db provided by the attenuators, plus the ability to control the transmitter power allows the system to operate under most ionospheric conditions.

3.6 THE RECEIVERS AND LOCAL OSCILLATOR

As explained earlier the design of the receivers used in the image-forming experiment was based on the receiver design used in an earlier experiment (Briggs *et al.* 1969). The differences between the new and old sets of receivers are listed below.

(1) Provision of an output for the 455 kHz I.F. signal.

(2) Use of a new mechanical filter, which increases the receiver bandwidth from 22 kHz to 28 kHz, thus allowing the use of narrower transmitter pulses which allows better range resolution.

(3) Improved matching between different receiver stages which increased the maximum gain from 106 db to 126 db.

(4) The use of specially selected transistors which were found to be necessary for receiver stability at high gain settings.

Table 3.1 summarises the performance characteristics of a typical receiver and allows a comparison between the original and new receivers to be made.

TABLE 3.1

	Old	New
Maximum gain	106 db	126 db
A.G.C. control range	75 db	0 db
Image rejection	32 db	43 db
Noise figure	9 db	7 db
Bandwidth (6 db points)	22 kHz	28 kHz
Signal to noise ratio (1 μvolt input)	4:1	4:1

The local oscillator was common to all receivers and provision was made for it to be used either in a continuous or in a pulsed mode (pulse widths were variable in the range 50 to 300 μseconds). Pulsed operations had the effect of suppressing the receiver output at all times except when the local oscillator was "on". Thus, by adjusting the delay of the local oscillator pulse relative to the transmitted pulse any ionospheric echo (first hop, second hop etc.) could be observed and the others rejected. This greatly simplified the task of selecting the correct pulse from those received by the receiving transducers, which included reflections of the acoustic signals from the top and bottom of the tank (see section 3.10).

Circuit diagrams and additional notes relating to the design of the receivers and the local oscillator are contained in Appendices 2 and 3.

3.7 THE POST-DETECTOR RECEIVER CIRCUIT

The detected outputs from the receivers and from the so called amplifying and detecting circuits (which processed the signals from the receiving array of transducers; see fig. 3.2) had to be converted into a suitable form for recording. The outputs from both these circuits consisted of a pulse, the amplitude of which varied slowly with time. In the case of the receiver outputs this was due to the normal fading of the echoes, and for the amplifier and detector outputs the variations were caused by changes in the amplitude and the direction of arrival of the ionospherically reflected signals. The major function of the post-detector receivers was then to produce a slowly varying d.c. voltage with

an amplitude proportional to the input pulse (derived from the detected output of the receiver or from the amplifying and detecting circuits). This d.c. signal was then used to drive the light emitting diodes and also to provide the input to the 100 channel digitiser for the magnetic tape records. One further output was produced. This was the control signal for the voltage controlled attenuators, which was produced by comparing the slowly varying d.c. output with a reference level and producing a signal (proportional to the difference) which was then fed to the attenuators so that the difference was minimised. The time constant of this feed back loop was variable, but for the experiments described in this thesis a value of about 100 seconds was used. Consequently this had little effect on the normal fading of the ionospheric echo which has a "period" in the range 1 to 20 seconds.

A diagram of this circuit may be found in appendix 4.

3.8 TRANSDUCERS AND TRANSDUCER HOLDERS

Considerable effort was directed into finding a suitable type of transducer and developing a transducer holder so that the two used together had the characteristics required for the experiment. The desired properties were,

(1) A bandwidth at least as great as the receiver bandwidth, i.e. greater than 28 kHz.

(2) Reasonable efficiency (so that cheap and simple driving circuits could be used).

(3) A polar diagram, wide enough to "illuminate" the entire transducer receiving array and narrow enough to avoid "wasting" acoustic energy. For this a beam width of approximately 6° to the half power points is required. This is determined by the diameter of the receiving array of transducers and by the dimensions of the tank.

(4) Reasonably robust with the ability to operate under water.

The first transducer tested was a disk, 1 cm in diameter and approximately 2 mm thick, made of a ceramic material (PZT-5A). It was nominally resonant in a thickness mode at 1 MHz. Unfortunately the small second harmonic content of the 455 kHz driving signal was sufficient to excite the transducer in its resonant mode with the result that measurements of the frequency response of the transducer indicated the presence of a resonance peak at 455 kHz. In practice the signal emitted by this type of transducer, when driven at 455 kHz, was very distorted and contained more power at the second harmonic than at the driving frequency.

The obvious possibility of using the transducers at resonance was considered and although a bandwidth (to the half power points) in excess of 30 kHz was obtainable, the value of the resonance frequency could not be guaranteed (by the manufacturers) to within less than

± 3% which is equivalent to an error of ± 14 kHz at 455 kHz.

The transducers finally selected were disks of PZT-5H (similar to PZT-5A), one cm in diameter and approximately 3 mm thick and nominally resonant, in a thickness mode, at 600 kHz. The "frequency response" was measured in the following way: a pair of transducers, separated by 1.65 metres in a tank of water, were used as a transmitter and receiver. The output from a variable frequency signal generator (output impedance 50 ohms) was pulse modulated (pulse duration approximately 100 μ seconds, repetition rate 50 Hz) and used to drive the emitting transducer. The amplitude of the signal received by the second transducer was measured. Fig. 3.8 is a plot of the normalised amplitude of the received signal as a function of frequency in the range 430-630 kHz. It can be seen that the amplitude of the signal received at the working frequency (455 kHz) is smaller, by a factor of about 10, than that received at the resonance frequency, however the response is relatively flat in this region. It should be noted that no attempt has been made to allow for the fact that, due to diffraction effects, the transducer beam patterns reduce in width as the frequency is increased. This leads to an apparent increase in the "tranducer efficiency" which is misleading if the term is to be thought of as the efficiency with which electrical energy is converted to acoustic energy.

As well as measuring the "frequency response" of the transducers, the polar diagrams were also measured by using a pair of transducers, one of which could be rotated in the horizontal plane about an axis perpendicular to the line joining the two transducers. Fig 3.9 is

Typical "frequency response" of a pair of transducers (see text). These transducers were nominally resonant, in a thickness mode, at 600 kHz.

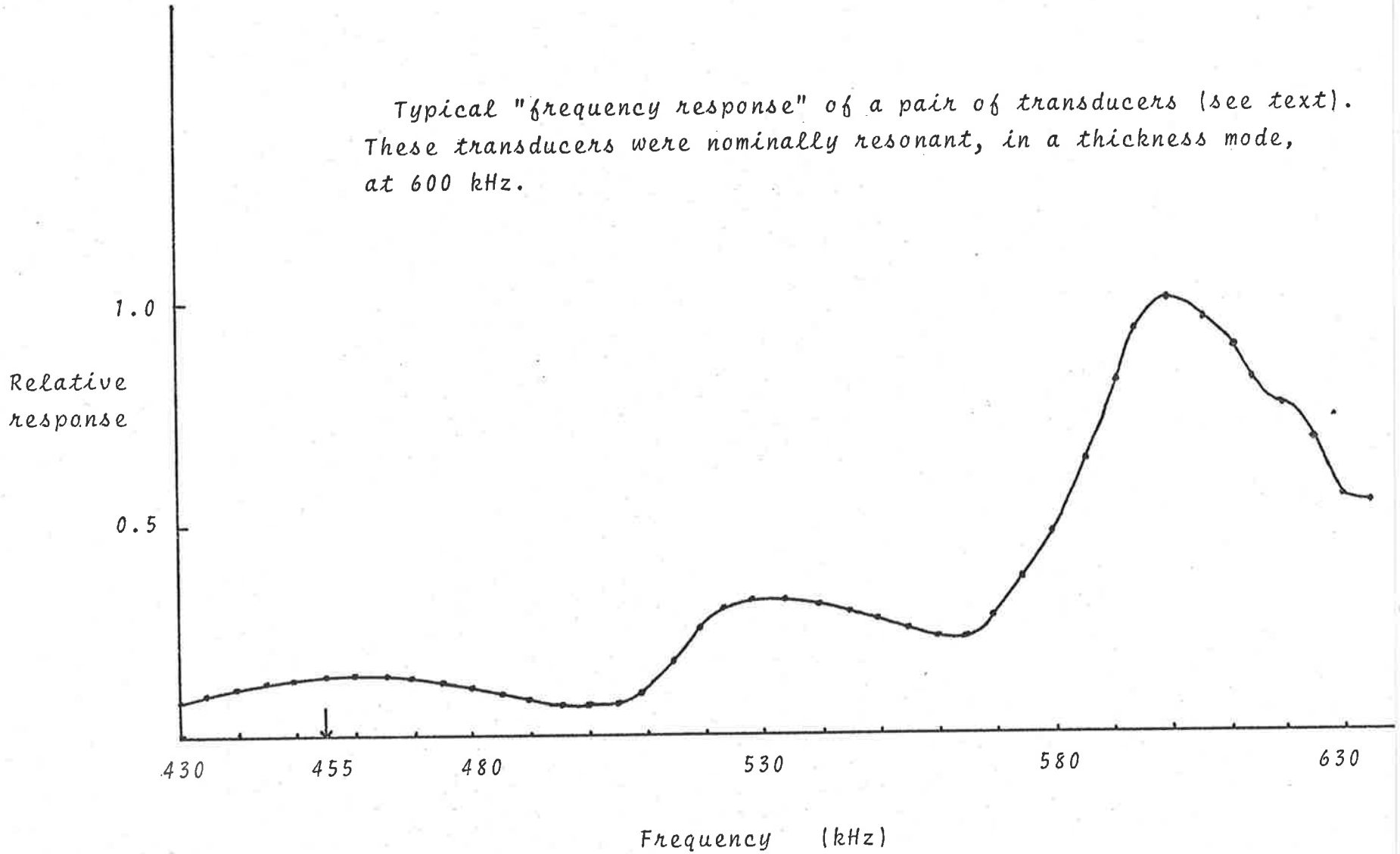

Fig. 3.8

Solid line is $$\left| \frac{2J_1 \left\{ \frac{kD}{2} \sin\theta \right\}}{\left\{ \frac{kD}{2} \sin\theta \right\}} \right|$$

where $k = \frac{2\pi}{\lambda}$

$\lambda = 0.32$ cm

$D = 0.9$ cm

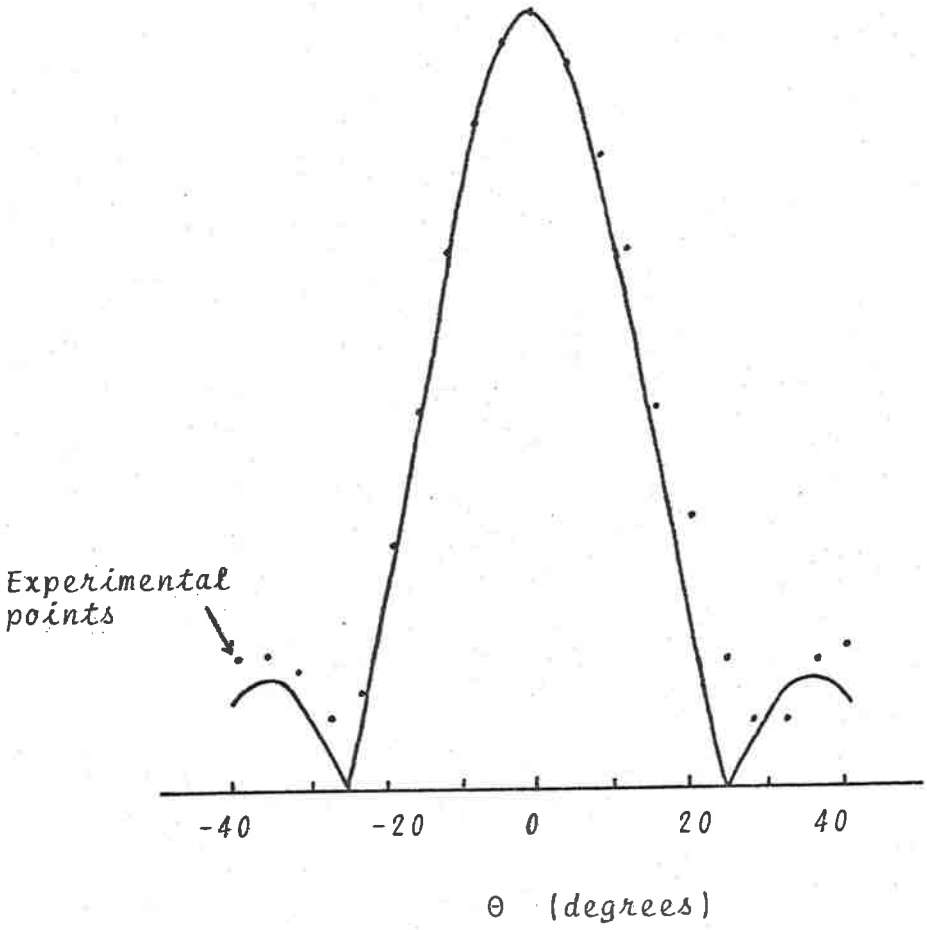

Normalised directivity function of a transducer

Fig. 3.9

a plot of the relative signal strengths received by the movable transducer for different orientations (θ). Also plotted is the theoretical polar diagram, calculated from diffraction theory, assuming that a signal of wavelength 0.32 cm (wavelength of 455 kHz ultrasound in water) is being emitted from a circular aperture 0.9 cm in diameter (effective diameter of the transducer in the transducer holder).

Comparison of the two curves indicates that the main lobe of the actual polar diagram is well described by the appropriate theoretical formula.

A number of different designs for transducer holders were considered. The one actually used is depicted in fig. 3.10. The mount consisted of a hollow, stainless steel tube with a very fine external thread (48 turns per inch) which allowed the holder to be screwed into a stainless steel plate and its position relative to the plate accurately adjusted (see frontispiece). The transducer was held in place by a brass insert and a teflon washer, which pushed the transducer against a ridge at the extreme end of the stainless steel tube (see diagram). The radiating face of the transducer, which was at earth potential, was protected from the water by covering it with an epoxy resin. The 455 kHz signal was applied to the transducer by a short length of enamelled wire feeding through a hole in the brass insert and soldered on to the centre of the back face of the transducer. The other end of this wire was soldered on to a Belling-Lee line connector which was attached to the brass insert. Signals from

Transducer Holder (not to scale)

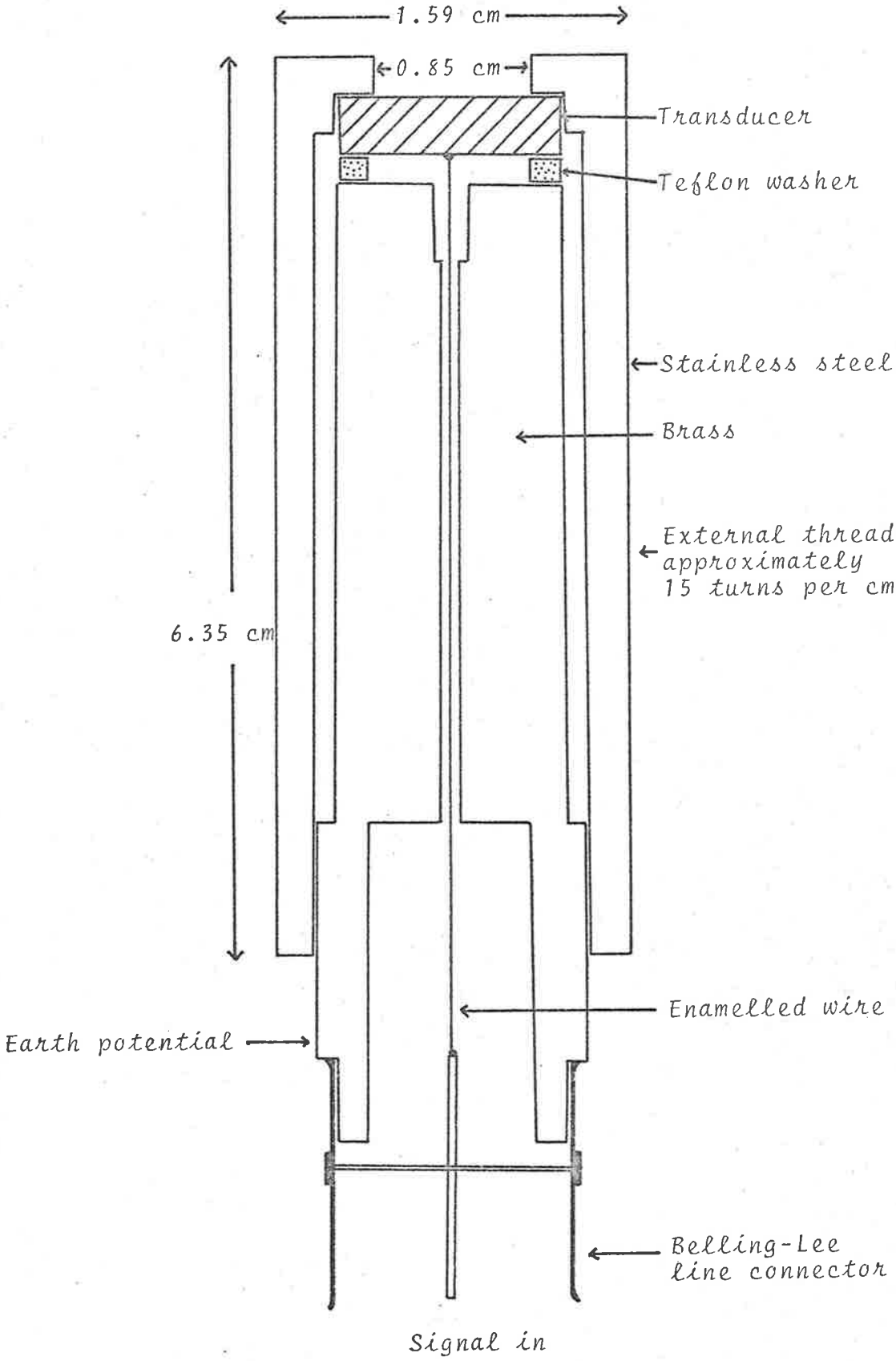

Fig. 3.10

the transducer driving circuits were carried by coaxial cables about 3 metres long to the Belling-Lee line connectors on the transducer holders.

The receiving transducer holders on the plate at the bottom of the tank were of the same type and were adjusted so that the top surfaces of the transducers lay in a plane parallel to the bottom of the tank. The external threads on the holders were then coated with a sealing material (Locktite) which set hard and produced a water tight joint. The transducers in the receiving array could thus not be easily adjusted.

No sealant was used with the top (emitting) array of transducers and their positions relative to the plate could be adjusted. The friction of the Belling-Lee plug and the cable was sufficient to prevent them from moving once in position.

3.9 TRANDUCER DRIVING CIRCUITS AND RELATED CONSIDERATIONS.

Before considering the design of the transducer driving circuits it is necessary to calculate an order of magnitude estimate of the way in which the voltage appearing across the receiving transducers is related to the driving voltage. This calculation is easily accomplished using standard formulas which relate the power output of a transducer to the driving voltage (see for example Hueter and Bolt 1955).

The power (W) radiated by one transducer, when driven by a driving voltage with an R.M.S. value of V_T, is given by the following

approximate equation

$$W \approx 4 \times 10^{-4} V_T^2. \qquad \text{(watts)}$$

Making simplifying assumptions about the transducer polar diagrams (see fig. 3.9), and knowing the separation of the transmitting and receiving arrays of transducers, it is possible to calculate the maximum intensity of sound I_{max} at the receiving array (assuming perfect focussing). This is found to be given by

$$I_{max} \approx 1.2 \times 10^{-4} V_T^2. \qquad \text{(watts cm}^{-2}\text{)}$$

Since the intensity of sound in the image plane is known, the force (F) on the receiving transducers may be calculated and the corresponding signal produced (V_R) can be determined. We find

$$V_R \approx 1.1 \times 10^{-3} V_T.$$

The design of the driving circuits and of the circuits which amplify and detect the signals from the receiving transducers are related. Clearly the larger V_T is the smaller the gain of the amplifying and detecting circuits needs to be.

A circuit diagram of the driving stage is shown in Appendix 5. The maximum voltage V_T available from this circuit was approximately 35 volts (100 volts peak to peak).

3.10 DESIGN CONSIDERATIONS FOR THE TANK

The general appearance of the tank can be seen in fig 3.3 and fig 3.11 is a schematic diagram showing the essential features and dimensions. The parts of the tank which come into contact with the water were made of stainless steel. As the photograph indicates the tank was supported on three legs, which had adjustable lengths, to facilitate levelling. The tank when full weighed approximately 1200 kg and the laboratory floor was strengthened to support this weight.

There are a number of design variables which determine the dimensions of the tank. These will be considered in more detail in chapter 5. It will suffice here to say that the length of the tank is determined by,

(1) the field of view of the instrument,

(2) the ratio of the diameter of the antenna array to the diameter of the emitting array of transducers,

(3) the ratio of the radio wavelength to the acoustic wavelength,

(4) the diameter of the receiving transducer array.

With the values chosen for these quantities the required length of the tank was 1.65 metres.

If the walls of the tank had been perfect absorbers of acoustic energy then the diameter would need to be no larger than the size of the largest transducer array. However the metal parts of the tank are very good reflectors and it is necessary to ensure that unwanted reflections do not interfere with the acoustic image.

Schematic diagram of the image-forming tank
(not to scale)

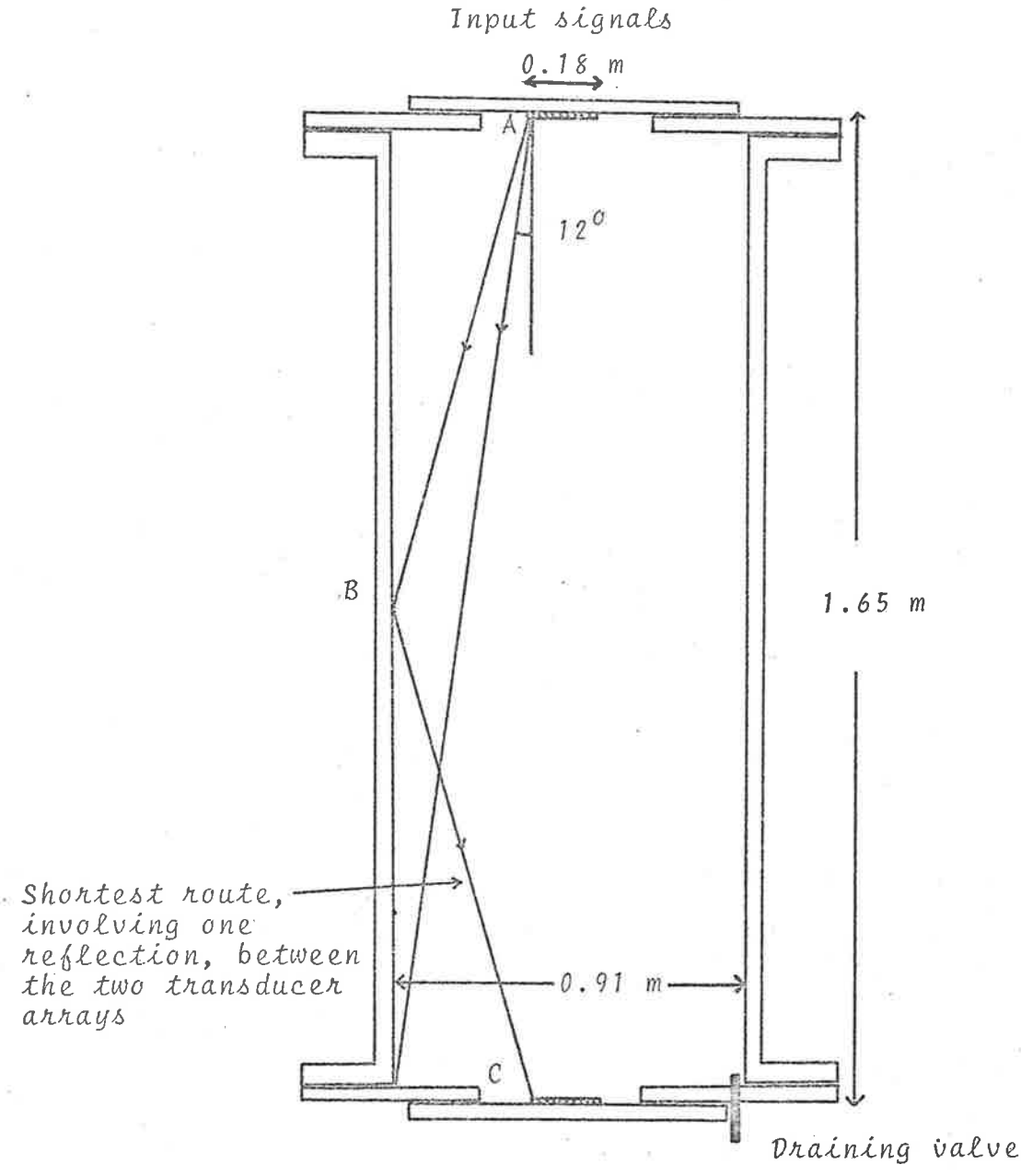

Fig.3.11

The problem of examining all possible reflections and determining what effect they will have is complex, and will not be dealt with in detail here. However the following arguments will suffice to show that unwanted reflections do not degrade the system.

Two types of reflections occur within the tank and these will be considered separately in two categories:

(1) reflections between the top and bottom of the tank,

(2) reflections from the curved sides of the tank.

A signal from the emitting array of transducers will always undergo a reflection of type (1). If a monitor transducer in the receiving array is used to detect signals from the emitting array, then the first signal to be detected is the direct pulse which will be delayed by approximately 1.2 m seconds, because it has to travel through the 1.65 metres of water that separate the two arrays. If there are no wall reflections then the next signal to be detected will occur approximately 2.4 m seconds later, and will be caused by the direct pulse being reflected up to the top of the tank and back again. Usually one, and very occasionally two of these types of reflections are observed (see fig. 3.12). Clearly reflections of this type will not interfere except for pulses with extremely long durations. However they do prevent the system from being used in a continuous mode, such as would be required for normal use in radio astronomy. By using the pulsed local oscillator, a continuous input at the antennas can be converted into pulsed signals and with this modification the system can be used for radio astronomy.

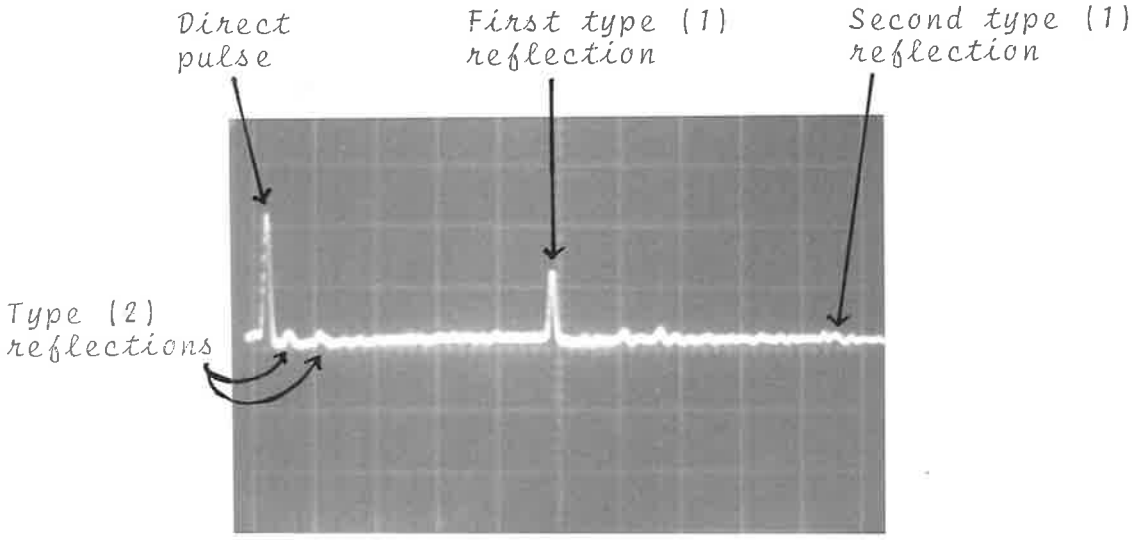

(Sweep speed 500 μseconds division^{-1}
Vertical scale 2 volts division^{-1}.)

Photograph shows the typical appearance of the amplified and detected output of a receiving transducer when all the emitting transducers are being driven by signals of the same amplitude and phase. This condition simulates the effect of a plane wave incident on the antenna array from the zenith.

Fig. 3.12

It should be noted that reflections of type (1) are difficult and probably impossible to eliminate, because, even if the material of the tank were perfectly absorbing, reflections will occur between the two arrays of transducers, which can not be made of a non reflecting material.

Reflections of type (2) (wall reflection) will only occur if the emitting array of transducers is transmitting at an angle of greater than 12° (see fig. 3.11). Since the first null of the polar diagram of the transducers does not occur until approximately 24°, then it is clear that reflections of this type are to be expected.

Fig. 3.13 is a photograph of an oscilloscope display illustrating the appearance of the signal received by a transducer when a single transducer in the emitting array is used as a transmitter. The photograph shows quite clearly the direct signal which is followed by a wall reflection, which has a complicated structure because the resultant signal is contributed to by reflections from different parts of the curved walls of the tank. The delay between reception of the direct pulse and the echo is seen to be slightly greater than 100 μseconds. This indicates that the signal has taken the shortest possible route, involving one wall reflection, to the receiving transducer. This is the route ABC shown on fig. 3.11. Other wall reflections with larger delays do occur but are not shown here.

At first sight, from this argument, it would seem that the maximum duration for a signal that can be used as an input to the system is approximately 100 μseconds. However, if the problem is to be

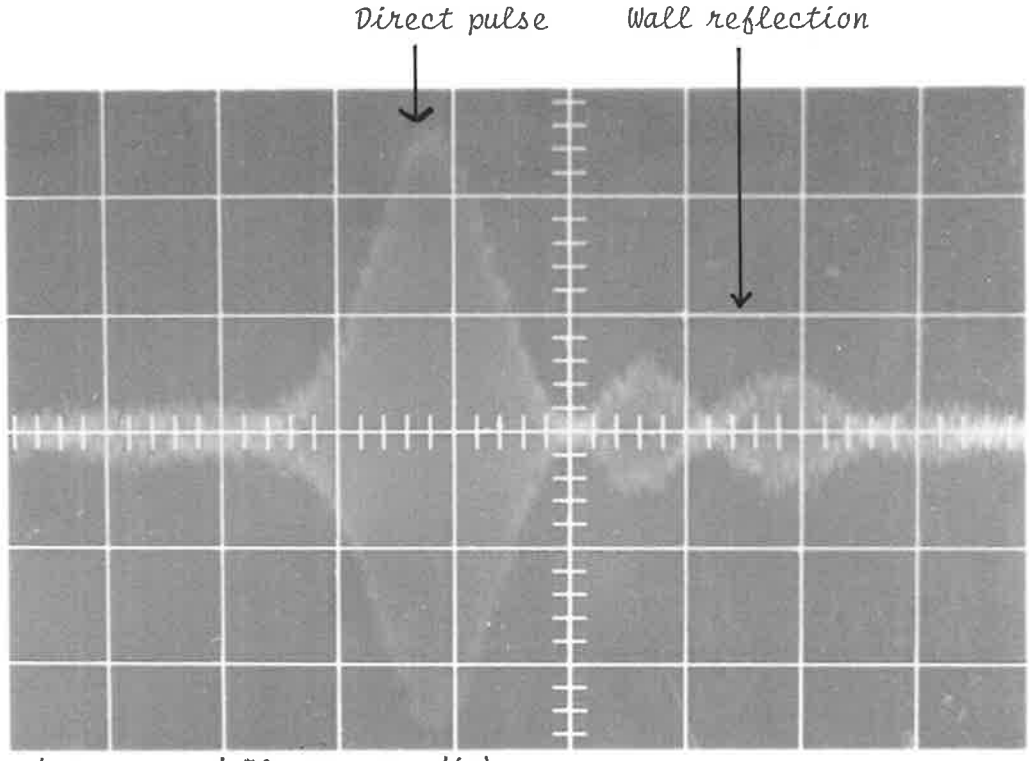

(sweep speed 50 μsec per div)

Photograph of an oscilloscope trace showing the direct pulse and a wall reflection. The emitting transducer in this case is being driven by a signal with the maximum available amplitude, thus the photograph gives some indication of the noise level in the system. When all 89 emitting transducers are being used then the signal to noise level is much improved.

Fig. 3.13

treated realistically, it is the polar diagram of the entire emitting array of transducers that must be considered when determining the effect of type (2) echoes, and not simply the polar diagram of a single transducer. Thus it is appropriate to examine the amplitude polar diagram of the emitting transducer array. Fig. 3.14 is a schematic representation of this pattern in polar coordinates. This figure has been calculated assuming that each transducer is driven by a signal of the same amplitude and phase. (The computer program used for the calculations required in the production of fig. 3.14 is discussed briefly in chapter 5.) It can be seen that grating sidelobes of the transducer array will give rise to wall reflections. The minimum delay between the direct pulse and these wall reflections can be calculated (from the geometry of the situation) and is found to be approximately 160 μseconds. If plane wave radio signals are incident on the antenna array from directions other than the zenith then the new beam pattern is obtained by roatating the pattern shown in fig. 3.14. For example, a plane wave incident on the array from a direction which make an angle of 28° with the zenith, will produce a pattern similar to that shown except that it is rotated through approximately 3° so that the main lobe intersects the bottom of the tank at the edge of the transducer receiving array.

Fig 3.12 shows that in practice two wall reflections are observed and that the delay between the wanted signal and the first wall reflection is approximately 200μseconds. The amplitude of the wall reflections relative to the wanted signal can also be determined

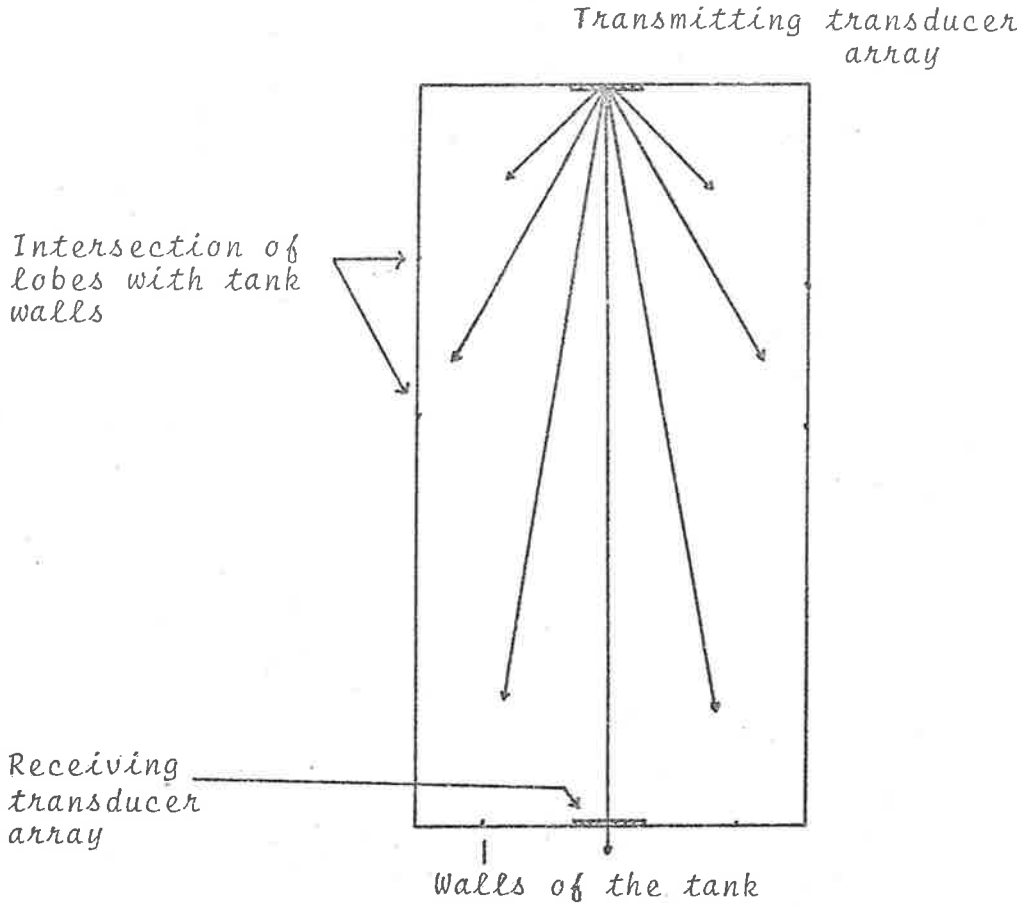

Polar diagram of the directivity pattern of the transducer array. The arrows show the directions in which the main lobe and the grating side lobes occur. The structure of these lobes cannot be shown on this scale, however the length of the arrow represents the relative amplitude of the signal emitted in the indicated direction.

Fig. 3.14

from this figure and it can be seen that they are small compared with the wanted signal. From this discussion the following conclusions can be made.

(1) Provided the input pulses have a duration of less than approximately 160 μseconds, then there will be no interference between the wanted signals and wall reflections.

(2) If the duration of the input pulses exceeds 160 μseconds then wall reflections will interfere with the wanted signal and small errors in amplitude may result. It should be possible to reduce the amplitude of the wall reflections by roughening the walls of the tank or using baffles perpendicular to the tank walls. These may prove desirable if the instrument is to be used for radio astronomy. However for the experiments described here these modifications have not proved necessary.

3.11 AMPLIFIERS AND DETECTORS

The purpose of these circuits was to amplify and detect the signals produced by the transducers which sample the acoustic image. The output obtained then provides the input for one of the sets of post-detector circuits (see section 3.7). To avoid loading the transducers, the circuit was designed to have a high input impedance and to compensate for the fact that not all the transducers had the same efficiency, the gains of the circuits were made variable in the range 0-40 db.

3.12 THE RECORDING SYSTEM

The modulus of the complex amplitude of the diffraction pattern and of the focussed image were recorded photographically using a 16 mm (VINTEN) ciné camera. Films were usually exposed at the rate of 4 frames sec^{-1} although exposure rates of 2 and 1 frames per second were also possible. The usual "play back rate" was 16 frames sec^{-1} representing a "speed up" factor of four.

The amplitude of the voltages of either the receivers or the amplifying and detecting circuits could be digitised and stored on magnetic tape as a sequence of 89 six bit numbers. To do this a 100 channel digitiser (eleven spare channels) was used. The sequence of 100 numbers from the digitiser was recorded by an incremental magnetic tape recorder approximately five times per second. The data flow was interrupted every 10 seconds and an end of record pulse and the time from a crystal clock were recorded.

Most of the results analysed in this thesis will be photographic records although some examples of contour plots made from the magnetic tape records will be shown.

CHAPTER 4

THE SETTING UP PROCEDURE

4.1 INTRODUCTION

This chapter outlines the procedure that has been used to adjust the positions of the transmitting transducers so that they produce signals with the correct phases in the image plane.

4.2 THE PROBLEM

The signals available to an experimenter in the central laboratory have the same phases and amplitudes (to within 6 db) as the signals received by the dipoles. However, before these signals are applied to the emitting transducers they pass through the attenuators, the r.f. stages of the receivers and the transducer driving circuits. It is important that the driving signals should have the correct relative phases and considerable effort was directed into measuring the phase characteristics of all of these units. It was found that the attenuators introduced a small variable phase error (up to $\sim 5^{o}$) which depended on the level of attenuation.

As far as the receivers were concerned it was found that if a pair of receivers had a common signal applied to their inputs then the phase difference between the two intermediate frequency output signals could be as large as 50^{o} (even larger if the receivers were not properly tuned). This phase difference was found to vary with temperature but under normal operating conditions it was stable and showed no detectable drift (i.e. less than $\sim 3^{o}$) over periods of several days. The temperature

dependance of the receivers was such that for a typical pair, a temperature difference of 20^{o}, would give rise to a phase change of 20^{o}(angle) between the output signals.In practice the receivers were all operated at close to the same temperature and any phase changes due to temperature variations were approximately the same for all receivers.

The transducer driving circuits, when properly tuned, introduced no phase errors.

Thus the driving signals at the intermediate frequency had large phase errors which were stable except for a small variable component introduced by the attenuators. The stable part of this error could have been compensated for electronically but it was found to be more convenient to make the adjustment mechanically by altering the positions of the emitting transducers so that the signals in the image plane were of the correct phase. The method used to accomplish this is described in the next section.

4.3 THE PROCEDURE

(1) Using a surface guage the transducer positions are adjusted so that they lie on part of the surface of a sphere which has a radius of curvature equal to the depth of the tank (1.65 metres).

(2) A continuous wave signal at 2 MHz is fed into the inputs of the receivers using the simple matching network shown in fig. 4.1. Under these conditions all receivers have at their inputs, signals with the same amplitude and phase. Thus the arrangement simulates the effect of a plane wave, incident from the zenith, on the antenna array.

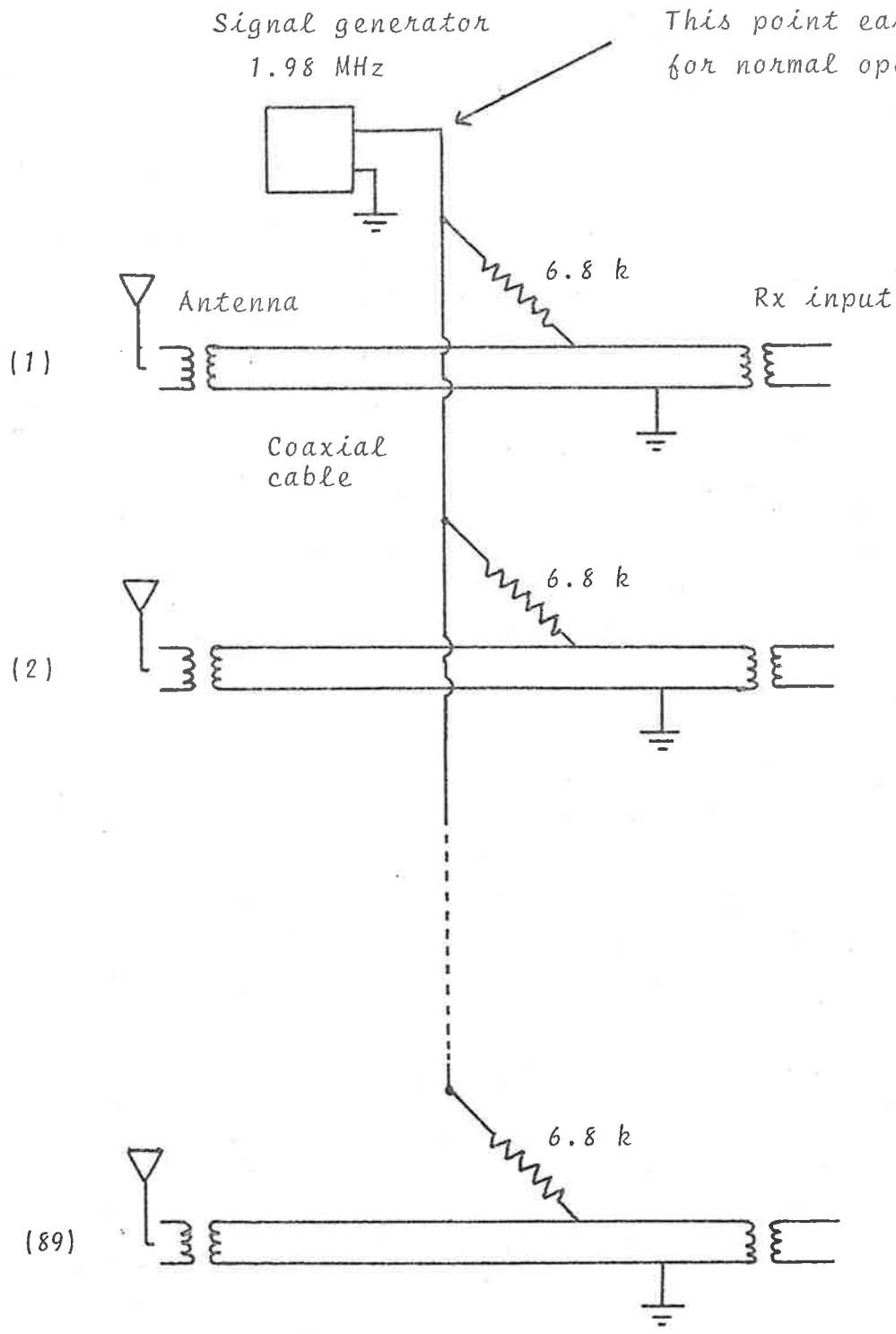

Matching Network for a
simulated plane wave input

Fig.4.1

(3) The local oscillator is switched to operate in the pulsed mode and adjusted so that the I.F. outputs of the receivers consist of approximately Gaussian envelopes and with durations of approximately 50 μsecs. These signals, after passing through the transducer driving circuits, are available for driving the appropriate emitting transducers.

(4) One particular transducer is selected (referred to from now on as the reference transducer) and its position is adjusted so that signals leaving it arrive at the centre transducer in the receiving array approximately 25 μsecs ahead of pulses from the other transducers. (A 50 μsec pulse of ultrasound in water is approximately 7 cm long, and therefore the radiating face of the reference transducer is approximately 3.5 cm in front of the other transducers.) The driving signal for the reference transducer is now applied and the signal received by the centre receiving transducer is monitored.

(5) An arbitrary transducer is selected and the appropriate driving signal is applied to it. The position of this transducer is adjusted until the monitored signal indicates that there is a phase difference of 180° between the two signals, at the position of the centre receiving transducer. Fig. 4.2 shows the appearance of the interference of two Gaussian shaped pulses which are displaced relative to each other and with the phases of their carrier signals differing by 180°. A sharp null will always be observed even though the amplitudes of the two pulses may be different. It was found to be more accurate to adjust the positions of the transducers to obtain a null than to adjust for a maximum. Using this method it is estimated

The interference between two Gaussian shaped pulses

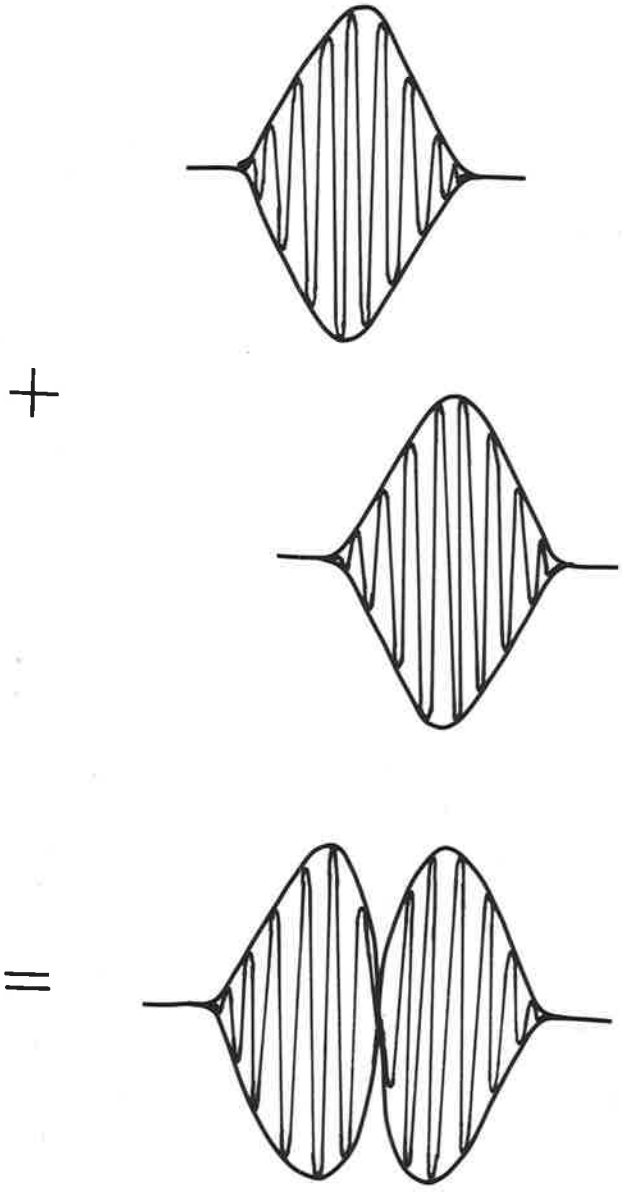

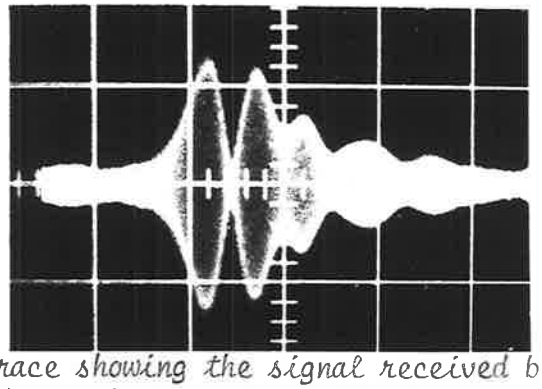

(sweep speed 100 usec. per div.)

Oscilloscope trace showing the signal received by the centre receiver transducer when the two emitted signals are out of phase by 180^{o}.

Fig. 4.2

that the resultant phase errors, which arise from errors in the positions of the emitting transducers, are less than 10^{o}.

(6) The remaining 87 transducers are now adjusted, individually, using this same method.

(7) Finally the reference transducer is repositioned and adjusted so that the signal from it interferes constructively (at the monitor transducer), with the signals from any one of the other 88 transducers.

4.4 COMMENTS AND CONCLUSIONS

The procedure described above is a fairly quick and effective method of"setting up" the image-former. It has the advantage that any constant phase error, that may be introduced by either the attenuators, the receivers or the transducer drivers, is compensated for. In addition, the matching network, which provides the simulated plane wave input, enables a rapid and convenient check to be made on the performance of the system. For example, to perform this check all that is required is that a continuous signal, at 2 MHz, be applied at the point shown in fig. 4.1. The input to the receivers is now the same as it would be if a continuous plane wave signal were incident on the antenna array from the zenith. The output of the receivers can be converted to a pulsed form by using the pulsed local oscillator and the acoustic image formed should have a maximum at the centre of the receiving array of transducers. This can be checked either visually, by looking at the light emitting diode display, or directly, by using an oscilloscope to measure the outputs of the receiving transducers. The whole pro-

cedure is simple and takes less than 5 minutes to perform.

Several other methods of comparing the phases from the transducers were tried. It was concluded that the method described was the most accurate and convenient for this particular problem.

CHAPTER 5

THEORY AND EVALUATION OF PERFORMANCE.

5.1 INTRODUCTION

The purpose of this chapter is to examine in more detail the principle of operation of the image-forming system. From these considerations it will be possible to derive an expression relating the angle of arrival of a radio wave, (measured from the zenith) and the position in the image plane of the corresponding acoustic image. Further, a computer model which simulates the action of the acoustic part of the system will be described. This model will be used to evaluate theoretically the effect that various errors could have on the overall performance of the system. Many workers, including Rayleigh (1879), Ruze (1952), Elliot (1958), Li (1959) and Bracewell (1961b), have studied the effects that errors in phase and amplitude have on the polar diagrams of antenna arrays, microwave focussing systems and optical devices. Although the principles involved in these studies are similar to those considered here it is not possible to use this earlier work directly, and a rather specialised approach to the problem has to be made.

5.2 DETERMINATION OF THE ANGLE OF ARRIVAL FROM THE ACOUSTIC IMAGE

Fig 5.1 is a schematic representation of a one dimensional system which converts radio waves into similar acoustic waves.

Schematic diagram for determining the relationship between Θ and Θ'.

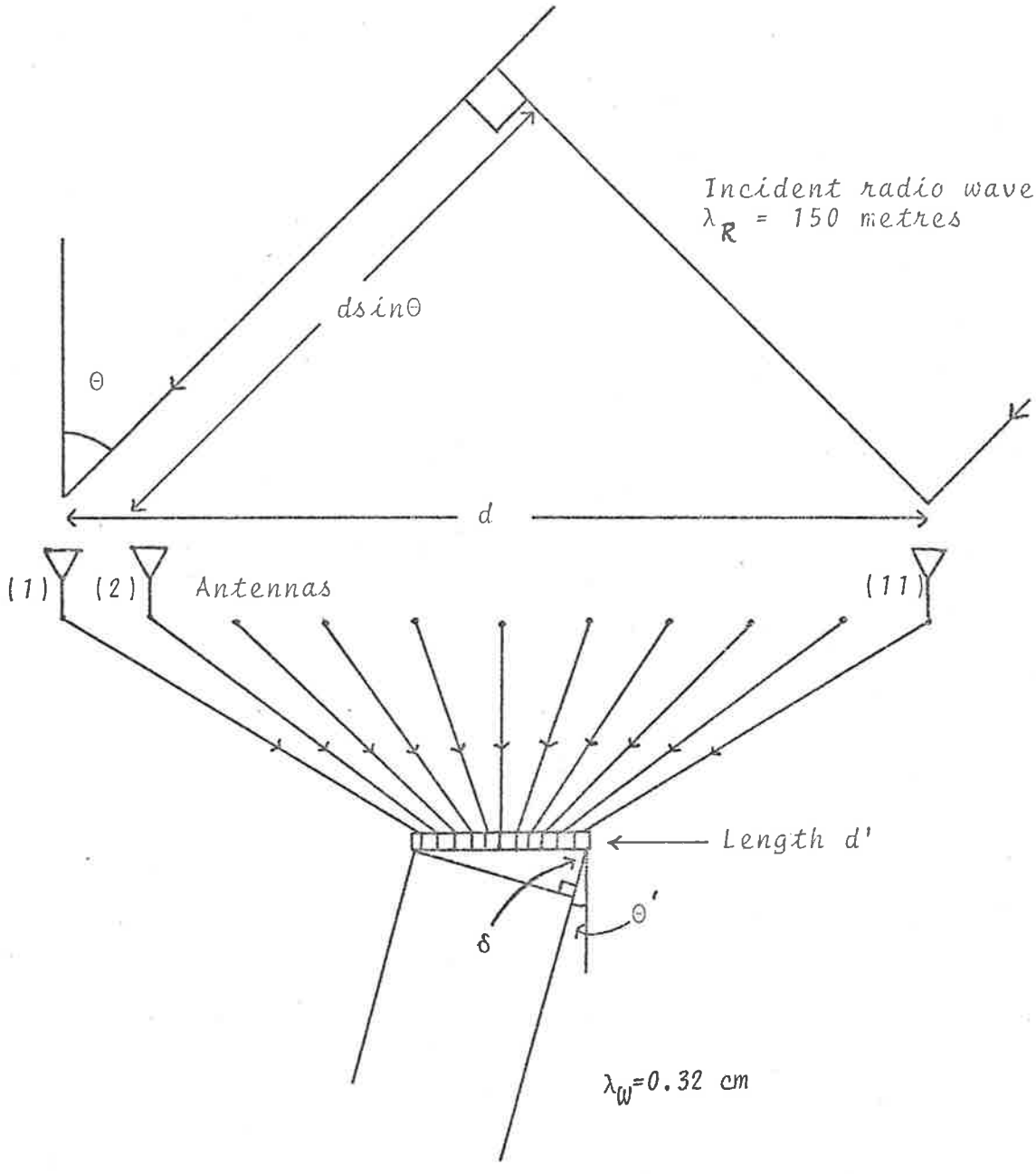

Image plane

Fig. 5.1

The signal received by antenna (1) lags in phase the signal received on antenna (2) by ϕ radians where,

$$\phi = \frac{2\pi d \sin\theta}{\lambda_R} \qquad 5.1$$

and d = length of the antenna array,

λ_R = radio wave length,

θ = angle of arrival of radio waves.

Therefore the signal emitted by transducer (1) lags in phase the signal emitted from transducer (11) by the same amount. With this knowledge, it can be seen that the length δ (see diagram) is given by

$$\delta = \frac{d \sin\theta \lambda_W}{\lambda_R} \qquad 5.2$$

where λ_W = wavelength of the acoustic waves in water.

Using equation 5.2 it is possible to calculate θ', the angle at which the acoustic plane wave is emitted from the transducer array (see fig. 5.1). It can be seen that θ' is given by the expression

$$\theta' = \arcsin \left\{ \frac{d\lambda_W \sin\theta}{d'\lambda_R} \right\} \qquad 5.3$$

where d' = length of the acoustic array.

The quantity $\left\{ \frac{d\lambda_W}{d'\lambda_R} \right\}$ will be called a scaling factor.

Substituting values for d, d', λ_W and λ_R for the instrument actually constructed (namely d = 1 km, d' = 18 cm, λ_W = 0.32 cm, λ_R = 150 metres

or 50 metres depending on the operating frequency) we find that

$$\theta' = \arcsin \{ 0.119 \sin\theta \} \qquad \text{for 2 MHz}$$

or

$$\theta' = \arcsin \{ 0.357 \sin\theta \} \qquad \text{for 6 MHz}$$

Equation 5.3 indicates that if a 2 MHz plane radio wave is incident on the antenna array at 15° then it will be converted into a similar acoustic wave leaving the transducer array at an angle $\theta' = 3.2°$. By adjusting the transducer positions so that they lie on part of the surface of a sphere a focussing effect is produced which is equivalent to using an acoustic lens. If the radius of curvature is R then radio waves arriving at an angle θ will produce an acoustic image having a maximum in intensity at a point, displaced a distance x, from the centre of the image plane, where x is given by

$$x = R\tan\theta' \qquad 5.4$$

Equation 5.3 can also be used as the basis for further discussion. For example, as we have already seen, the angle θ' at which the acoustic plane wave is emitted from the array will not be the same as θ (the angle of arrival of the incident radio waves); i.e. there is a scaling factor involved which depends on d', λ_W, d and λ_R. From a general point of view all these quantities are variable but for the particular experiment described here λ_W, d and λ_R are fixed and only the quantity d' is a design variable. If d' could be made small enough then the acoustic array could be made so that it exactly modelled the antenna array i.e. the acoustic array would have a length to wavelength

ratio the same as the antenna array. In this case the scaling factor would be one. However in practice this would be difficult to achieve because it would require very small transducers spaced very closely together. In fact, to obtain a scaling factor with a value unity, the diameter of the transducer array would have to be approximately 2 cm. In any case there is no advantage to be gained in doing this.

It can be seen from fig. 5.1, that for a given value of d', the field of view of the instrument will depend on the size of the receiving transducer array and the distance of this from the emitting array. For the instrument actually constructed the field of view was determined by the anticipated ionospheric conditions and for convenience it was decided that both the emitting and receiving arrays should be of the same size. Thus the separation of the transducer arrays is determined and hence the focal length of the emitting array is also fixed and this fixes the length of the tank. If either one of the arrays can be moved, in the horizontal plane, as is the case with the present equipment, then although the angle of view cannot be changed, the actual field of view can be varied. In other words the centre of the field of view does not have to be directed towards the zenith.

One further point that can be made is that in the conversion of the acoustic image into a useful form, care must be taken to ensure that the image is sampled on a fine enough grid so that no information is lost. The density of sampling with the present equipment is best seen by referring to fig. 5.7. From this figure it would seem that a cross section of the peak in the acoustic image is sampled by three

transducers, but in fact the instrument is two dimensional and a total of five transducers are actually used to sample each peak in the image.

At this point it is relevant to mention that at 2 MHz the resolving power of the instrument which is determined by the beam width of the antenna array is approximately 9° and the field of view is (normally) ± 28° from the zenith. Thus there are approximately 27 independent image points which is the same as saying that the instrument measures the angular spectrum in 27 independent directions. If the system is operated on 6 MHz, then although the resolving power is improved by a factor of 3, the field of view is correspondingly decreased. This occurs because the scaling factor (see equation 5.3) is changed by the decrease in the value of λ_R, which occurs in changing to the higher frequency.

5.3 THE COMPUTER MODEL

The operation of the acoustic stage of the image-forming system can be simulated using a computer program, and this provides a convenient method of testing the effects that various imperfections (e.g. errors in phase and amplitude imposed by practical considerations) will have on the system's performance. It is also helpful to know what tolerances are required in order that a satisfactory performance may be achieved.

The output of the image-forming system is a focussed acoustic image which is formed by the interference between the signals emitted by 89 piezo-electric transducers, which, ideally, lie on part of the surface of a sphere. The phase and amplitude at any point in the image

is calculated by adding together (taking proper account of phase) the contribution due to each transducer. If this calculation is performed a large number of times at a grid of points in the image plane then the form of the acoustic image can be studied. Fig. 5.2 illustrates the geometry of the problem. Two planes, parallel to one another and separated by a distance equal to the focal length of the system, are defined. The top plane is divided into an 11 x 11 grid, each point of which has coordinates (x_l, y_m). These points represent the positions of the emitting transducers before they have been adjusted to lie on the focussing surface. On the second plane, another, more closely spaced grid of points is defined. These have coordinates (x_i, y_j) and are the points at which the acoustic image is to be calculated. The positions of the points in the grid on the upper plane are now displaced vertically by different amounts so that the points lie on part of the surface of the focussing sphere.

It is now a straight forward, but messy, geometrical problem to calculate the distances from each point on the upper surface to each point in the lower plane. For the actual instrument a total of 89^2 such distances are involved, but for the computer model the number of grid points in the upper and lower surfaces are 121 and 441 respectively. Therefore the number of distances actually calculated is much larger (53,361). The distance between the point (x_l, y_m) and (x_i, y_j) will be represented by the symbol r_{ij}^{lm}.

Having described the geometry of the situation it is now possible to write down a formula for the quantity that is actually

Schematic diagram showing the geometry for the computer model

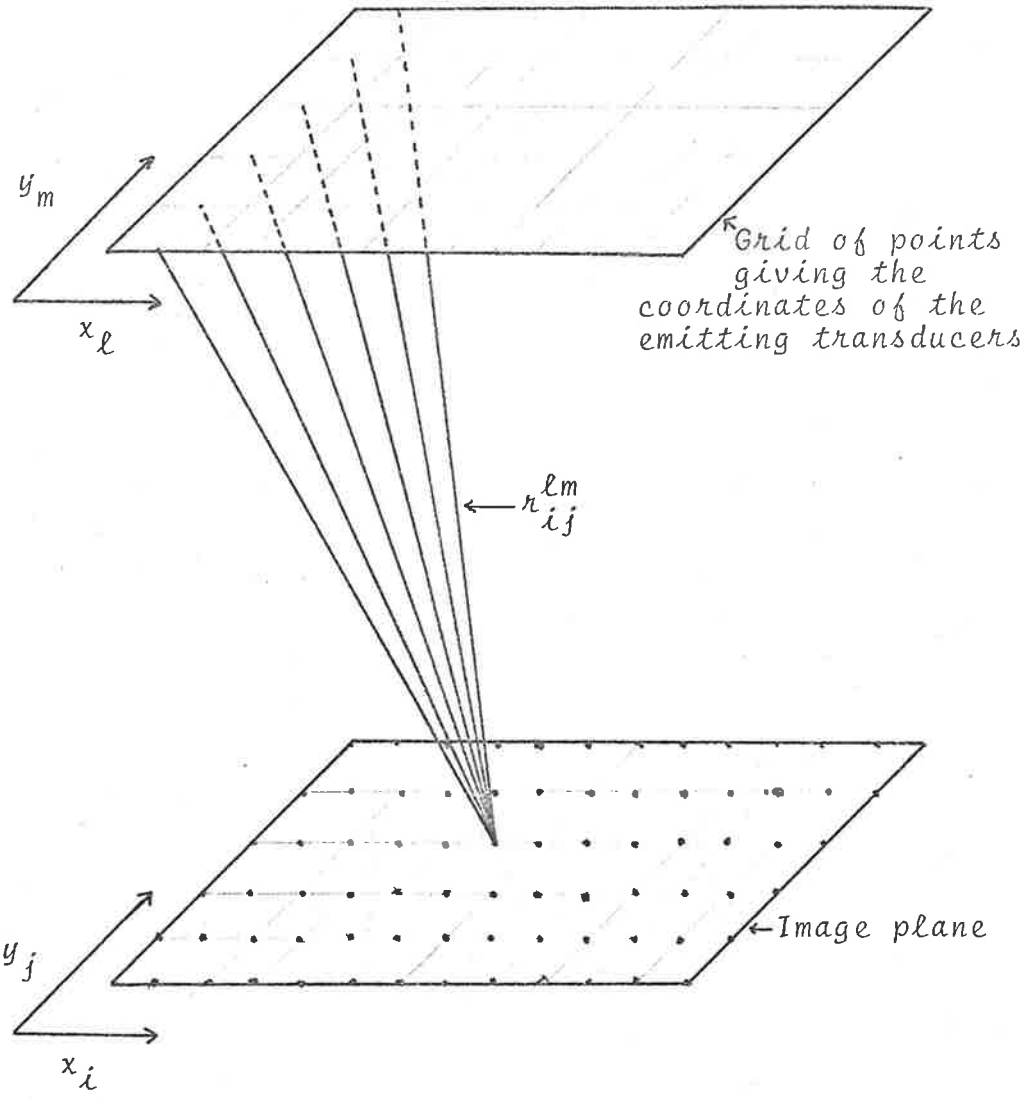

Note (1) Not all the distances required for the calculation of the image at the indicated point are shown.

(2) The curvature of the emitting points is not shown.

(3) Some of the grid points in the upper plane do not correspond to transducer positions. In the model these points emit signals with zero amplitude.

Fig. 5.2

calculated in the image plane. This is as follows

$$F(x_i, y_j) = \sum_{\ell=1}^{n} \sum_{m=1}^{n} A(x_\ell, y_m) \exp \left\{ \frac{2\pi i \, r_{ij}^{\ell m}}{\lambda_w} \right\}, \qquad 5.5$$

where $F(x_i, y_j)$ = a complex function representing the phase and amplitude of the acoustic image,

$A(x_\ell, y_m)$ = a real function describing the amplitude of the signal from each transducer,

and the other quantities have already been defined. (Note for certain grid points, $A(x_1, y_m)$ is set equal to zero). Calculations of this type are easily undertaken using a digital computer. Further terms can be introduced into 5.5 to take into account the beam patterns of the individual transducers. Also changes to the model can be introduced to simulate errors in the positions of the transducers. These result in a more complicated equation which will not be written down here.

The equation 5.5 and fig. 5.2 allow an interesting comparison to be made between a conventional phased array and an acoustic image-forming system. It will be recalled that to direct the beam of a phased array in a given direction a certain combination of phase or delay networks must be used to introduce phase shifts into the signals from each antenna before the summing network. For the image-forming system a given point in the image plane corresponds to signals arriving from a given direction, thus there is an obvious analogy between the distances r_{ij}^{lm} which are introduced by geometrical factors in an image-forming system and the phase or delay networks usedby a phased array.

In practice the calculated image can be displayed in a number of ways. For detailed study it is useful to present the image as a set of numbers arranged in a matrix corresponding to the grid points. The figures may be used to produce cross sectional plots, usually, of the modulus of the complex amplitude of the acoustic image. If less detail is required then contour plots can be drawn. An alternative display method, which has been used here, is to present computer"drawn" density plots. Here ten different "shades of grey" are used to represent the amplitude of the signal at different points in the grid. This type of display provides a representation which is similar to that presented by the photographic records, except that in this case regions of high acoustic amplitude are represented by dark areas. For the photographic records the opposite is true.

5.4 THE EFFECT OF THE TRANSDUCER BEAM PATTERNS

Ideally the transducers should be isotropic sources of acoustic signals, however in chapter 3 it was shown that the experimentally measured polar diagram is closely described by the pattern expected from diffraction theory, and the pattern is therefore not isotropic.

To test the effect of this on the acoustic image the computer program was used to calculate the modulus of the complex amplitude of the acoustic field over the receiving transducer array. It was found that, if a plane wave is incident from the zenith, then the error introduced by the non isotropic transducers is less than 6% within the field of view of the instrument. This was considered to be negligible.

The result is not surprising since the transducers have

polar diagrams that are considerably broader ($\sim 24^{\circ}$) than the angle subtended by the receiving array of transducers at the emitting transducers ($\sim 6.4°$).

All modelling "experiments" referred to from now on include the effect of the non isotropic transducers.

5.5 THE EFFECT OF RANDOM PHASE ERRORS

In chapter 4 it was explained that the positions of the focussing transducers could be adjusted to compensate for any phase errors that might be introduced by the attenuators, the receivers or the transducer drivers. The accuracy with which the transducers can be positioned is such that the resulting phase errors are less than $\pm$ 10°. However in practice, when the system is operating, the attenuator control voltages are allowed to vary and further (variable) phase errors of up to $\pm$ 5° might be introduced. Thus an estimate for the total phase error in the emitted acoustic signals is $\pm$ 15°.

Using the computer program to simulate the system it is possible to determine the effect that errors of this type will have. Fig. 5.3 and 5.4 show cross sectional plots and two dimensional density plots of the acoustic images that would be formed by systems introducing random phase errors of differing amounts. It is important to point out that the errors ($\pm \Delta\phi$) referred to in these diagrams are not rms.errors but are maximum errors. Further, the error distribution function is such that, for a quoted error of $\pm \Delta\phi$, the phase error of the emitted signals can lie anywhere within the range $\pm \Delta\phi$

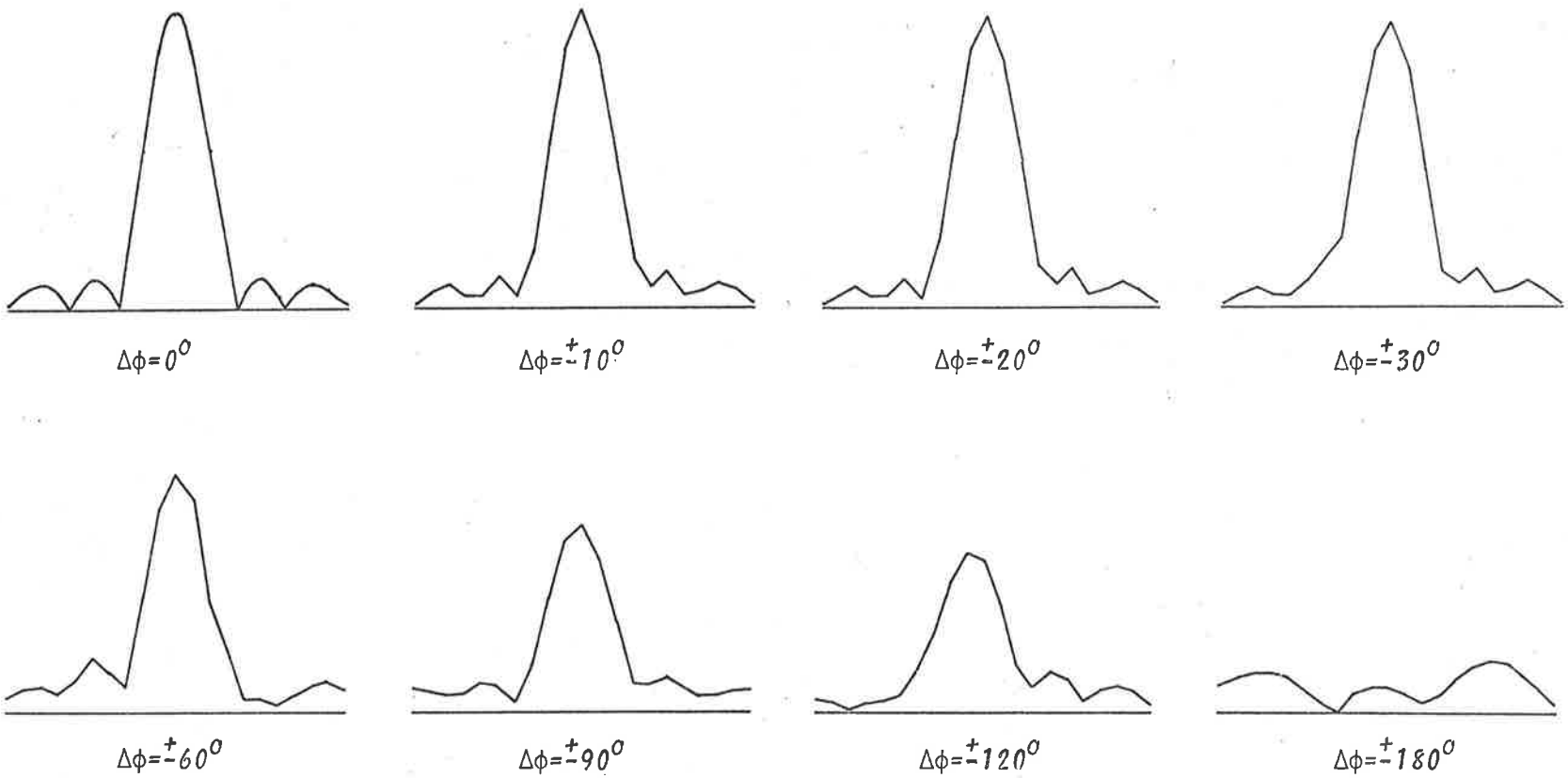

Cross sections of the density plots shown in fig. 5.4

Fig. 5.3

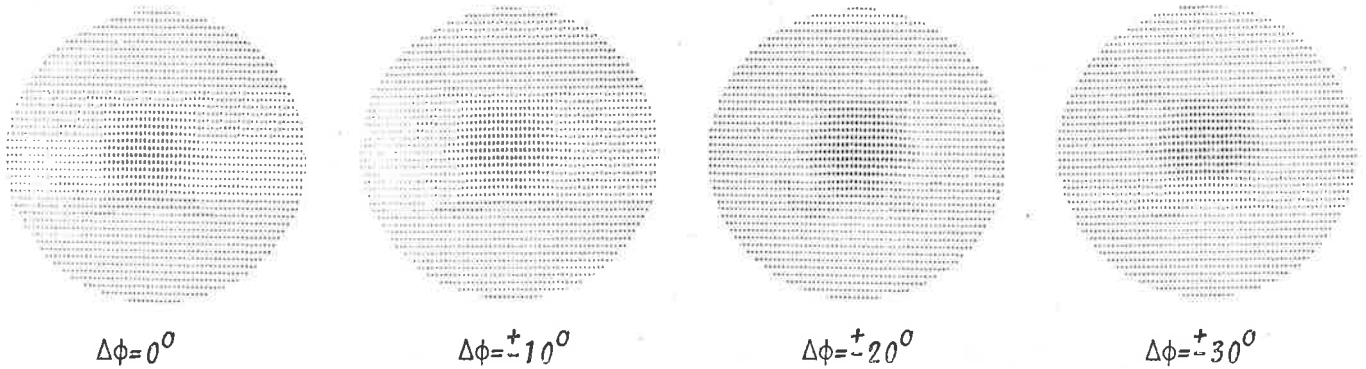

Density plots showing the effect of random phase errors.

Fig. 5.4

with equal probability, however no errors will fall outside this range. The phase errors were generated from a computer library function which produced random uncorrelated numbers. It was appropriate that the phase errors should be uncorrelated because the error in the position of any transducer is independent of the positions of the neighbouring transducer. If the focussing array had been a continuous surface then this would not have been the case.

The density plots show that there is little deterioration in image quality until the phase errors ($\pm \Delta\phi$) are of the order of $\pm 60°$. Note that there is a pointing error of 2.8° for $\Delta\phi = 120°$.

The cross sectional plots depicted in fig. 5.3 show that phase errors also affect the "gain" of the acoustic array. The density plots have been normalized and therefore this effect is not apparent in this form of display.

5.6 THE EFFECT OF RANDOM AMPLITUDE ERRORS

The most important source of this type of error occurs because different transducers have different efficiencies. The histogram in fig. 5.5 shows how the relative efficiencies of the emitting transducers are distributed. The histogram was obtained by driving each transducers in turn with the same signal and monitoring the amplitude received by a single transducer in the receiving array. The relative "emitting efficiency" (x) has then been defined (for this histogram) as the amplitude of the received signal (A) divided by the mean amplitude ($\bar{A}$) of the monitored signals.

Histogram showing the distribution of relative "emitting efficiencies" (x) among a sample of 89 transducers.

Note: 89% of the transducers have efficiencies lying within the range $\bar{x} \pm .5\bar{x}$, where $\bar{x}$ is the mean "emitting efficiency".

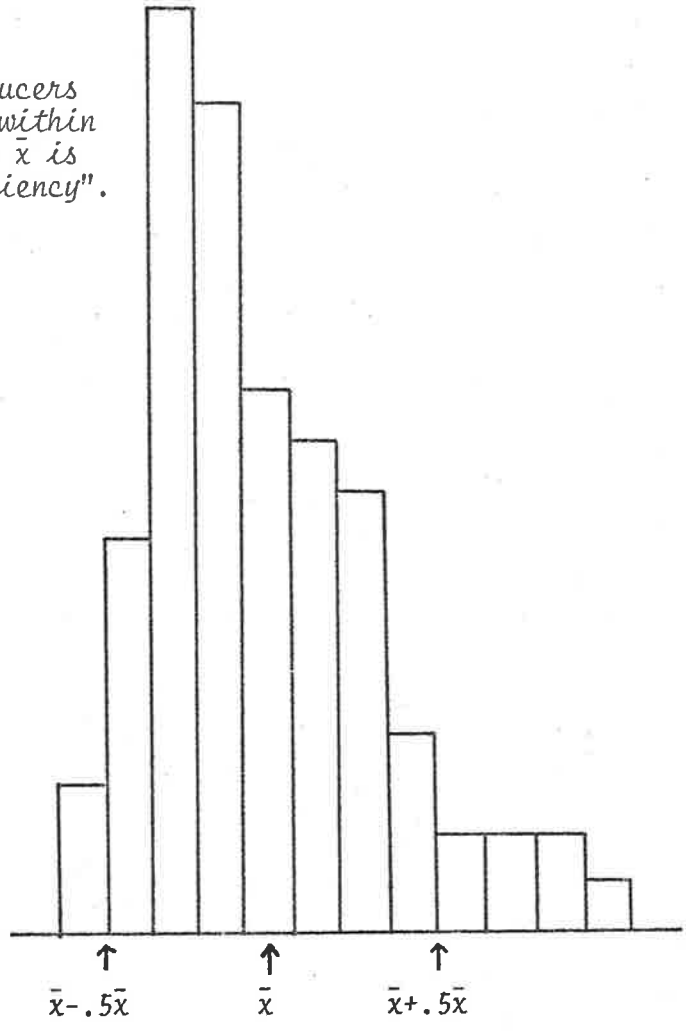

Fig. 5.5

The effect of these errors on the acoustic image is studied in the same way as the effect of phase errors. Fig. 5.6 shows a series of density plots drawn for different amplitude errors, $\pm \Delta A$. Once again, for simplicity, the error distribution function has been chosen so that any error within the range $\bar{A} \pm \Delta A$ has an equal probability of occurring and errors outside this range do not occur. From these plots it can be seen that quite large errors in amplitude can be tolerated. The effect of errors of a slightly different kind, caused by the failure of either a transducer driving circuit or a transducer, were also investigated. In this particular type of failure the emitting transducer emits no signal. The density plots show that this can happen to several transducers without producing any serious deterioration of the acoustic image.

So far in this study we have been concerned with the effect that imperfections in the focussing part of the system may have on the acoustic image but errors are also important in the conversion of the acoustic image into a visible form. It is known that different transducers have different efficiencies and if these differences were not compensated for then serious distortion of the image would result. For this reason the gains of the amplifying and detecting circuits are variable and have been adjusted to allow for the differences between receiving transducers. In order to do this a single transducer is used to radiate to the receiving array and the gains of the amplifying and detecting circuits are adjusted so that they all give the same output.

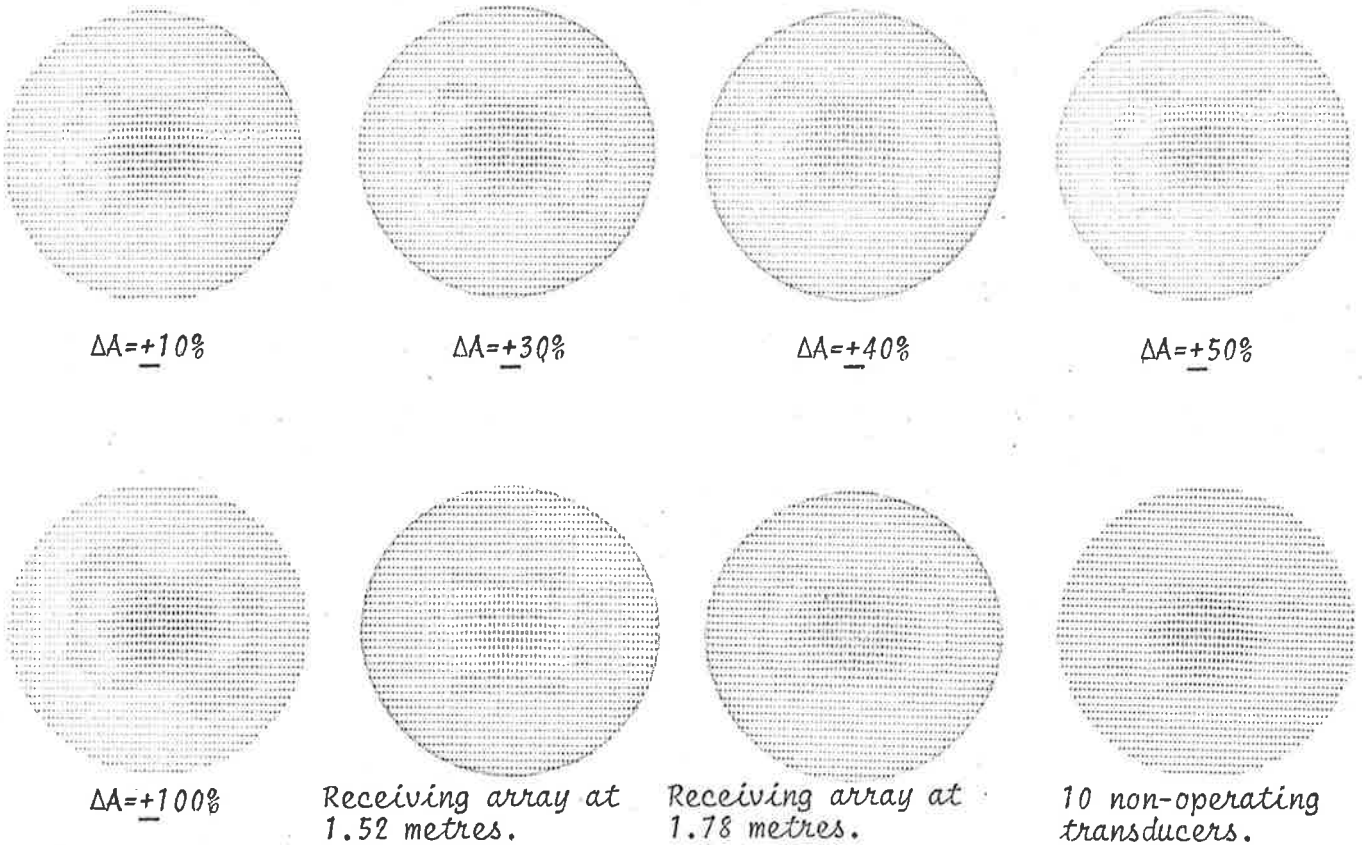

Density plots showing the effect of amplitude errors, errors in the position of the receiving array and the effect of transducer failures.

Fig. 5.6

5.7 THE EFFECT OF DELAYS

The computer assumes a continuous wave input for the system and the effects of internal reflections are ignored. In practice the system is pulsed, and for the acoustic image to be formed, it is necessary that the contributing pulses overlap over a significant portion of their lengths. To check that this occurs a study must be made of the delays introduced by various parts of the system including the feeder cables, the tank and the delay caused by the $d\sin\theta$ component which is characteristic of all phased arrays (see fig. 5.1).

In practice it is difficult to calculate an exact value for the maximum difference in the delay between signals being processed by different channels in the system. However an upper limit can be found by adding together the maximum delays which can occur at each stage. It is found, that provided the angle of arrival of incoming signals does not exceed 28° (from the zenith) then the maximum delay will not exceed 10 μseconds. This is in fact an over-estimate because delays in the acoustic part of the system will partially compensate for the delays that occur in earlier stages.

Thus pulses with durations of 50 μseconds will overlap over approximately 80% of their lengths in the image plane and pulses received by neighbouring antennas in the array will overlap over approximately 98% of their lengths. Therefore no serious degradation of the image should occur from operation in a pulsed mode provided the pulses have durations of not less than say 50 μseconds.

5.8 DEPTH OF FOCUS

The "setting-up" procedure, described in chapter 4, outlines the method by which the focussing transducers are positioned. It is apparent from this description that the transducers are adjusted so that the image plane lies in the same plane as the transducer receiving array. In other words the focal length of the system is adjusted so that the image plane lies in the desired position. Thus since the receiving transducer array automatically lies in the image plane, then from a practical point of view, the depth of focus is not important. Nevertheless it is interesting to examine the quality of the image in planes which are parallel to the image plane but at different distances from the focussing array. Fig. 5.6 shows the appearance of the computer calculated image at 1.52 metres and 1.78 metres from the focussing array; both show some broadening when compared with the ideal image (see fig. 5.4, $\Delta\phi = 0$), which is produced in a plane 1.65 metres from the focussing array.

5.9 DEPTH OF FIELD

The discussion, so far in this chapter, has assumed that the ionosphere is at infinity and that the "best image" will lie in the focal plane of the focussing array. This is equivalent to assuming that a point source of radio waves in the ionosphere will give rise to plane wave fronts incident on the array. If the point source is assumed to be in the E region (height of 100 km) then it is easy to show that the phase errors across the antenna array, which arise from

approximating the actual wave by a plane wave, are of the order of 3°, (even less for the F region) and it has already been shown (section 5.5) that errors of this order have little effect on the image quality. Of course, if the instrument is intended to operate as a two dimensional Fourier transformer, then in order to obtain the angular spectrum of the returned energy, it is theoretically correct for it to be focussed "for infinity" whatever the actual height of the ionosphere may be.

5.10 COMPARISON BETWEEN THEORETICAL AND ACTUAL IMAGES

It is interesting to compare the image obtained by the actual instrument using a simulated plane wave input with that produced by the computer model when proper account has been taken of the errors in phase and amplitude which will exist in the real system.

As an approximation to the real system the simulation program has been used to calculate the image obtained when a plane wave from the zenith is "processed" by an instrument which introduces phase errors of ± 15° and amplitude errors of ±50%. In addition to these errors, random amplitude errors of up to ± 10% have been introduced into the calculated acoustic image to allow for the distortion that may be introduced in the converting the image into either the visible or digitised form. A cross sectional plot of the result is shown in fig. 5.7. Also plotted on the same figure are two sets of points which correspond to direct measurements made of the signals

Graph, showing the theoretically and exprimentally obtained images. The quantity plotted is the normalised modulus of the complex amplitude of the acoustic image.

⊙ North-South

× East-West

• Points calculated from the computer model

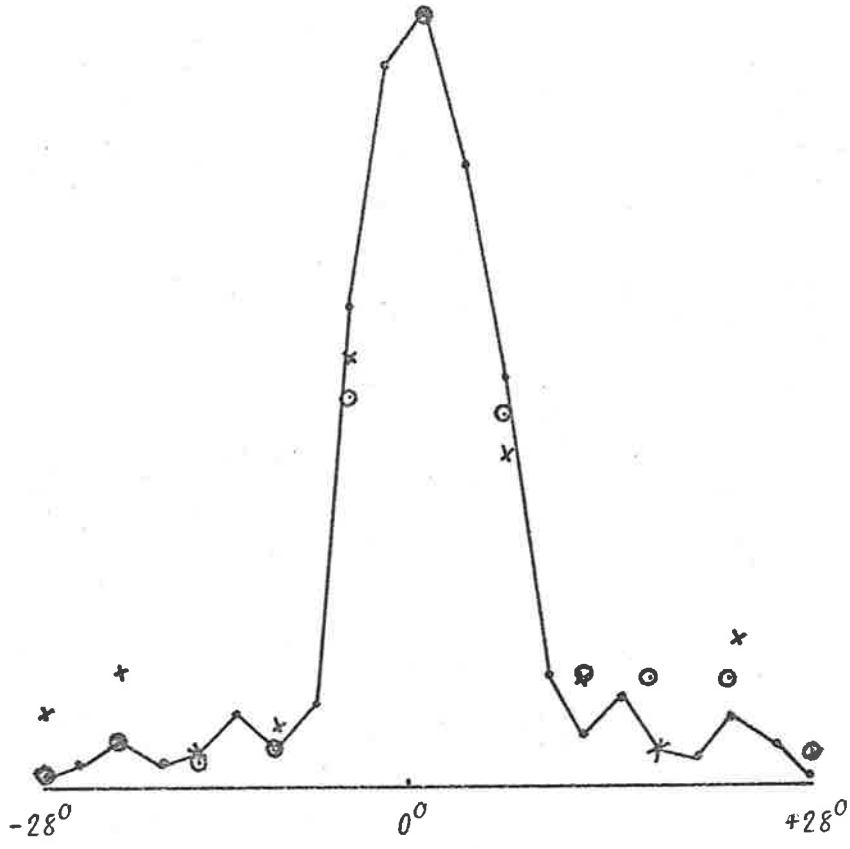

Fig. 5.7

appearing on the transducers in the North-South and East-West rows of the receiving array. At the time these measurements were made the input to the system was an artificial plane wave (see section 4.4).

Fig. 5.8 is a photograph of the light emitting diode display (with and without the diffusing screen) made at the same time.

Finally fig. 5.9 is a microdensitometer trace of the photograph of the light emitting diode display with the diffusing screen in place (see fig. 5.8). The shape of this graph depends on characteristics of the light emitting diodes, the film and the developing process, and it has been presented here for interest rather than for comparison with other plots.

5.11 CONCLUSION

The discussion in the first part of this chapter has shown how the angle of arrival of a radio wave (θ) is related to position of the peak in the corresponding acoustic image. The later part of the chapter has been concerned mainly with discussing the effects that amplitude and phase errors will have on the system. Finally, some data are presented which show that the performance of the system is fairly close to that expected theoretically. In particular the resolving power of the system (beam width to the half power points) is approximately $\pm 4.5°$ and the amplitude of the maximum sidelobes is approximately 14 db. down on amplitude of the main lobe.

Photograph showing the appearance of the light emitting diode display when the input to the system is an artifcial plane wave (see section 4.4)

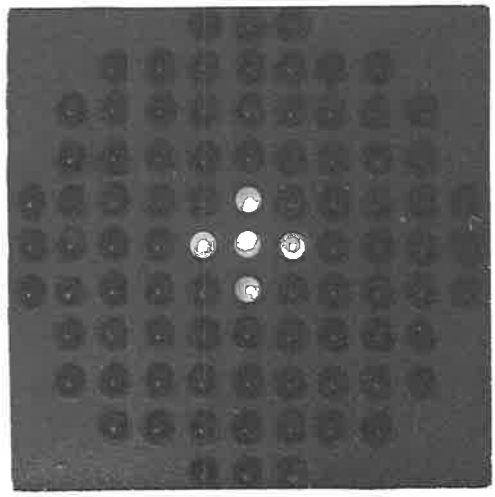

Without the diffusing screen

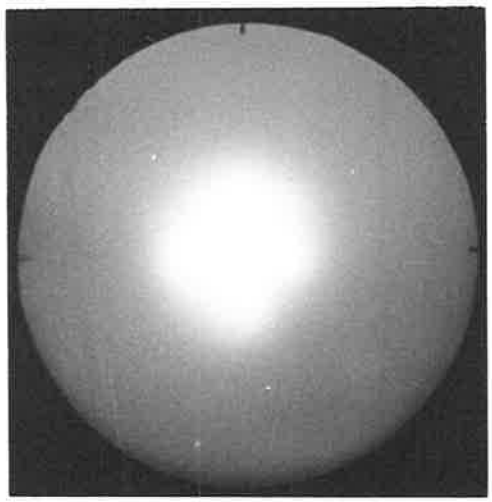

With the diffusing screen

Fig. 5.8

Microdensitometer trace; a cross-section of the diffuse image shown in fig. 5.8

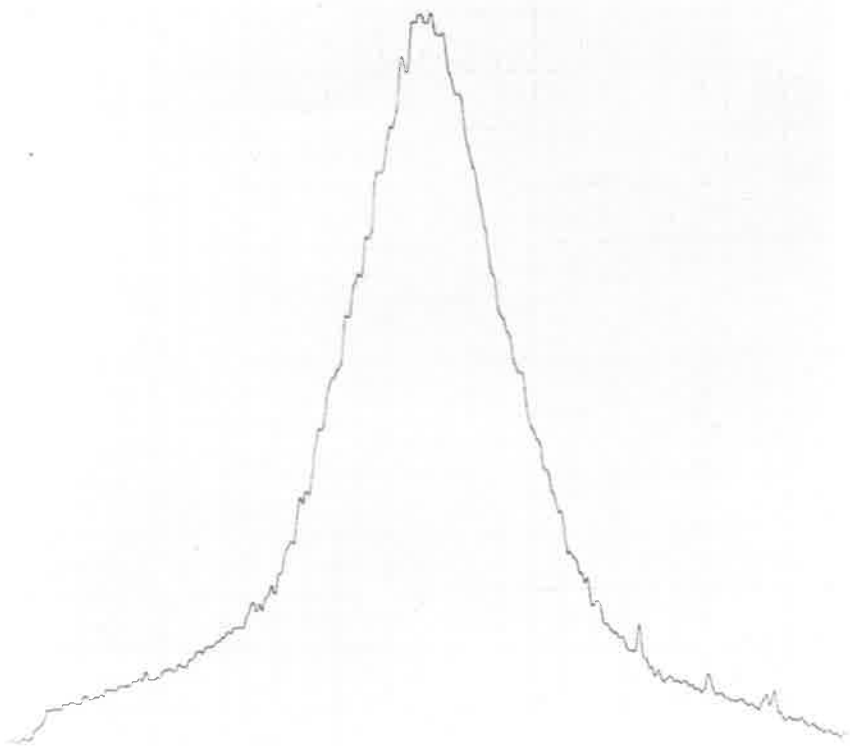

The shape of the graph depends on the type of film used and the developing process. The plot has been presented for interest rather than for comparison with other plots.

Fig. 5.9

CHAPTER 6

MODELS OF THE REFLECTION PROCESS AND SOME RESULTS

6.1 INTRODUCTION

Before discussing the results that have been obtained it is useful to consider in some detail how the data is measured and also to consider some geometrical arguments which may be used to develop an understanding of the relationship between the quantities that are measured and the corresponding ionospheric conditions.

Some computer models of the reflection process will also be considered in this general discussion and it is shown, in section 6.3, that all the different types of diffraction patterns that have been observed can be produced by the interference between a few specularly reflected rays.

In section 6.4 some geometrical arguments, concerned with the focussed image will be presented. Later parts of the chapter (see sections 6.5 and 6.6) will be concerned with an examination of the photographic records which have been made of the different types of diffraction patterns and angular spectra that have been observed.

Finally, in section 6.7, some theory which has been developed for use in oceanography and radar astronomy, will be considered. The arguments presented will be concerned with the theory of specular reflections from random surfaces.

6.2 THE QUANTITIES MEASURED

It has already been explained in chapter 3 that the information obtained from the system relates to the structure of the

diffraction pattern over an area of ground covered by the array and to the form of the angular spectrum of radio waves received from the reflecting layer. This information is recorded in two ways;

(1) in analogue form on 16 mm ciné film (normal photographing rate is four frames per second),

(2) in digital form on magnetic tape.

The photographic records contain information about both the angular spectra and the diffraction pattern. However, with the present experimental arrangement, the magnetic tape records contain information either about the diffraction pattern or the angular spectrum. In most cases the angular spectrum has been recorded.

For the topics that are to be discussed in this thesis it is more convenient to use the photographic records. However to provide some indication of the use that can be made of the magnetic tape records fig.6.1 is presented. This is a set of three different contour plots of the angular spectrum from an E region (100 km) reflection as recorded in digital form, on the magnetic tape recorder. These plots differ only in the number and the range over which the contours are plotted. Fig. 6.1a shows 20 equally spaced levels plotted between 40% and 100% of the maximum amplitude in the image, 6.1b is a similar plot between 20% and 100% of the maximum amplitude, and 6.1c is a plot showing 30 equally spaced levels between 0% and 100% of the maximum amplitude in the image. Much of the structure in this plot (6.1c) is due to the side lobes of the instrument and is not indicative of the true structure of the angular spectrum. The side lobe levels are such that fig. 6.1b is the optimum presentation.

Contour plots of a digitised focussed image output
(E region reflection)

(a)

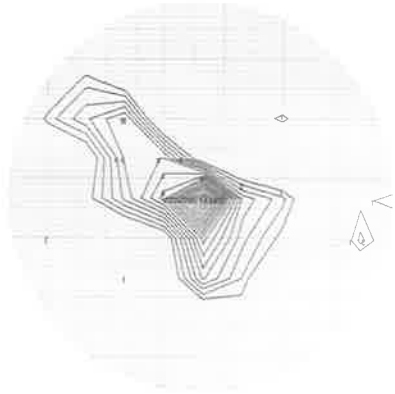

(b)

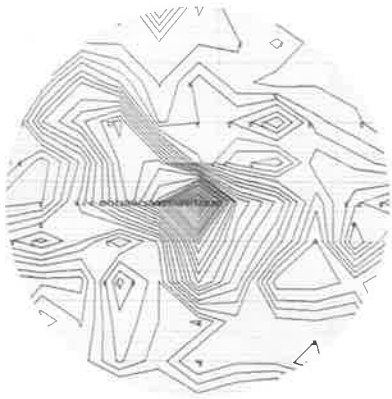

(c)

Fig. 6.1

6.3 PRELIMINARY DISCUSSION (1)-SOME GEOMETRICAL ARGUMENTS CONCERNING THE DIFFRACTION PATTERN.

The arguments considered here refer to the case in which radio waves, totally or partially reflected from the ionosphere, can be considered as having been reflected from a discrete (group) range. Partial reflection processes in which the reflected power is returned from a large volume of space, such as might occur in the case of reflections from the D-region, are not considered.

The term group range is used here in its conventional sense, i.e. if r' is the group range and r is the geometric range then,

$$r' = \int_0^r \mu'(r)\, dr \quad ,$$

where $\mu'(r)$ = the group refractive index of the ionosphere along the ray path.

Fig. 6.2a is a schematic representation of an oscilloscope display referred to as an A-scan. The horizontal axis of the scan refers to time and the vertical axis displays the amplified and detected signal received by a single dipole (used as the receiving element of a fixed frequency ionospheric radar sounder). The first signal received (on the left) is the ground wave and the second is the first reflection from the ionosphere, which will be referred to in this discussion as the echo. If the ionospheric reflection surface (which for practical purposes is a surface of constant electron density) can be considered to be smooth then the reflection will be specular and ray theory can be applied. The ionosphere can be considered to be smooth in the neighbourhood of some point if the deviations of the

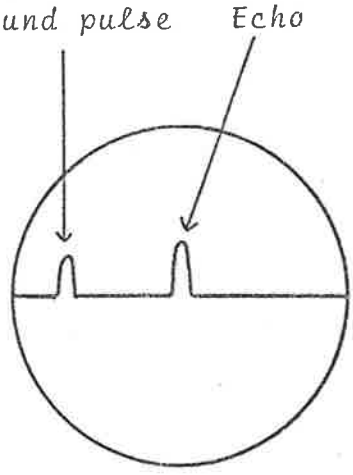

Echoes from a single point or from points at the same range (a)

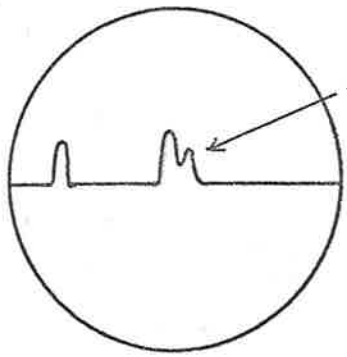

Echoes reflected from different (group)ranges (b)

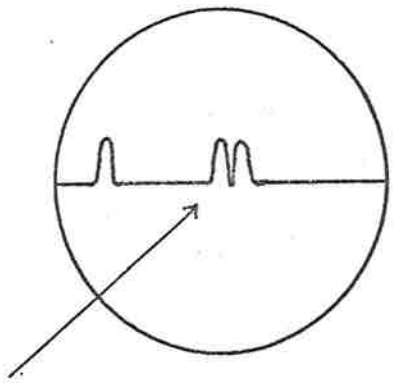

Echoes from two points with (group) range differences greater than $c\tau/2$ (c)

Fig. 6.2

reflecting surface from a tangent plane at that point are very much less than the wavelength of the probing signal (150 metres at 2 MHz). Here the neighbourhood of some point is considered to be an approximately circular region surrounding the point with an area equal to that of the first Fresnel zone. At 2 MHz and at a range of 100 km this is an area approximately 7.7 km in diameter. At 250 km the diameter is approximately 12.2 km. With this "definition" it can be seen that on occasions parts of the ionosphere will give rise to specular reflections while for other parts this approximation will not be appropriate (see chapter 7).

If the transmitter emits a pulse (with duration τ) and this is reflected from a single reflection point in the ionosphere, then the duration of the echo will also be τ. If, however, there are a number of reflection points at different (group) ranges then a series of echoes will be returned each with different delays. This will cause the received echo to be spread as shown in fig. 6.2b. Consider the case in which there are two reflection points and where differences in the (group) ranges are greater than the length of the transmitted pulse, then, in this case the reflected pulses will not overlap and two separate echoes will be observed, (see fig. 6.2c). If the two pulses do overlap then the resulting echo will have a shape which will depend on the relative amplitudes and phases of the two echoes. In this case a spread echo will be produced.

A single reflection point returning a signal to the receiving array will produce a diffraction pattern which will show no

structure, since each antenna will be receiving a signal of the same amplitude.

If there are two reflection points and the differences in (group) ranges are such that the echoes can overlap, then the diffraction pattern wi show a band structure, analogous to Young's interference fringes, with the spacing of the bands being determined by the angular separation of the reflection points. If the (group) range difference is such that echoes do not overlap then the band structure will not be present. If the overlap is partial then only the overlapping parts of the echo will exhibit the band or fringe structure. However, the electronic equipment which is used to display the diffraction pattern is such that the fringe structure, under these conditions, will be apparent but the depth of modulation of the fringes will not be correctly represented.

This argument may be extended to any number of reflection points. Each pair of reflection points, which produce overlapping pulses, can be shown to give rise to a set of fringes. The resultant pattern is then the superposition of these fringe systems, proper account being taken of the phases of the signals being added. The following very simple model can be used to show that this is so.

Consider the static situation which is represented by fig. 6.3. Three non-colinear reflection points (1,2 and 3), with coordinates (x_1, y_1, z_1), (x_2, y_2, z_2) and (x_3, y_3, z_3), reflect circularly polarised radio waves back to the ground. We are interested in calculating the form of the diffraction pattern at a grid of points in the neighbourhood of a central point B (see diagram). Let the amplitudes of the signals received from the reflection points (1, 2 and 3) be A_1, A_2 and A_3.

If a specular reflection model is assumed, then each reflection point may be considered to produce an approximately plane wave at the array. In practice it will be shown that it makes little difference in this problem whether the reflected waves are considered to be plane or spherical. The relative phases of the reflected waves at the reflection points will depend on the distances from the transmitter to these points. In the static case these phases can be represented by ϕ_1, ϕ_2, and ϕ_3. The phases that the reflected waves will have at the two dimensional grid of points (the grid points have coordinates x_{nm}, y_{nm}, 0) can be calculated using a computer. Ignoring the time dependent part, the wave from reflection point (1) at (x_{nm}, y_{nm}, 0) in the grid can be represented mathematically by the term

$$A_1 \exp i(\underline{k}_1 \cdot \underline{r}_{1_{nm}} + \phi_1),$$

where,

$i = \sqrt{-1}$

$\underline{k}_1 = \frac{2\pi}{\lambda} \hat{\underline{u}}_1$,

$\lambda =$ radio wavelength,

$\hat{\underline{u}}_1 =$ a unit vector in the direction of propagation of the wave from point (1),

$\underline{r}_{1_{nm}} =$ a vector from reflection point (1) to the point (x_{nm}, y_{nm}, 0) on the ground. For the model $|\underline{r}|$ is a geometric distance and no

Diagram showing the geometry for the computer calculation of the diffraction patterns

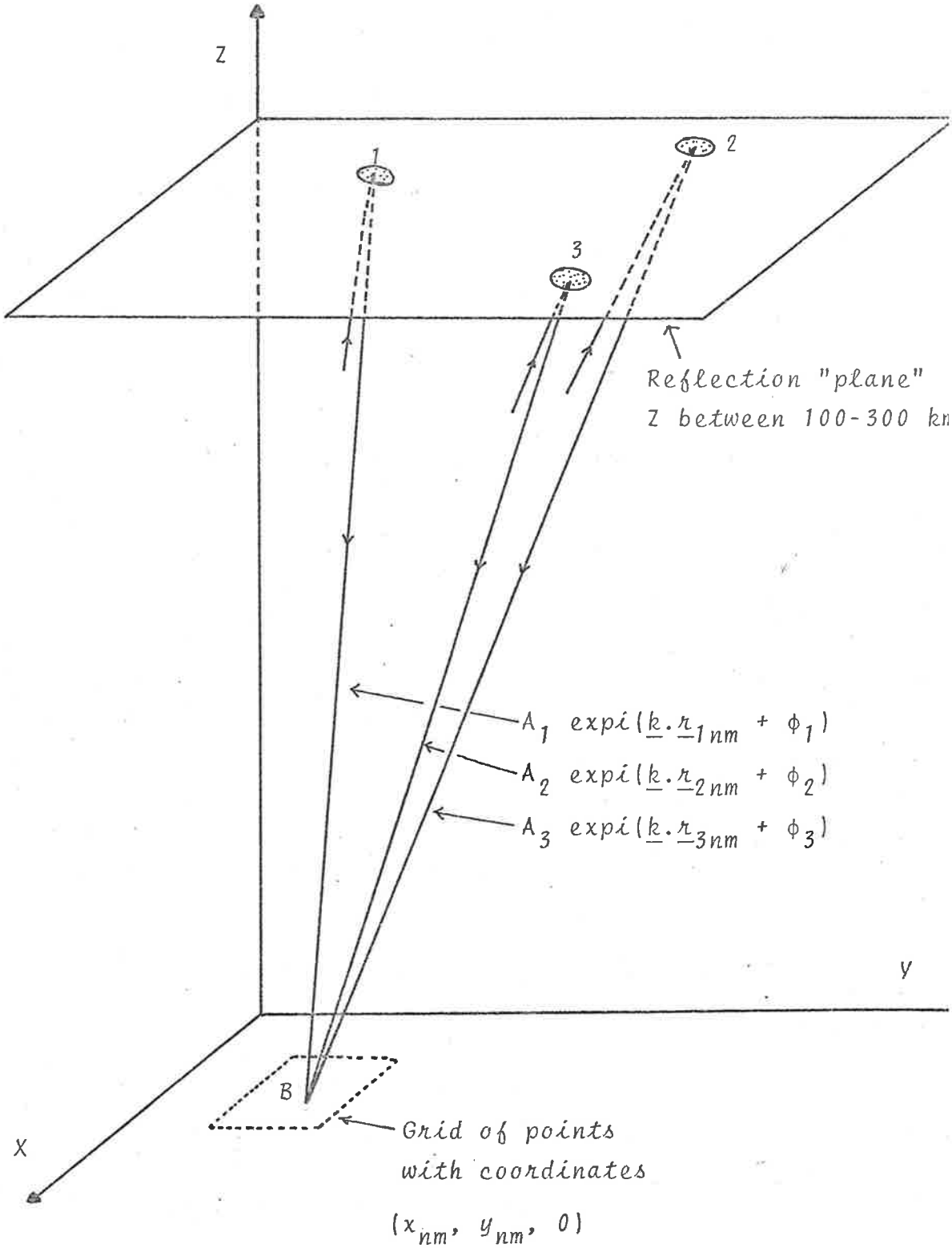

Fig. 6.3

attempt has been made to allow for variations of the refractive index below the reflection level.

The total field strength at the point $(x_{nm}, y_{nm}, 0)$ from (in this case) the three contributing waves is equal to A_{nm} where,

$$A_{nm} = A_1 \exp i(\underline{k}_1.\underline{r}_{1_{nm}} + \phi_1) + A_2 \exp i(\underline{k}_2.\underline{r}_{2_{nm}} + \phi_2) +$$

$$A_3 \exp i(\underline{k}_3.\underline{r}_{3_{nm}} + \phi_3)$$

It should be noted that the $\underline{k}.\underline{r}$ terms, appearing in the exponents, can be written in the form $kr\cos\theta$ where

$k = |k|$

$r = |r|$

θ = the angle between the vectors $\underline{k}$ and $\underline{r}$.

In practice we are interested in calculating the modulus of the complex amplitude of the diffraction pattern at points defined on a small area around B. If this region is a square, with sides of 1 km, with the point B in the centre, then θ will be small and $\cos\theta$ will not differ from 1 by more than 3×10^{-5} for an E-region model (even less for F-region). Therefore the $\underline{k}.\underline{r}$ terms can be replaced by kr which, as far as the phase of the wave is concerned, is equivalent to replacing the plane waves from the reflection points by spherical waves. With this approximation an analytical expression for the intensity of the diffraction pattern, (at the point $(x_{nm}, y_{nm}, 0)$), i.e. the square of the

modulus of the complex amplitude, has the form

$$A_{nm}^{\ 2} = A_1^2 + A_2^2 + A_3^2 + 2A_1A_2\text{Cos } k(r_{1_{nm}}-r_{2_{nm}}) +$$

$$2A_2A_3\text{Cos } k(r_{2_{nm}}-r_{3_{nm}}) + 2A_3A_1\text{Cos } k(r_{3_{nm}}-r_{1_{nm}}).$$

The last three terms give rise to the fringe structure. The number of fringes produced depends on the number of reflection points contributing to the pattern. If there are k such reflection points then $\frac{k}{2}$! sets of fringes will be produced.

Distance attenuation of the reflected waves has of course been left out in this model, but since all the waves are attenuated approximately equally the form of the diffraction pattern will not be affected significantly.

A computer model, based on the mathematical treatment presented above, has been used to produce contour plots which show the structure (modulus of the complex amplitude) of the interference pattern produced by different numbers of specularly reflected waves whose reflection points are arranged in different configurations. The pattern produced by a single ray shows no amplitude variations and is therefore not shown. Fig. 6.4 shows the simple fringe structure which results from the interference between two specularly reflected rays. Fig. 6.5 shows the pattern produced by three non colinear reflection points and Fig. 6.6 is a similar pattern produced by a different configuration of reflection points and plotted on a different scale. Although these patterns have a regular structure it is not immediately obvious that they contain three sets of fringes lying in different orientations. In fig. 6.6 the fringe

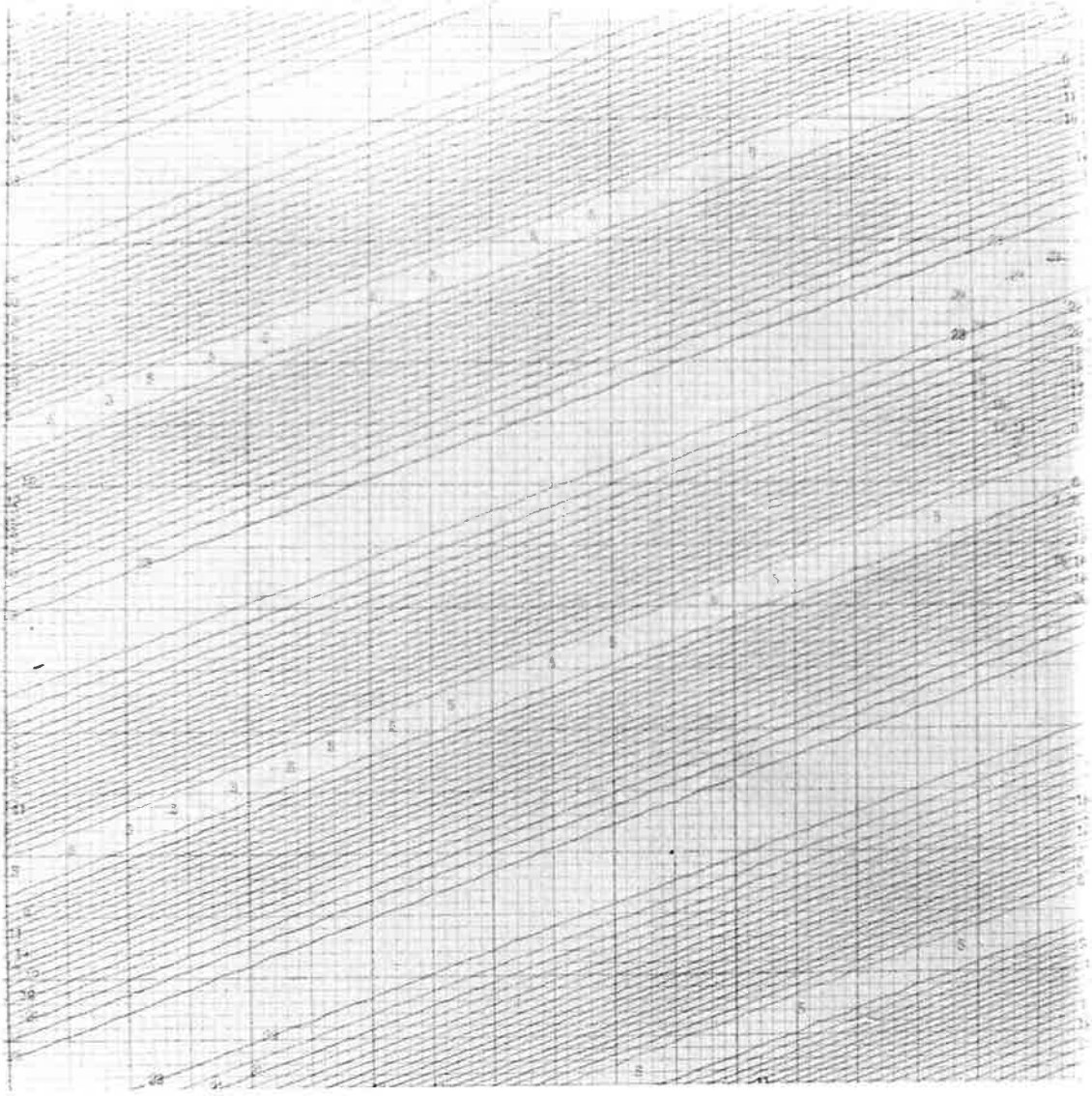

Contour plot of the modulus of the complex amplitude of the diffraction pattern formed by the interference between two specularly reflected rays. The pattern shows a fringe structure, a cross section of which, has the form of a rectified sine wave, i.e. sharp minima and broard maxima. The fringe spacing is as would be expected from the angular separation of the reflection points which were used in the calculation.

Fig. 6.4

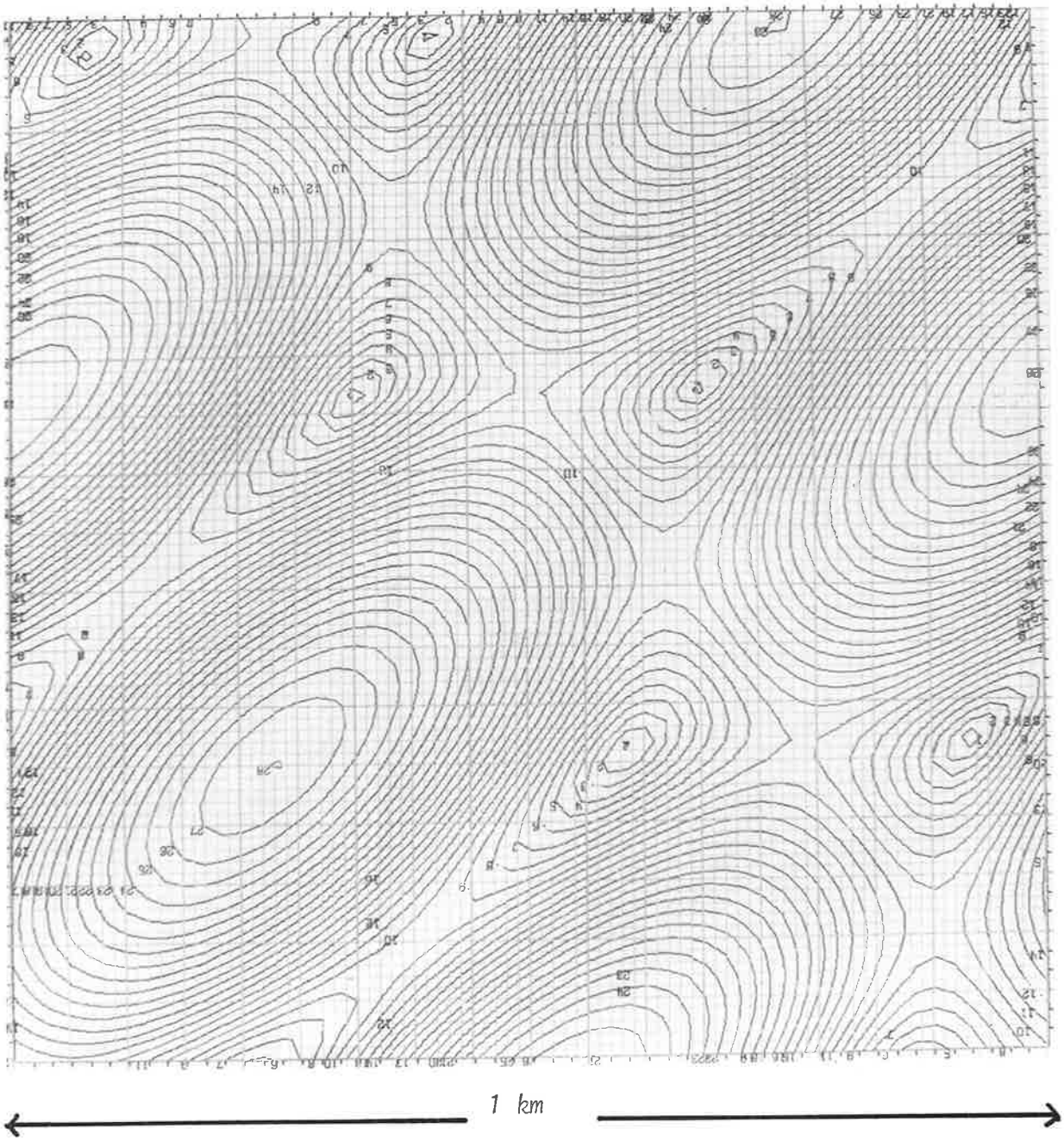

Contour plot of the modulus of the complex amplitude of the diffraction pattern formed by the interference between three specularly reflected rays.

Fig. 6.5

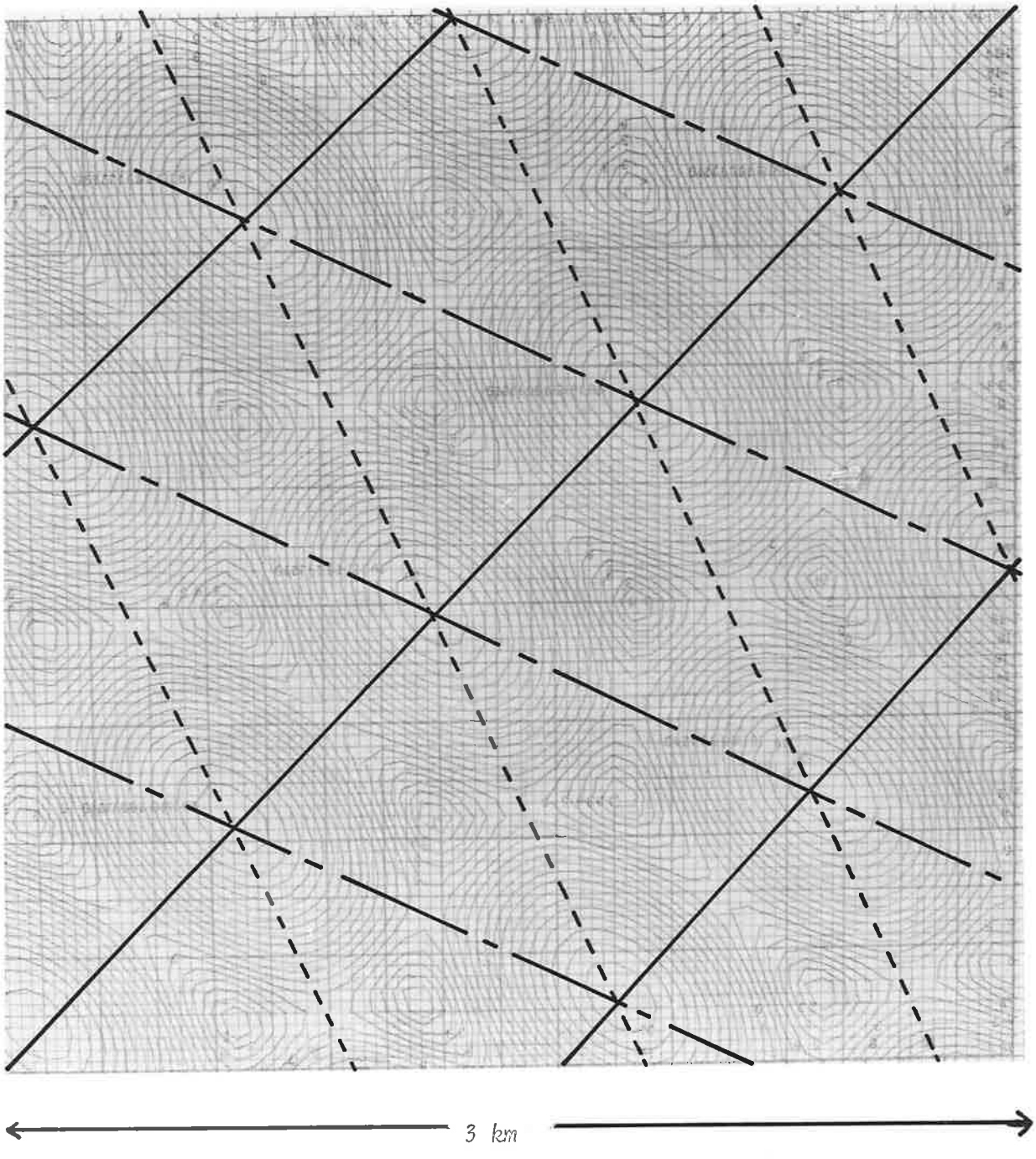

Contour plot of the modulus of the complex amplitude of the diffraction pattern formed by the interference between three specularly reflected rays. The inked in lines show the orientations of the fringe systems that are produced. These have been determined from a knowledge of the configuaration of the reflection points.

Fig. 6.6

orientations (determined from a knowledge of the positions of the reflection points) are shown. It can be seen that the elongations of the "blobs" in the pattern are determined by the two sets of fringes which are most nearly parallel.

One further interesting result is that if the three reflection points in the ionosphere 1, 2 and 3 are approximately centred over a coincident transmitting and receiving system, i.e. the circumcentre of the triangle 123 is vertically over the system, then the crests of all three fringe systems will intersect at common points (see fig. 6.6) at least in the neighbourhood of the transmitting and receiving system. This statement can be seen to be approximately true by letting the points 1, 2 and 3 be "sources" of plane waves, which are"emitted" with equal phases and are travelling in directions such that they arrive at the receiving system. Each pair of waves will produce a set of fringes, and for the conditions described, it can be seen that if the three perpendicular bisectors of the sides of the triangle 123 are projected on to the ground then these projected lines will be coincident with one of the crests from each of the three sets of fringes and hence, in the diffraction pattern, the fringes will intersect at the projection of the circumcentre of the triangle 123 on the ground. Since the three fringe systems are periodic then it follows that the structure of the pattern, at the projected circumcentre, will be repeated. This result is true, even if the waves from 1, 2 and 3 are not "emitted" with the same phases. The only difference

is that the projected circumcentre will not coincide with a point of intersection of three crests.

If four specularly reflected waves are contibuting to the pattern then the result is much more complex and in fact the structure appears to be random. In this case there are twelve sets of superposed fringes and further not all the fringe crests intersect in common points. Fig. 6.7 is a contour plot that illustrates this point. Finally fig. 6.8 shows the pattern that would be obtained if the four reflection points were situated at the corners of a square. This is not of course, a situation that would be expected to occur in practice.

Many workers in the past (e.g. Booker *et al.*, 1950 and Ratcliffe, 1956) have assumed that diffraction patterns with apparently random structures are produced by the interference between rays which have a continuous distribution of their angles of arrival. The angular power spectrum in this case is often assumed to have a Gaussian profile so that off zenith directions contribute less power than those closer to the zenith. However the work described above shows that the interference between four specularly reflected waves will also give rise to a random looking pattern. Thus it is not possible from observations of the pattern structure alone, to determine which is the more realistic ionospheric model. To do this direct measurement of the two dimensional angular spectrum is required.

Studies of the diffraction pattern by Felgate (1969) showed that on many occasions fringe structures were observed and this supported the specular reflection model. The results reported in this thesis

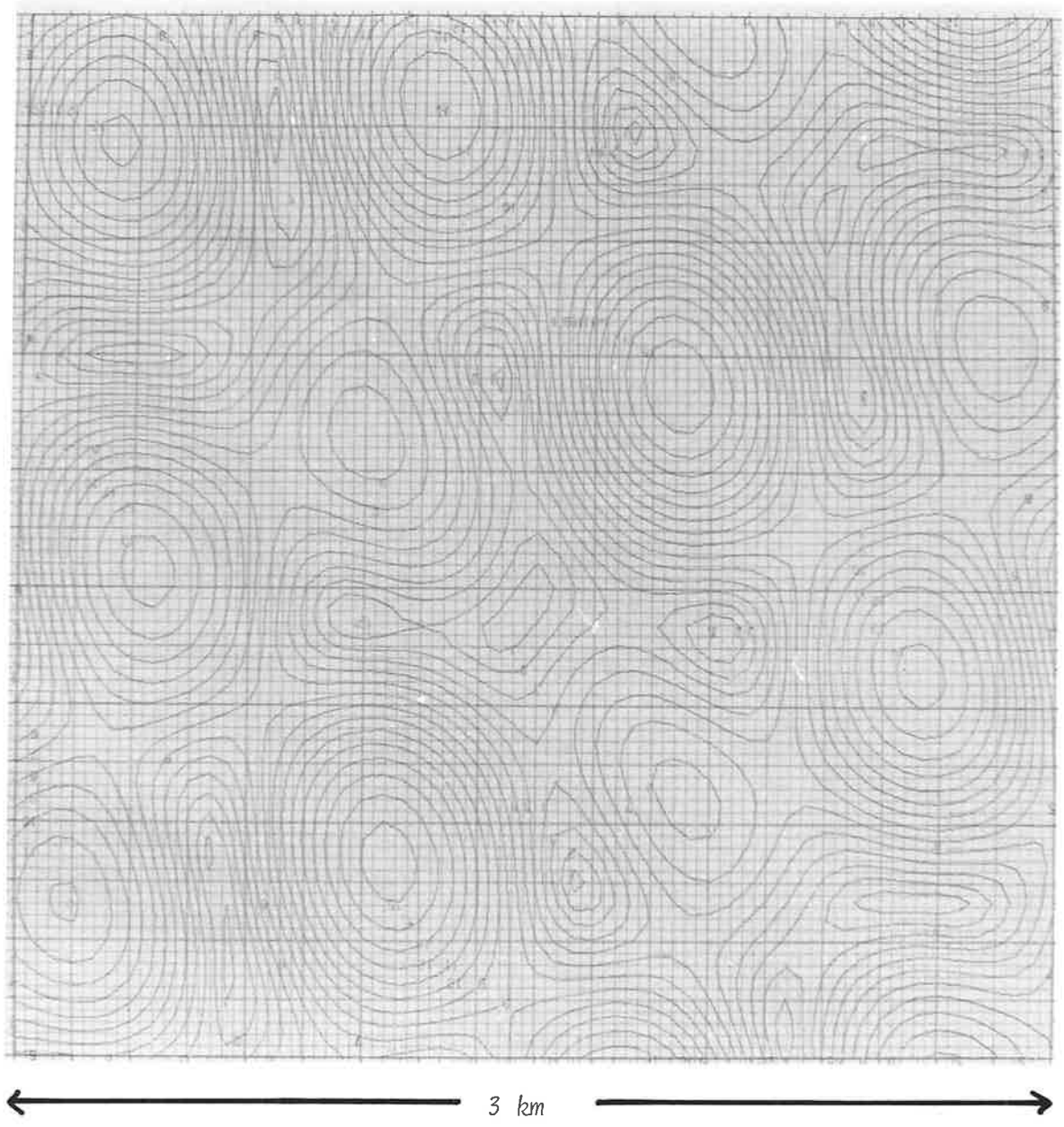

Contour plot of the modulus of the complex amplitude of the diffraction pattern formed by the interference between four specularly reflected rays. The pattern has a random appearance.

Fig. 6.7

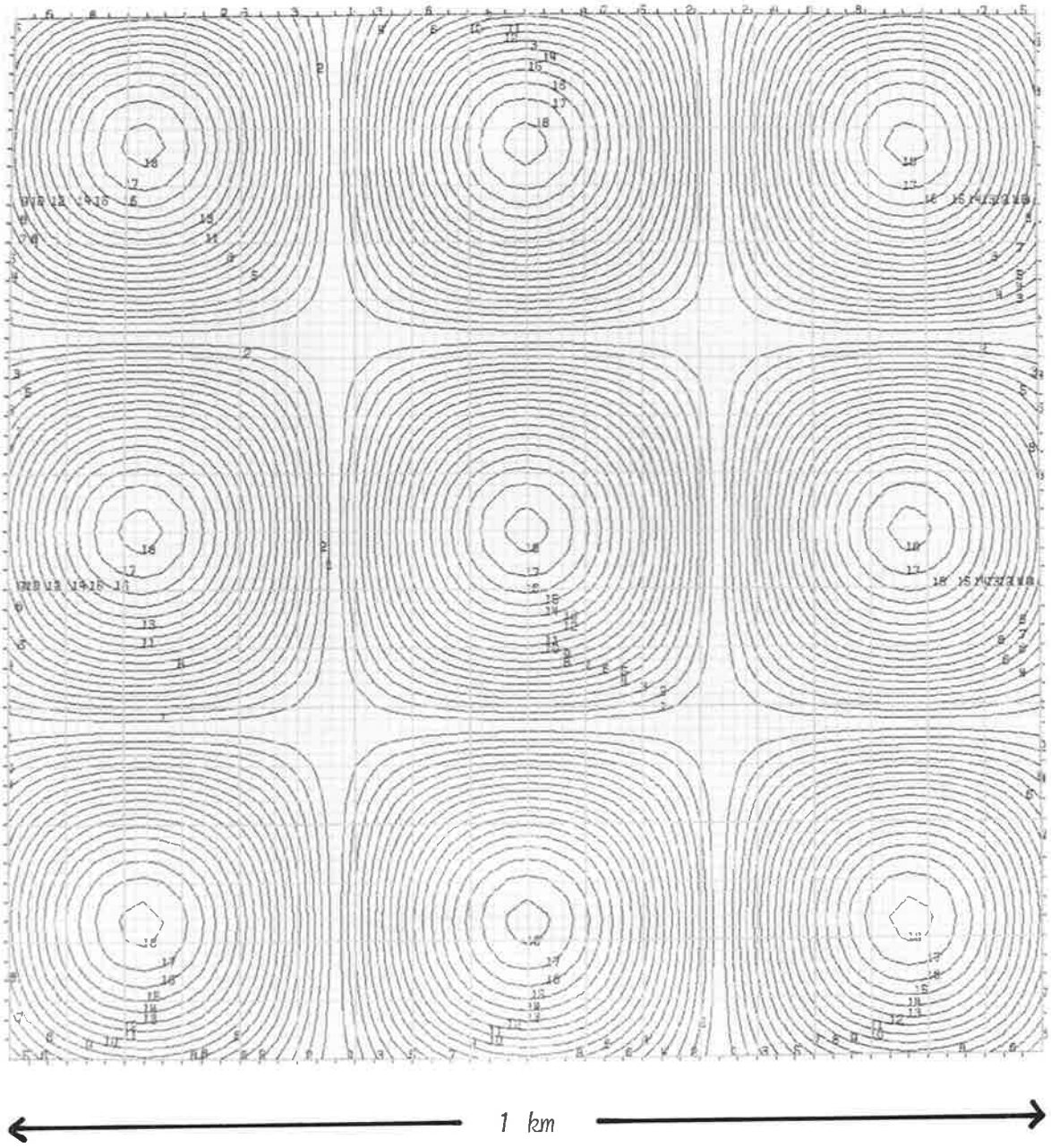

Contour plot of the modulus of the complex amplitude of the diffraction pattern formed by the interference of four specularly reflected rays arranged at the corners of a square which is centred over the transmitter/receiving system.

Fig. 6.8

(see TABLE 6.2) and recent work by Brownlie *et al.* (1973a) in Brisbane also support the specular reflection model.

These results have important consequences for experiments which estimate the ionospheric "drift velocity" from measurements made on the diffraction pattern. For example, if the pattern is formed by the interference of rays from a colinear set of reflection points then only that component of the "drift velocity" which is perpendicular to the fringe system that is produced, can be measured.

In addition another problem arises because movement of the diffraction pattern can now be caused by the vertical or horizontal motions of the specular reflection points and these are not necessarily the result of the bodily movement of ionization. A recent review paper by Briggs (1972) discusses this problem in more detail.

Another important consequence of using a specular reflection model is that the older idea, that the "scale" of ionospheric irregularities is of the order of a few hundred metres (Briggs and Phillips 1950), must be abandoned. These estimates were made using a model which assumes that the angular distribution of the reflected waves consists of a filled in cone with a Gaussian profile and further it is assumed that the phase modulation imposed on the reflected wave by the ionospheric irregularities is small (very much less than one radian). If this is the case then it can be shown (Ratcliffe 1956), subject to some conditions (see Briggs and Phillips, 1950), that the "scale" of the irregularities at the reflecting layer is equal to the "scale" of the

variations in the complex amplitude of the reflected wave. Here the term "scale" is conventionally taken to be the distance at which the autocorrelation function, of either the function describing the irregulariries or the function describing the reflected wave field, fall to a value of $^{1}/_{e}$. This result implies that the scale of the ionospheric irregularities can be estimated from the structure of the (complex) diffraction pattern. However if the ionospheric irregularities are large, with "scales" of tens of kilometres such as are required for specular reflection, then the phase modulation imposed on the reflected wave will usually be much more than one radian and if this is so then the "scale" of the diffraction pattern will be much smaller than that of the ionospheric irregularities.

The important points that have been discussed in this section may be summarised as follows.

(1) If the diffraction pattern is formed by the interference between discretely reflected waves then the pattern will consist of fringes the spacings of which will depend on the angular separation of the reflection points.

(2) The duration of the echo provides an indication of the (group) range differences between the reflection points which in some cases can be considered to be a measure of the angular spread. However, deductions of this nature should be treated with caution since it is possible to imagine a curved reflecting surface with the receiving array at the centre of curvature, which would give rise to a broad angular spectrum with very little range spreading. A similar situation

could arise if the distribution of ionization below the reflection surface was such as to equalize the group ranges of the reflection points.

(3) If the diffraction pattern is formed by the interference of four or more specularly reflected rays then the structure will appear to be random.

(4) Finally, with the specular reflection model it will no longer be true that the "scale" of the ionospheric irregularities is approximately the same as the "scale" of the structure in the diffraction pattern.

6.4 PRELIMINARY DISCUSSION (2) - SOME GEOMETRICAL ARGUMENTS CONCERNED WITH THE FOCUSSED IMAGE.

The discussion so far has been confined to what may be deduced about the ionosphere and the angular spectra of reflected signals by studying the diffraction pattern, and the echo on the A-scan. It will be useful to proceed with a similar discussion for the output of the image-forming system.

In the usual mode of operation, the ionospheric echo of interest (first hop, second hop, etc.) is selected by adjusting the delay of the signal from the gated local oscillator, so that it occurs at the same time as the echo. In this way the receiver outputs contain only the selected echo. The ground pulse and other echoes are suppressed. Suppression of the ground pulse is not total, but under most conditions it is well below the amplitude of the selected echo.

It will be recalled that the signal received by any given transducer in the image plane is produced by a radio signal from a given direction, and, in the case of total reflection, the radio signal will have come from a reflection point at a well defined range. Therefore if the acoustic signal from one of the receiving transducers is displayed on an oscilloscope in the same way as an A-scan then the echo should never be spread. This form of display is equivalent to an A-scan of ionospheric reflections from a given direction. So far, even on occasions when echoes on the normal A-scan have been observed to be very spread the echoes from a given direction have always been of the same duration as the transmitted pulse.

A further point that should be noted is that the spread of an A-scan echo can be controlled by the width of the gating local oscillator pulse. Naturally the duration of the echo can not be increased beyond its true value, but it can be made narrower. The effect of the pulsed local oscillator is then to accept only those echoes for which the (group) ranges to the reflection points, lie within certain bounds, which are determined by the width and delay (relative to the transmitted pulse) of the local oscillator pulse.

To illustrate this point consider the following geometrical argument. A situation is envisaged in which the ionosphere is returning a very spread echo from a totally reflecting layer. If this is so then the leading edge of the echo is produced by signals which are reflected from points having the least range, which in general will

be signals with angles of arrival close to the zenith. The trailing edge of the echo will be produced by contributions from greater ranges which will usually be from echoes which are further from the zenith. Thus if the pulsed local oscillator is set so that only the leading edge of a spread echo is seen on the A-scan then the output of the image-former will indicate that the angular spectrum of the reflected signals is narrow and centred close to the zenith.Conversely if the local oscillator is set so that only the trailing edge of the echo is observed then the image-former output will indicate that the angular spectrum is broad and furthermore echoes will appear to come mainly from large off zenith angles. Fig. 6.9 illustrates the geometry of this situation and fig. 6.10 is a series of photographs of the image-former display showing the output obtained from a broad angular spectrum when firstly (top figure) the local oscillator pulse has been set on the trailing edge of the echo thus excluding the echoes from close to the zenith, and secondly when the pulse has been set on the leading edge of the echo and finally when the pulse is set so that the whole echo is processed. In practice it is not difficult to ensure that in normal operation the gating local oscillator has a width such that echoes from all contributing angles are processed.

6.5 CLASSIFICATION OF RECORDS (1) - THE DIFFRACTION PATTERN

Felgate and Golley (1971) studied the diffraction pattern using the 89 element antenna array at Buckland Park. The working frequency for their experiments was 2 MHz and the equipment used to display the pattern was similar, but not identical, to that described in chapter 3. The study involved the analysis of some 50 hours of photographic

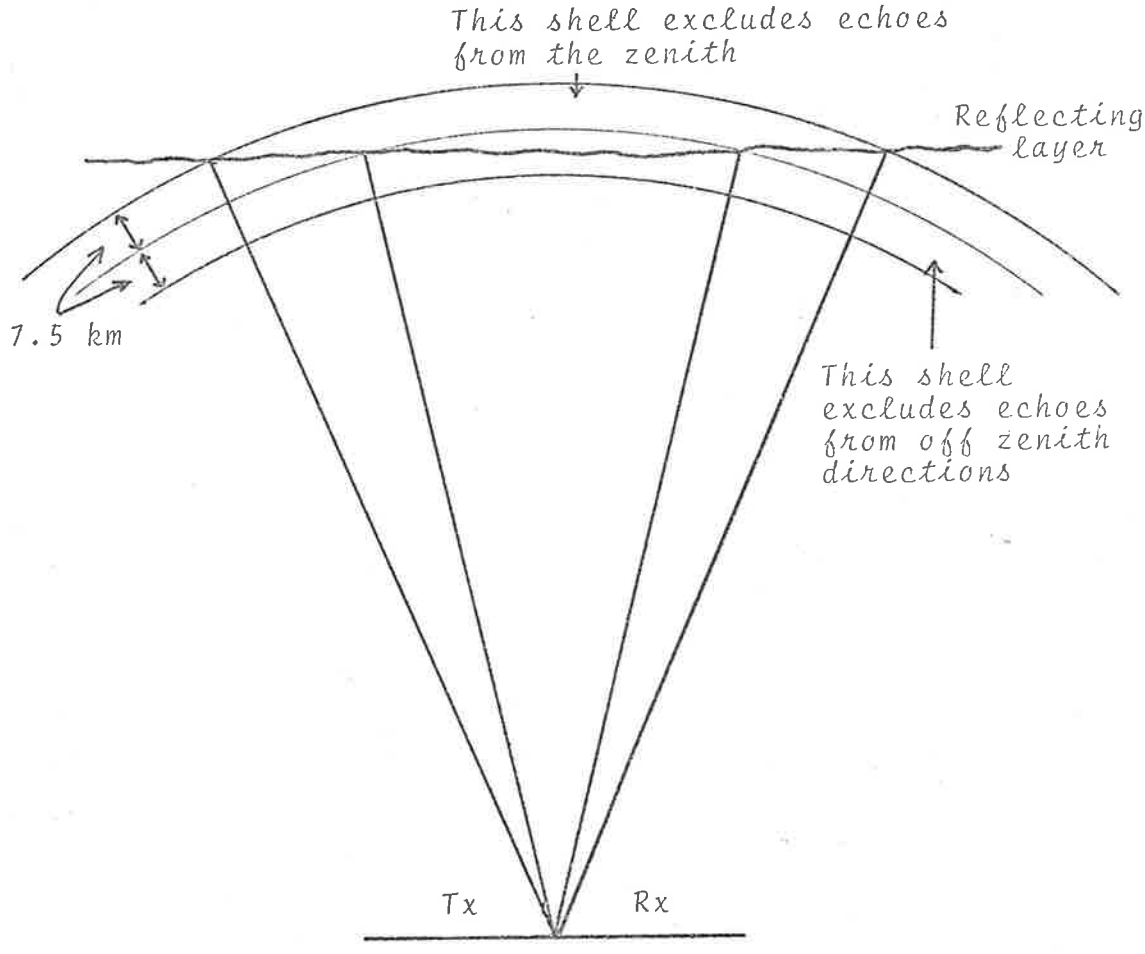

Diagram illustrating how the duration and position of the local oscillator pulse can affect the observed angular spectrum.

If the pulse has a duration of 50 μseconds then the system will only accept echoes from a spherical shell 7.5 km thick. The diagram shows that if the diameter of this shell is varied then the observed angular spectrum can be affected.

Fig. 6.9

The effect of the local oscillator on the focussed image output

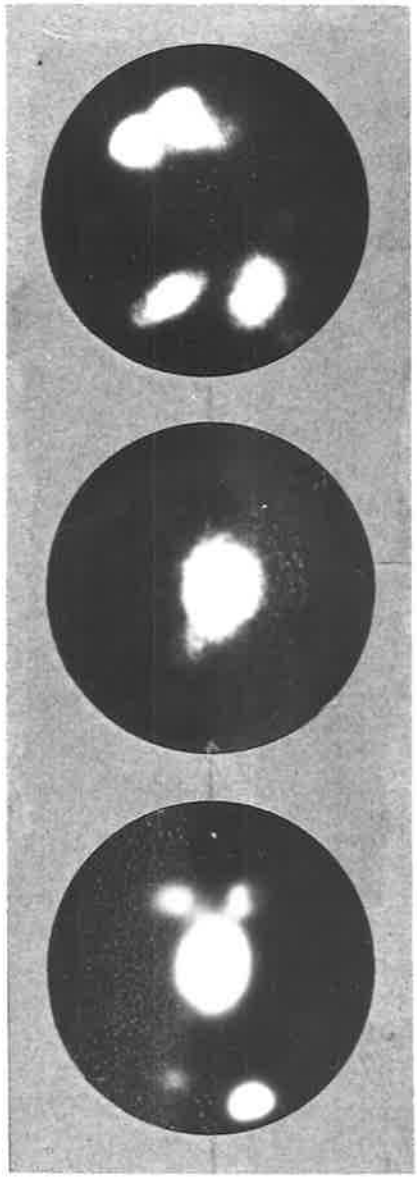

Zenith echo excluded

Off zenith echoes excluded

All echoes processed

Fig. 6.10

records, the majority of which were made during the period 12-12-68 to 8-1-69. It was found that the pattern could be classified into seven different types in the following way:

Type (1). Large scale patterns:

Patterns with a scale much larger than the size of the array.

Type (2). Periodic fringe patterns:

These consisted of alternate dark and bright bands which were observed to move across the display. The distance between successive bands was observed to vary from approximately 400 metres to over 1000 metres.

Type (3). Crossing fringe patterns:

These consist of two sets of superposed dark and bright bands which move in different directions with different speeds and often with different spacings.

Type (4). Random patterns:

These consist of isometric regions of strong signal in random positions all moving with approximately the same velocity. The patterns are observed to undergo some random changes as they move.

Type (5). Combined random and fringe patterns:

These are similar to type (4) patterns, however occasionally one or two sets of fringes may be observed for brief periods.

Type (6). Random changing patterns with rapidly changing directions of motion:

These are similar to type (4) but the speed and direction of movement of a given feature in the pattern may change drastically as it crosses the array.

Type (7). No fading at all:

This category needs no further description.

As well as classifying the various types of patterns observed Felgate and Golley have also measured the relative frequency of occurrence of different pattern types for different ionospheric reflections. Their results are summarised in TABLE 6.1. Also shown are the results of a similar survey made by the writer in 1973 using that part of the image-forming system which displays the diffraction pattern (see chapter 3). The photographic records, analysed for this survey, were made at irregular intervals from 2-3-73 to 30-7-73, however it should be noted that approximately 90% of the records were made in the period 2-5-73 to 30-7-73: (i.e. during late autumn and winter as opposed to the observations made by Felgate and Golley which were made during the 1968/1969 summer).

In all a total of 4800 feet of film has been used representing 12 hours of recording time. Although the recording method has varied from time to time the most common approach has been to record for 5 minutes every 30 minutes. Of the 12 hours of records, 40% were from the day time E region, 26% were from sporadic E layers (made during day time or night time) and 34% were from the night time F region.

TABLE 6.1

1968/1969 (After Felgate and Golley)

Pattern Type	E	E_s	F
1 Large Scale	12%	19%	46%
2 Fringes	10%	34%	18%
3 Crossing Fringes	24%	20%	7%
4 Random	17%	3%	3%
5 Random with some Fringes	23%	14%	-
6 Random with varying Direction	12%	6%	2%
7 No Fading	2%	4%	24%

1973 (present results)

Pattern Type	E	E_s	F
1 Large Scale	17%	22%	24%
2 Fringes	6%	3%	2%
3 Crossing Fringes	6%	-	-
4 Random	42%	49%	42%
5 Random with some Fringes	21%	4%	2%
6 Random with varying Duration	4%	22%	25%
7 No Fading	4%	-	5%

The most significant difference between the results obtained in the two surveys is the increase in the number of records classified as random and the decrease in the frequency of occurrence of those classified as consisting of fringes or crossing fringes. This is probably a seasonal effect although a longer survey is required to confirm or refute this.

In chapter 7 it is argued that some of the observed fringe systems are caused by the interference of rays specularly reflected from ionospheric irregularities which produce isoionic surfaces with a corrugated structure. As suggested by Hines (1960), internal atmospheric gravity waves could produce suitable irregularities. On the basis of this model it would be envisaged that in summer, the irregularities are caused by the presence, more frequently, of an isolated internal atmospheric gravity wave travelling through an otherwise unperturbed ionosphere while in winter the irregularities would be produced by either a different mechanism or alternatively by several waves travelling in different directions thus producing isoionic surfaces with a more complicated structure. This would result in more specular reflection points which would not necessarily be colinear; thus a diffraction pattern with a more complicated form would be produced. Of course it is not necessary that the winter ionospheric irregularities be caused by waves. Turbulence particularly in the E region might produce the required reflecting surface. However it seems necessary to assume some kind of wave motion in order to explain the type of observation described in chapter 7.

6.6 CLASSIFICATION OF RECORDS (2) - THE FOCUSSED IMAGE

The photographic records of the focussed image display have also been classified. Five different categories have been used and these have been chosen on the basis of patterns that have actually been observed and also on various models that have been suggested for the reflection process (see for example, Briggs and Phillips (1950), Booker *et al.* (1950),Bramley (1951), Ratcliffe (1956) and Pfister (1971)).

The following are the classifications chosen:

Type (1). A single specular reflection from the zenith:

This type of pattern (see fig. 6.11) is characterised by the presence of a steady bright spot in the centre of the focussed image display. The size of the spot is small indicating that the reflection is specular (i.e. the incident signal is a plane wave). A flat smooth reflecting surface is required to produce this type of spectrum (see fig. 6.12a). The corresponding diffraction pattern shows no fading. If the reflecting surface were to be rough, on a small scale, then the angular spectrum would have the form shown in fig. 6.12b. The spectrum in this case contains a strong specular component with weaker off vertical contributions. There is some indirect evidence that this model is appropriate (Bramley 1951, Lindner 1973). However in this survey it has not been possible to discriminate between these two models. The

reason for this is that the apparent size of the spot on the focussed image display depends on the signal amplitude. Broadening of the spectrum beyond 3 or 4 degrees would be apparent and such cases would not be included in this category. A more sensitive way of determining whether a reflection is specular or not is to plot the shape of the acoustic image using the digitised results. Such plots confirm that the reflections are indeed specular.

Type (2). A single moving specular reflection:

For this type of spectrum the display shows a single spot which moves usually, although not always, with a random motion close to the centre of the display (see fig. 6.11). The probably reflecting surface for this type of pattern is shown in fig. 6.12c. Once again small scale irregularities as depicted in fig. 6.12d could be present.

Type (3). Multiple moving specular reflections:

In this case the focussed image display shows several spots which move usually, though once again not always, in a random manner around the centre of the display (see fig. 6.11). Often single spots are observed to split into two, and on other occasions two spots may join together. The discontinuous appearance and disappearance of spots is another feature of this type of pattern. Figs. 6.12e and 6.12f show reflecting surfaces which would give rise to this type of pattern. The

differences between surfaces, which produce type 2 and type 3 spectra is that type 3 are produced by surfaces for which the amplitude of the undulations is large whereas for type 2 the amplitude variations must be small compared with their horizontal extent.

Type (4). Glinting patterns:

These are similar to type 3 patterns (see fig. 6.11) except that the movement of the reflection points is more rapid and discontinuous appearances and disappearances are more common. In general there are more specular reflection points (approximately 5-9) and these points produce signals of smaller amplitude than those observed in type 3 patterns. These patterns are probably produced by a rapidly changing type 3 reflecting surface (see figs. 6.12e and 6.12f) with possibly even larger amplitude undulations.

Type (5) A broad cone of reflected signals:

An irregular reflecting surface is required to produce this type of angular spectra and in addition, the scale of the irregularities must be such that the surface cannot be considered to be smooth over areas greater than approximately one Fresnel zone. Fig. 6.12g depicts the type of surface envisaged. The early models of the ionosphere assumed a structure of this type (see Booker *et al.* 1950). In the present survey this type of pattern was not observed for either E or F region reflection but it has been included as a possible model for D-region reflections, although the few

Examples of focussed image outputs

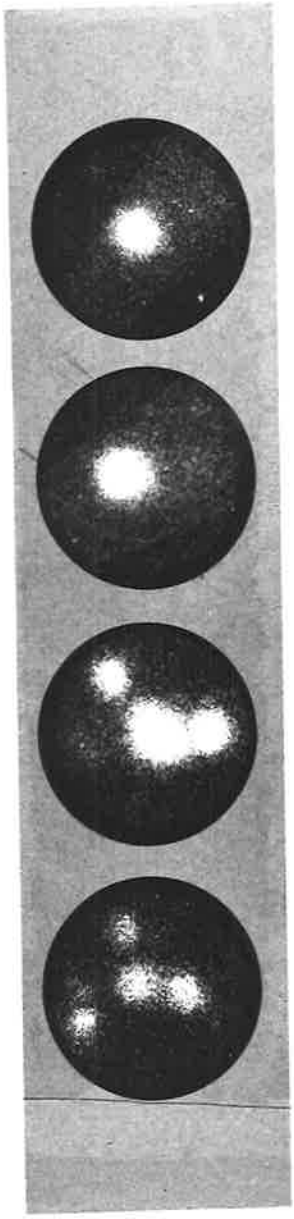

Type 1. Single specular reflection from the zenith.

Type 2. Single moving specular reflection.

Type 3. Multiple moving specular reflections.

Type 4. Glinting specular reflections.

Fig. 6.11

Schematic diagram of possible ionospheric reflecting surfaces

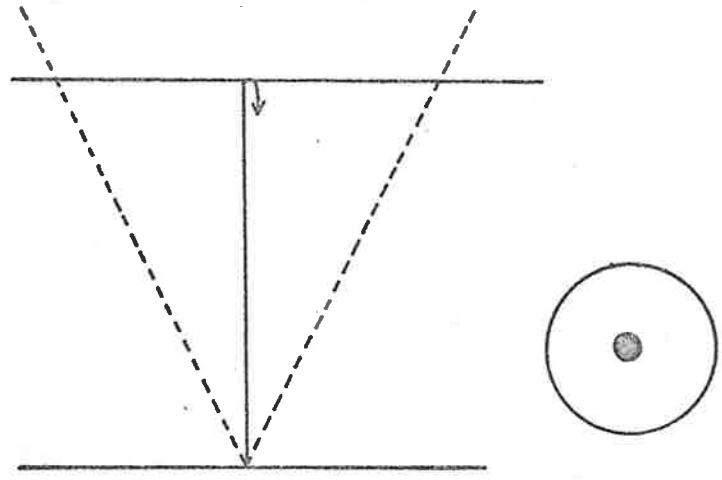

Schematic diagram of the focussed image display

(a)

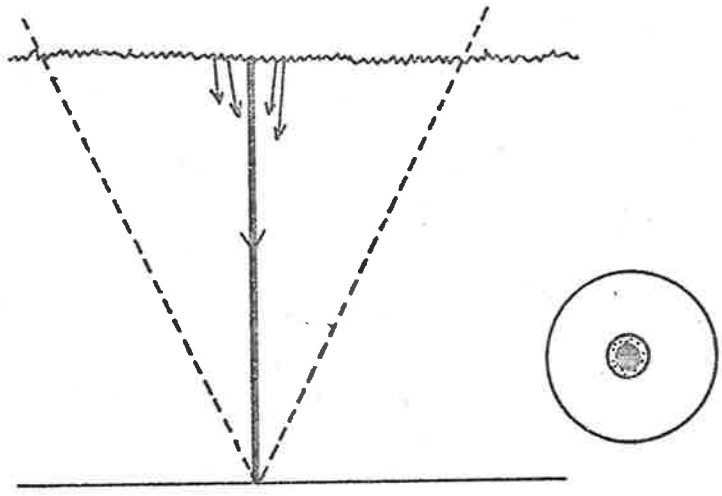

(b)

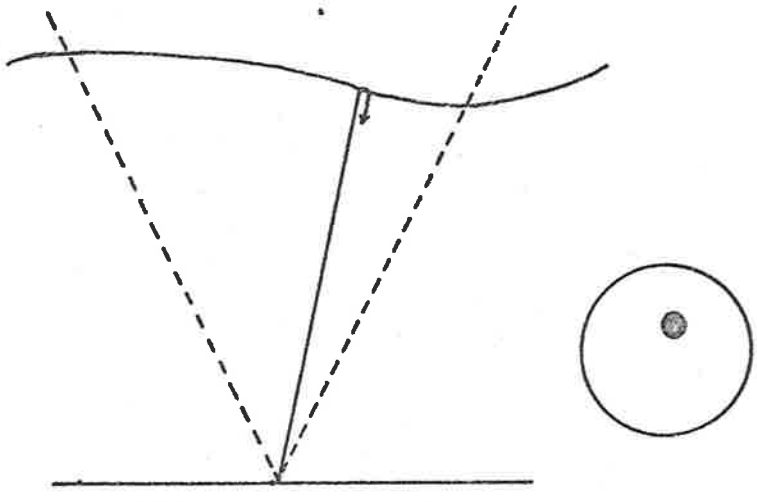

(c)

Fig. 6.12

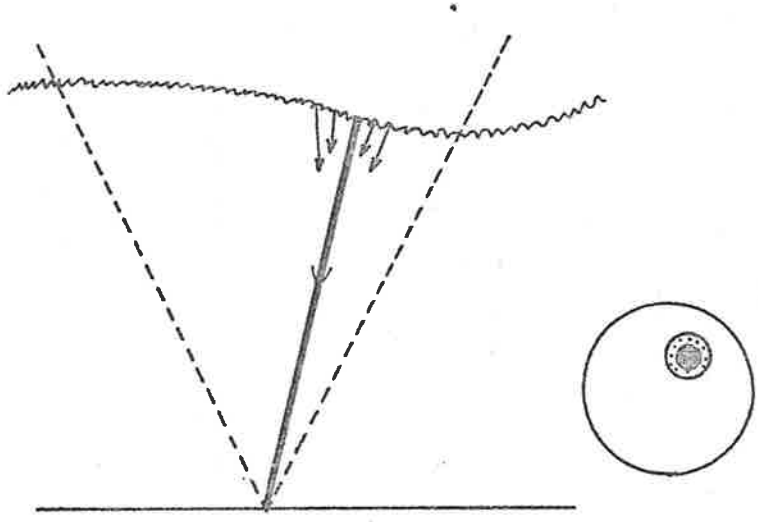

(d)

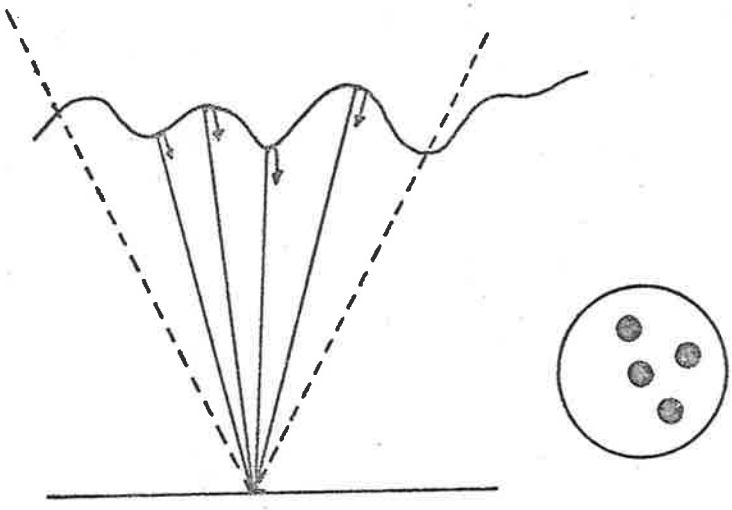

(e)

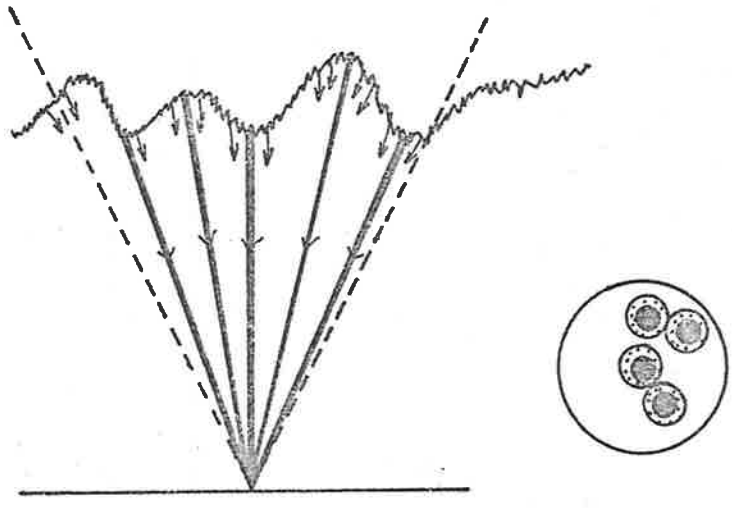

(f)

Fig. 6.12 cont.

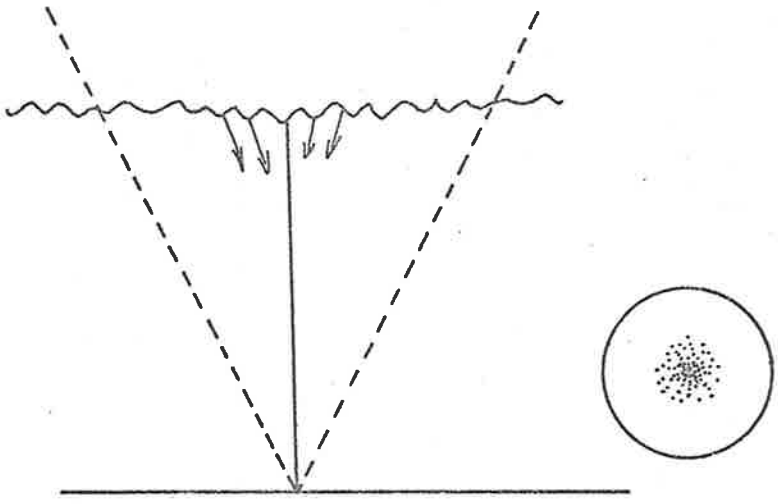

(g)

Fig. 6.12 cont.

D-region observations that have been made (approximately 55 minutes of observing on one day) were of type 4.

Table 6.2 shows the relative frequency of occurrence of the different types of observed angular spectra, from different ionospheric regions.

TABLE 6.2

(Frequency of occurrence of different types of angular spectra)

	Type of angular spectra	E	E_s	F
1.	Specular Reflection From Zenith	11%	9%	10%
2.	Moving Single Specular Reflection	13%	9%	19%
3.	Multiple Moving Specular Reflections	74%	67%	71%
4.	Glinting Specular Reflections	2%	15%	-
5.	Broad Cone of Reflected Signals	-	-	-

6.7 SOME THEORY RELEVANT TO THE PROBLEM OF SPECULAR REFLECTIONS

The problem of specular reflections from both random and regularly disturbed surfaces is relevant not only in ionospheric physics but also in oceanography and in radar astronomy; see for example Longuet -Higgins (1960(a), (b), (c)) and Barrick (1968).

The theory developed by Longuet-Higgins is concerned with the reflections of light from a point source off the ruffled surface of water, and is anologous to the ionospheric problem. In this situation the observer sees images of the light source at different points on the surface. As the surface changes the specular points, as the images are called, are observed to move and change in intensity. Occasionally pairs of points are observed to come together and disappear while at other times pairs of reflection points spontaneously appear. The annihilation or creation of pairs of points is called a "twinkle". These observations are very similar to the patterns described as type 3 and type 4 for the ionospheric reflection of radio waves, and it is interesting to see whether some of the statistical properties of the ionospheric reflecting surface can be deduced from experimentally determined information about the angular spectrum. The discussion that follows will show that unfortunately very little useful information can be extracted in this way.

Part of the theory developed by Longuet-Higgins is applicable to reflections from an isotropic, random surface, for which the deviations from a mean plane surface have a Gaussian distribution. Further, the first and second derivatives of the surface are also assumed to have Gaussian distributions.

Clearly, in view of suggestions made by Hines (1960) that ionospheric irregularities can be caused by gravity waves, a random isotropic surface would not always be a suitable model for the reflecting layer. However, the reflecting surface that gives rise to angular

spectra of type 4 may well be described by a random two dimensional function with the above properties and such a surface could be produced by a spectrum of waves travelling in different directions, or alternatively, by turbulence.

If this is assumed, then a formula relating the number of specular reflection points to the surface statistics can be derived, provided the distance of the observer and illuminating source from the surface are known. The desired formula is equation 4.11 from Longuet-Higgins (1960b) which states:

$$N = 1 + \left(\frac{2A}{\sqrt{3}}\right) \exp\left(-\frac{1}{3A}\right) , \qquad 6.1$$

where N = the number of specular points

and $A = < \left(\frac{\partial^2 \zeta}{\partial x^2} + \frac{\partial^2 \zeta}{\partial y^2}\right)^2 >_{av} 4h_o^2$

$\zeta = \zeta(x,y)$ (the function representing the surface)

h_o = the distance from the observer/source to the reflecting surface.

For the ionospheric problem the quantity h_o is the reflection height and

$$< \left(\frac{\partial^2 \zeta}{\partial x^2} \quad \frac{\partial^2 \zeta}{\partial y^2}\right)^2 >$$

is the average square of the "mean curvature" of the surface. Clearly the mean curvature must depend on both the rms deviations of the reflecting surface and the correlation length of the surface. Unfortunately it does not appear to be possible to separate these two quantities and, unless a separate estimate for one of them, say the correlation length, can be obtained, then the only information that can be

extracted from a knowledge of the number of specular points is information relating to the average square of the mean curvature which can be considered as a measure of the roughness of the surface. But this is not as informative as separate information about the rms deviation and the correlation length.

Fig. 6.13 shows the way in which the values for A, which is related to the average square of the "mean curvature" vary, with the number of specular reflection points. Two comments concerning the use of this graph should be made. Firstly N, in equation 6.1, refers to the total number possible specular points. In practice the field of view and field of illumination of the image-forming system appear to be large enough to enable the observation of all reflections. However, the second point which should be made, is that the power from each reflection point is not known and it is possible that some mathematically permitted reflection points may not be observed.

6.8 DISCUSSION AND CONCLUSIONS

This chapter has been concerned with a number of topics including models of the reflection process and the presentation of some preliminary results obtained with the equipment described in chapter 3. Also discussed have been some geometrical arguments, which were considered because they helped to develop a framework within which the results could be interpreted.

The most important result of the modeling "experiments" has been the demonstration that all the different types of diffraction patterns observed in practice, including those with apparently random structures,

Graph showing the way in which the number of specular reflection points is related to the quantity A (see text). (After Longuet-Higgins 1960b)

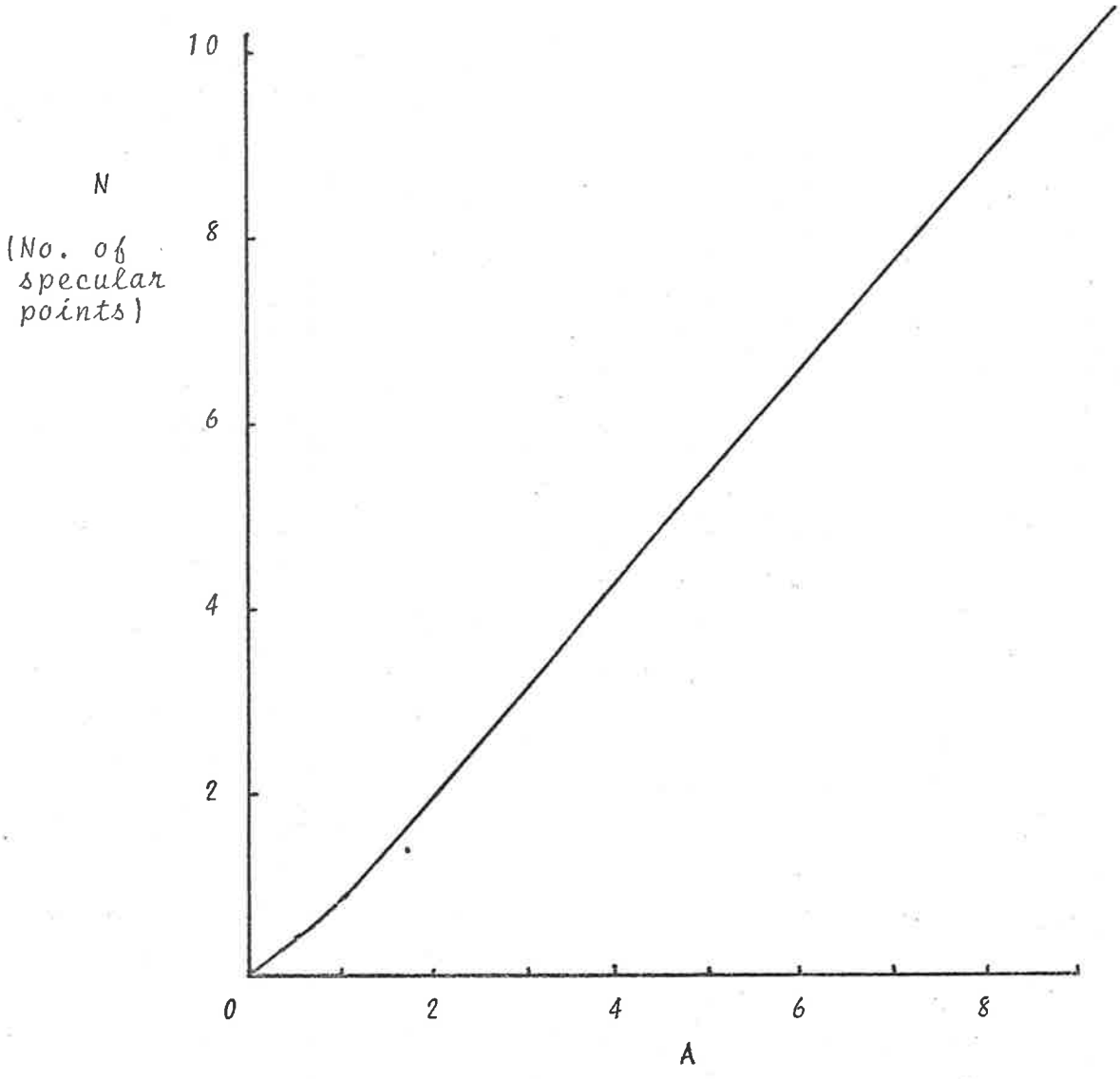

Fig. 6.13

can be produced by the interference between a few discretely reflected rays. Further, direct observations made of the angular spectra from E and F region reflections indicate that the specular reflection model is the appropriate model. This has important consequences for the estimates of the "scales" of ionospheric irregularities made in earlier experiments. In particular estimates of the "scales" of irregularities made by Briggs and Phillips (1950) will be too small.

In section 6.5 the classification of the types of diffraction patterns which occur has been discussed with particular reference to the work of Felgate and Golley (1971). Their results have been compared with the result obtained using the present equipment and the differences in the frequencies of occurrence of different pattern types have been tentatively attributed to seasonal effects.

In section 6.6 a survey, similar to that carried out on the diffraction pattern records, has been performed on the focussed image results. It was found that all the angular spectra observed consisted of rays discretely reflected from ionospheric structures which had "scales" of the order of several kilometres or more. Spectra consisting of a filled in cone of rays which would be produced by reflections from an ionosphere with irregularities with "scales" of only a few hundred metres were not observed. Incoming rays, were observed making angles as large as 28° from the zenith (the normal field of view of the instrument is ± 28° from the zenith). However these were rare and most echoes were observed to occur within

15^{o} of the zenith.

Clearly there should be some connection between the types of angular spectra observed and the corresponding diffraction patterns. For example spectra of types 1 and 2 should produce patterns of types 1 and 7 and spectra of types 3 and 4 would be expected to produce patterns of types 2, 3, 4 and 6. The relative frequencies of occurrence show that these expectations are approximately met.

Angular spectra of type 3 may be further subdivided into cases in which the reflection points move in a regular and periodic fashion, such as might be expected to be produced by a wave-like disturbance which distorts the isoionic surfaces so that they have an undulating periodic structure. An observation like this is discussed in chapter 7, but since spectra of this type are rare (at least in the survey described here) the observation has been included in category 3. However in the Felgate and Golley survey 1968/1969 (mostly summer) the incidence of fringe systems is higher, and since these patterns appear to be produced by the interference of specularly reflected rays from several colinear reflection points (see chapter 7), it may prove necessary, in subsequent surveys, to introduce a separate category for patterns of this type.

Reflections from E_s structures showed angular spectra of types 1, 2, 3, and 4 with the most significant difference between E_s and normal E layer reflections being the more frequent occurrence of type 4 spectra. This probably indicates that the E_s layers observed had a rather patchy structure. About 90% of these observations (E_s)

were made during the day time and angular spectra of type 4 were observed during both day and night, but the number of records are not sufficient to allow the day and night time observations to be treated separately.

Angular spectra for the F region are based on night time observations only. Some of these observations were made at times when ionograms (from an ionosonde at Salisbury, approximately 17 km south-east of Buckland Park) showed the presence of spread F . Although on some, fairly rare occasions, echo spreading (mainly frequency spreading) was observed at frequencies as low as 2 MHz, none of these coincided with times at which measurements of the angular spectra were available. Echo spreading (on ionograms) is more common at higher frequencies and when the image-forming system is operating at 6 MHz it should be possible to study the angular spectra, from spread F structures in detail.

Finally the theory of specular reflections from random surfaces has been considered briefly, with a view to estimating the statistical properties of the surfaces which give rise to type 4 and possibly type 3 reflections.

CHAPTER 7

EVIDENCE FOR INTERNAL ATMOSPHERIC GRAVITY WAVES.

7.1 INTRODUCTION

This chapter will be concerned mainly with the examination of a single 15 minute photographic record made using the equipment described in chapter 3. It will be argued that the motions of the ionospheric reflection points, for this record as observed using the image-forming system, are best explained by assuming that the air density, and hence the electron density, in the ionosphere has been perturbed by the passage of an internal atmospheric gravity wave. Estimates for the wavelength and "amplitude" of this wave are made.

Before proceeding with a description of the experimental results a brief discussion of some of the theoretically predicted properties of gravity waves will be presented.

7.2 PRELIMINARY DISCUSSION

The properties and basic theory relating to internal atmospheric gravity waves have been discussed by several workers including Eckart (1960), Hines (1960), Tolstoy (1963) and Midgley and Liemohn (1966). These waves may be thought of as long period pressure waves which can propagate through the atmosphere. They belong to the same family of waves as ordinary sound waves, the only difference being that the effects of gravity have been taken into account. (Waves with extremely long wavelengths, for which Coriolis forces and the earth's curvature are important, are excluded from this discussion).

The energy sources for these disturbances are thought to lie, for the most part, in the troposphere. Possible tropospheric sources include cold fronts, mountain waves, earthquakes, volcanic eruptions and nuclear explosions. Tidal motions which attain large amplitudes in the upper atmosphere have been suggested as high level sources of energy for gravity waves through non-linear processes. (Rishbeth and Garriot, 1969).

Waves generated in the lower atmosphere may propagate upwards and, if dissipative effects are ignored, the wave amplitude will grow exponentially with height. (The density of the atmosphere decreases exponentially with height and thus, for energy to be conserved, the wave amplitude must increase with altitude to compensate.)

The spectrum of waves generated in the lower atmosphere that reach a given height is determined by the temperature and wind structure of the atmosphere below that height. Hines (1960) has produced a diagram which shows the spectrum of gravity waves that can reach a given height. The figure is reproduced here as Fig. 7.1. It can be seen that many of the waves generated in the lower atmosphere are reflected in the mesosphere. Further, waves can be removed from the spectrum by viscous damping. The diagram shows that at any given height the shorter period waves are more severely attenuated by this effect. Other papers, notably by Pitteway and Hines (1963), Midgley and Liemohn (1966) and Einaudi and Hines (1970), give further consideration to the problems of reflections and the viscous dissipation of internal atmospheric gravity waves.

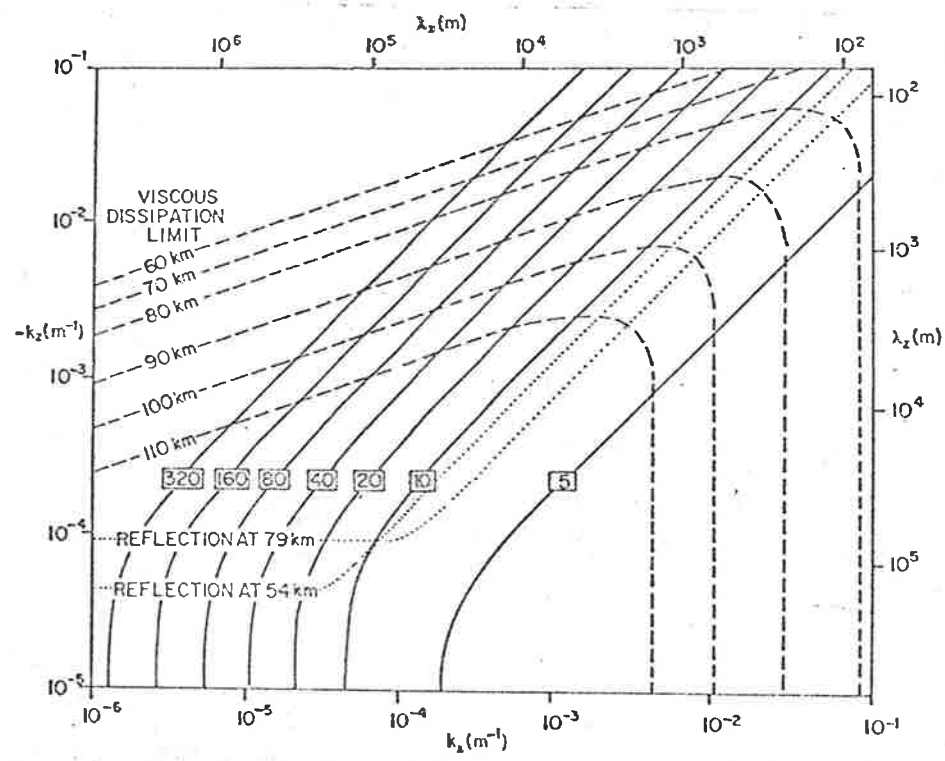

The diagram shows the permitted spectrum of gravity waves at various heights. The broken lines show the limits of the spectrum determined by viscous damping. The dotted lines show that part of the spectrum, which if generated in the lower atmosphere, will be reflected at the indicated heights. The figures in boxes refer to the period of the waves in minutes. (After Hines, 1960 fig. 11)

Fig. 7.1

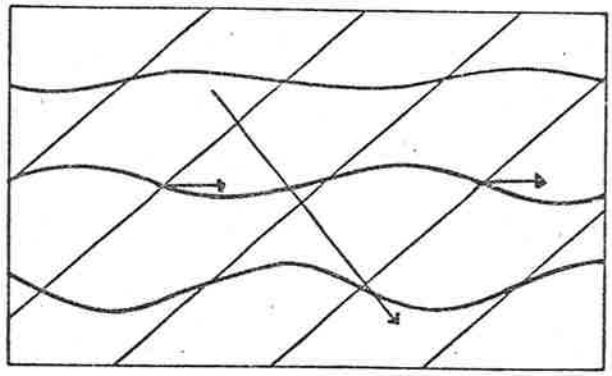

This figure shows how a gravity wave propagating downward (light arrow) will produce deformations in the isoionic contours which will appear to propagate horizontally (heavy arrows). (After Hines, 1965 fig. 6.9)

Fig. 7.2

7.3 THE EFFECT OF INTERNAL ATMOSPHERIC GRAVITY WAVES ON THE IONOSPHERIC REFLECTION OF RADIO WAVES

Fig. 7.2, which is derived from Fig. 6.9 of Hines (1965), shows how a gravity wave could produce ionospheric irregularities. Electron density variations are produced as the compressions and rarefractions of the wave change the ambient air density. The same figure shows how the isoionic contours would assume a sinusoidal or quasi-sinusoidal form with a horizontal wavelength equal to the horizontal component of the wavelength of the gravity wave.

The phase path technique, which is a useful method of measuring small changes in the reflection height of radio waves, often shows that the isoionic contours vary in a quasi-sinusoidal manner, (Landmark 1957, Vincent 1972). The distortion of the contours is similar to that which would be produced by a gravity wave propagating in an ionosphere which has little or no horizontal variation in electron density except that which is produced by the wave itself.

Several workers including Bramley (1953), Vincent (1967), McGee (1969), Pfister (1971) and Afraimovich (1972), have considered the effect that a sinusoidal or quasi-sinusoidal perturbations will have on the reflection of radio waves. Of particular interest is the number of possible specular reflection points and the angle of arrival, from which the slope of the effective reflecting surface can be determined. Munro (1953) has considered a similar problem although in this case the perturbation was not sinusoidal. Brownlie *et al.* (1973c) and Guha and Geller (1973) have considered the more general problem of

reflections from a surface which has been produced by a large number of waves of different wavelengths, travelling with different velocities.

Fig. 7.3 illustrates the geometry of the problem in which the isoionic contours can be represented by a sine wave. The wave should be imagined as having long wave fronts so that in two dimensions the isoionic surfaces are like ripples on the surface of the water. If the surface is assumed to be smooth (although undulating) the reflections will be specular, and ray theory can be applied. Thus the reflection points that will return power to the receiver, which is close to the transmitter, are determined by the normals shown in the figure. (Austin (1967) has developed a simple method of calculating the positions of the reflection points. His approach is similar to that followed below.) Refraction below the reflecting surface is neglected.

A cross section through the reflecting surface can be represented by f(x) where,

$$f(x) = A\sin(\omega t + kx) + h_o \qquad 7.1$$

where A = the amplitude of the wave

ω = angular frequency of the wave

$k = \frac{2\pi}{\lambda x}$

x = the horizontal coordinate.

The slope of the reflecting surface as a function of x is found by differentiating f(x) with respect to x.

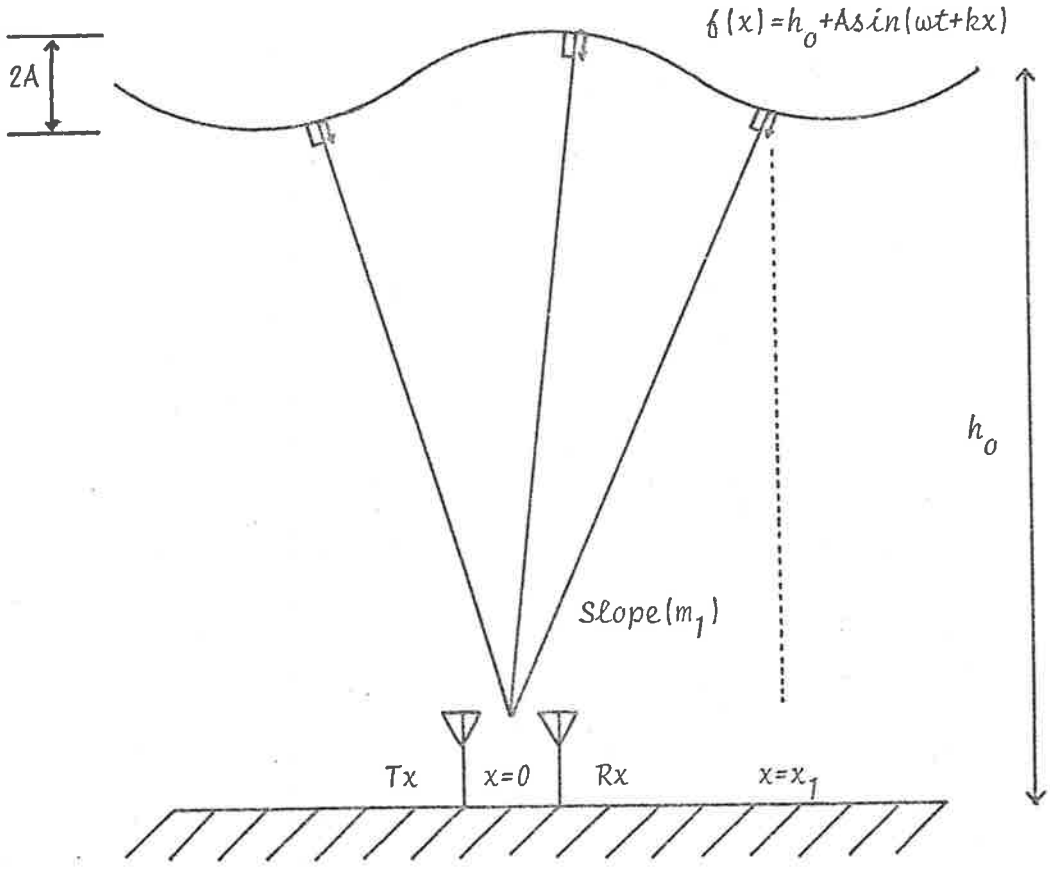

Diagram illustrating the geometry of the problem of the specular reflection of radio waves from a sinusiodal reflecting layer.

Fig. 7.3

$$f'(x) = kA \cos(\omega t + kx) \qquad 7.2$$

The slope of a line drawn from the receiver to the reflecting surface so that it intersects the reflecting surface at an arbitrary point x_1, can be seen to be equal to m_1 where,

$$m_1 = \frac{h_o + A \sin(\omega t + kx)}{x_1} \qquad 7.3$$

The requirement that this line be normal to the reflecting surface is met by demanding that

$$f'(x_1)\, m_1 = -1 \qquad 7.4$$

i.e. $$x_1 = h_o kA \sin(\omega t + kx_1) + \frac{kA^2}{2} \sin(2\omega t + 2kx_1) \qquad 7.5$$

For practical cases $\frac{kA^2}{2} \ll h_o kA$ and therefore equation 7.5 reduces to

$$x_1 = h_o kA \sin(\omega t + kx_1). \qquad 7.6$$

This is a transcendental equation which can either be solved numerically or graphically to yield values of x_1 for which signals will be specularly reflected back to the transmitter/receiver system. This can be done for different values of time (t) and thus the movement of these reflection points relative to the transmitter can be calculated. This will be done for the particular wave that best matches the experimental observations, but first these will be described.

7.4 EXPERIMENTAL OBSERVATIONS

Early observations of the structure of the diffraction pattern (formed by radio waves reflected from the ionosphere) showed that in many cases the structure was simple and consisted of a system of fringes travelling in a well defined direction. Several workers including Gossard (1967), Gossard and Paulson (1968), and Felgate and Golley (1971) have interpreted these fringe structures as being the radio analogue of Young's interference fringes, the radio fringes being formed by the interference between two specularly reflected signals. On a number of occasions these fringe systems were observed to persist for long periods of time, of the order of 30 minutes.

Film records (of an E-region (100 km) reflection) from the image-forming system beginning at 1310 hours on the 14th of March 1973, show a clearly defined set of fringes travelling towards the south-west with a velocity (estimated by measuring the time taken for the crest of a fringe to cross the array) of between 80 and 100 metres sec^{-1}, corresponding to an ionospheric velocity of between 40 and 50 metres sec^{-1}. The fringe system was observed to persist for the duration of the record which was 15 minutes (the time taken to expose 100 feet of film at 4 frames sec^{-1}). The following record, which commenced at 1348 hours on the same day also shows a set of fringes travelling in the same direction. However this pattern was disturbed at times and these fringes were crossed by another set travelling towards the north-west.

Fig. 7.4 is a sequence of frames, taken at intervals of 0.25 seconds, from the film record which began at 1310 hours. The fringe system is clearly seen on the diffraction pattern display. The focussed image shows a pair of spots which at first sight would appear to correspond to two specularly reflected rays. As time progresses these two spots appear to merge forming first an elongated spot and finally a broad, almost circular spot. The fringe structure is visible in all the frames indicating that the circular spot consists of rays arriving from at least two unresolved directions. Careful examination of the record revealed that the focussed image displayed the two spot structure on three separate occasions. The sequence of film shown is typical of these occasions. The two spots are resolved for short periods of time approximately 6 or 7 frames of film corresponding to approximately 2 seconds of observing time. For the major part of the record the appearance of the focussed image is similar to that shown on frame labelled t=2.5 sec. in fig. 7.4. The interval between the appearances of the two separate spots on the focusse image display was found to be 5.3 minutes and 5.9 minutes.

These observations can be explained by assuming that the isoionic contours at the reflection height have a sinusiodal or quasi-sinusoidal shape similar to that which would be produced by the passage of an internal atmospheric gravity wave.

In order to satisfy the observations the wave would have the following properties:

(1) a period of between 5.3 and 5.9 minutes (say 5.6 minutes),

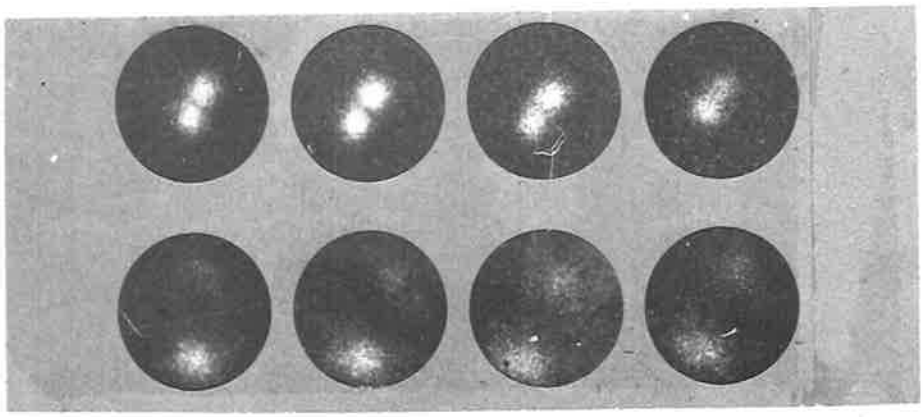

t=0 sec.

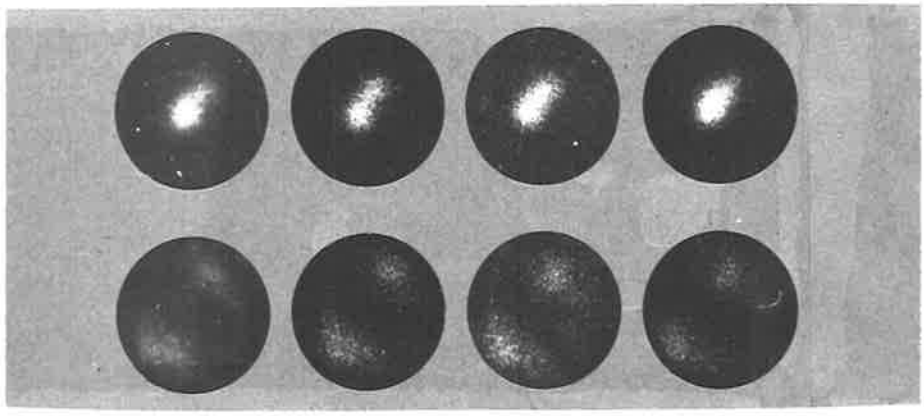

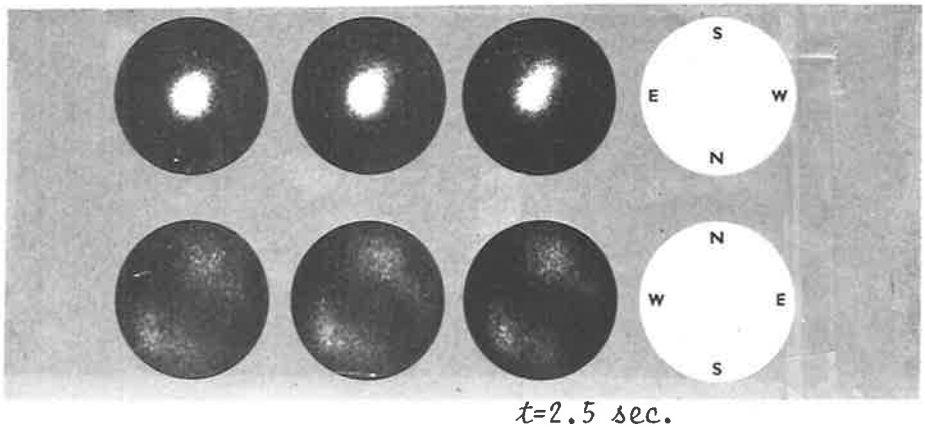

t=2.5 sec.

A sequence of frames from the cine film taken at .25 second intervals.

Fig. 7.4

(2) a phase velocity, relative to an observer on the ground, of approximately 45 metres sec^{-1};

(3) from (1) and (2) it can be deduced that the horizontal component of the wavelength (λ_x) would have to be approximately 15 km.

It should be noted that both the period of the wave and its phase velocity as observed from the ground will depend upon the component of the velocity of the medium (ionosphere) in a direction perpendicular to the wave fronts. However the wavelength, as calculated from the product of these two quantities, will not be affected by any background motion.

From the photographic records the maximum angular separation of the reflection points can be measured and is found to be approximately 14°. From this the spatial separation of the reflection points can be calculated and is found to be approximately 25 km, which is greater than the estimated wavelength of the disturbance (15 km).

From Fig. 7.4 it can be seen that the two spots in the focussed image display are displaced by equal distances from the centre. This implies that either a crest or a trough of the wave is overhead. The absence of an echo from the overhead position implies that it is a trough of the wave that is directly overhead. The situation envisaged is depicted in Fig. 7.5. The curvature of the reflecting surface in the overhead position results in a defocussing effect and thus no echo is observed from this position.

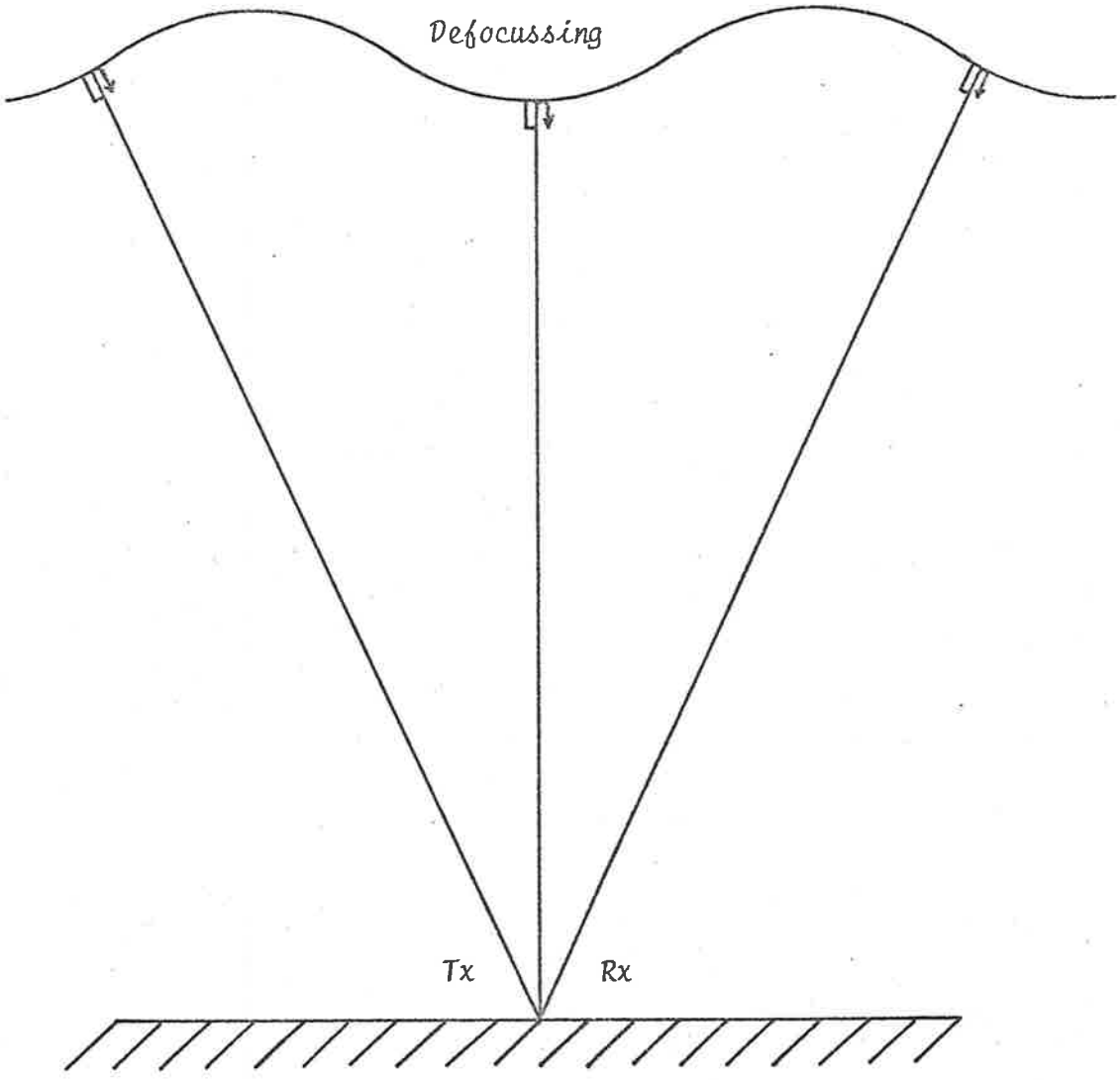

Diagram showing the envisaged position of the isoionic contour (at the reflection level) that would be required to produce the image-former output shown in fig. 7.4 (t=0). The ray from the zenith is defocussed and is therefore not observed on the focussed image display.

Fig. 7.5

If Fig. 7.5 is a correct representation of the situation then it is possible, knowing the position of the reflection points and the wavelength of the disturbance, to calculate an estimate for the amplitude of the wave (A). A value of A equal to 338 metres is appropriate.

Using all the data available, relating to the amplitude of the wave, the wavelength and the reflection height (h_o), which is 100 km, it is possible to solve equation 7.6 and to find the x-coordinates of the reflection points as a function of the position of the crest of the wave. These are plotted in fig. 7.6. The horizontal axis in this figure, labelled ωt, corresponds to the position of the crest of the wave. When $\omega t = 2n\pi$ ($n = 0, \pm1, \pm2, \ldots$) the reflecting surface overhead is concave, i.e. appropriate for focussing and when $\omega t = n\pi$ ($n = \pm1, \pm3, \ldots$) the reflecting surface is as depicted in fig. 7.5. The vertical axis, labelled x, gives the x-coordinates of the reflection points. When $\omega t = 0$ the crest of the wave is vertically overhead. There are seen to be three reflection points whose x-coordinates are approximately -6.3, 0 and +6.3 km. Under this condition the angular separation of the outside reflection points is approximately 7° and the angular separation between the neighbouring pairs of reflection points is approximately 3.5°. The resolving power of the instrument is approximately 9° and therefore we would expect the focussed image to consist, in this instance, of an elongated spot rather than three resolved spots. When $\omega t = \pi$ this corresponds to a trough of the wave being overhead. The intersections

Diagram from which the x-coordinates of the specular reflection points can be determined (see text)

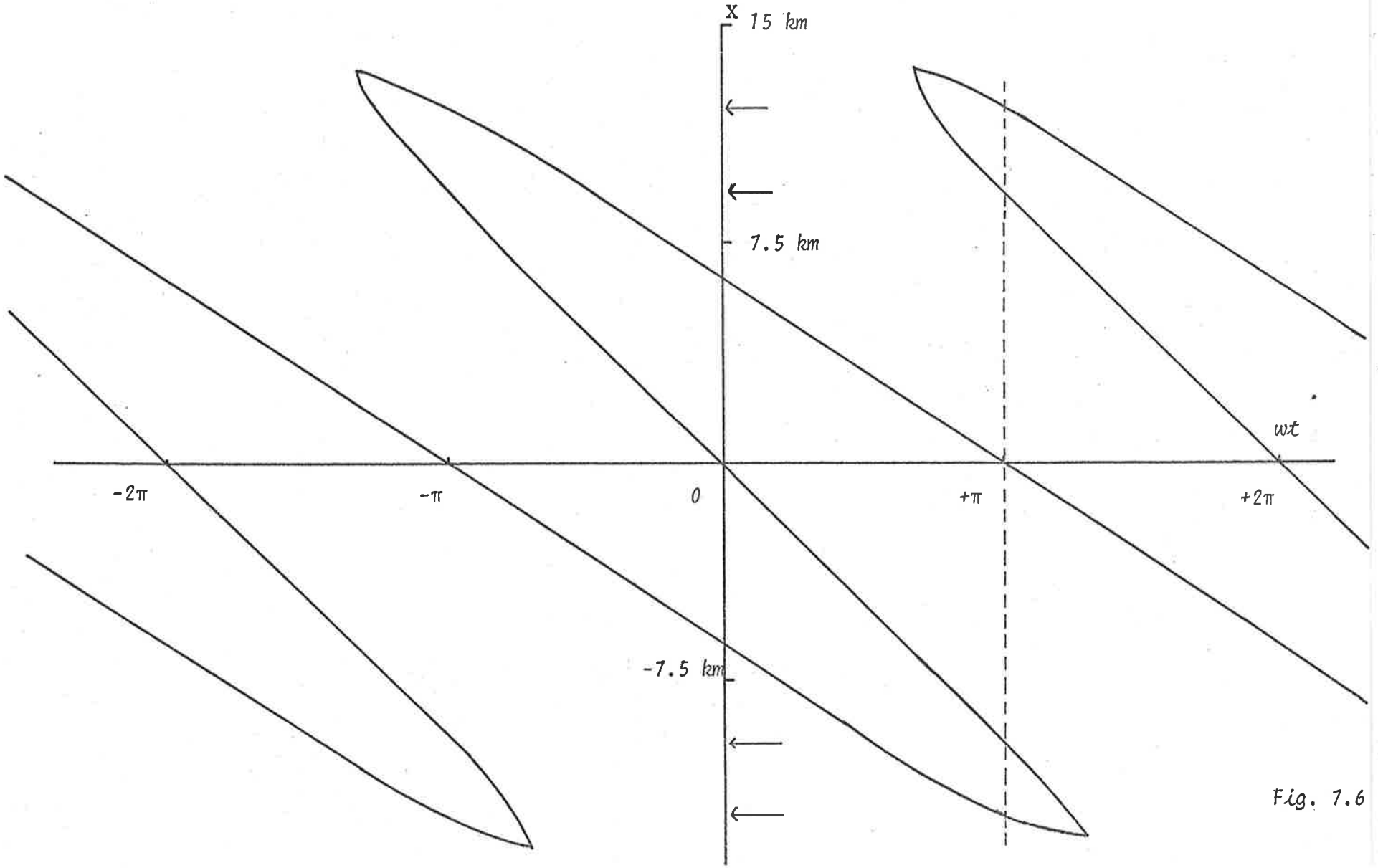

Fig. 7.6

of a line drawn perpendicular to the x-axis and the curve shown in fig. 7.6 indicate that there are five possible specular reflection points with x-coordinates of -12, -9.4, 0, +9.4 and +12 km. The angular separation between the reflection points at 12 and 9.4 km is approximately 1.5° and therefore the pair will not be resolved. As has been explained earlier the reflection from the zenith is defocussed and is therefore not observed. An average value for the angular separation of the two outer-most pairs of reflection points is approximately 12°. Therefore these should be resolved as is observed (see fig. 7.4). However if the central reflection point were to contribute to the image then the image would once again appear as an elongated spot. The defocussing condition will last only for a short time. This explains why the appearance of the two spots is so transitory.

From fig. 7.6 it can be seen that, for the wave observed, there will always be at least three reflection points. Thus it is expected that the fringe system would be always observed. This is the case.

The model described above explains the observations and, in view of the period and the deduced wavelength of the structure, it seems reasonable to assume that the distortion of the isoionic contours is due to the passage of an internal atmospheric gravity wave, rather than just random fluctuations in the ionisation density caused by say turbulence. However, it is necessary to point out that with the radio reflection technique used here it is not possible to discriminate

between wave motions and the bodily motion of irregularities.

Fringe systems existing for fairly short periods of time, showing three or four fringes, are observed frequently (see Table 6.1). However most of these do not appear to be associated with any periodic disturbances. The record considered in detail above is the only one of its type among the 12 hours of photographic records taken. In fact no other patterns of this type were observed in over 100 hours (made mostly during winter) of visual observations for which no photographic records were taken.

CHAPTER 8

CONCLUSIONS AND SUGGESTIONS FOR FUTURE WORK

8.1 CONCLUSIONS AND SUGGESTIONS

Probably the most important feature of the work described here has been the demonstration that the acoustic image-forming technique is feasible. The problems of the phase stability of the receiving system have been overcome by operating at a fixed gain and a reasonable dynamic range for the system has been achieved by using voltage controlled attenuators to vary the amplitudes of the inputs to the receivers so that they are of an appropriate value for the chosen receiver gain settings. Systems designed to work purely in conjunction with a nearby transmitter could probably be made to operate over a sufficiently wide dynamic range by varying the transmitted power, so that the received signal was of a satisfactory amplitude. This approach would not be useful when using distant transmitters for which the power could not easily be controlled. It has also been demonstrated that the apparatus can be adjusted to obtain a resolving power close to that expected theoretically.

The acoustic image-forming method is not only applicable to large filled in arrays but should also prove useful with other systems such as linear or "sparsely" filled arrays.

One technical area, in which further research is required, is in the conversion of the acoustic image into a useful form, e.g. a visible image. This problem also arises in the field of medical

physics where ultrasonic techniques are used to create low resolution pictures of internal organs. It is likely that improved image conversion techniques may be developed in the fairly near future.

The computer modelling program used in chapter 5 provides some idea of the tolerances (of the phases and the amplitudes of the signals being processed) that are required for instruments of this type. It is worth re-emphasising that the phase errors allowable in the image-forming system are double those which are permitted, for the same performance, in a conventional reflecting type of image-forming instrument. This has obvious advantages.

As far as the ionospheric observations are concerned, it is noted that echoes from the E and F layers as well as from sporadic E structures appear to be of a specular or quasi-specular nature. These results are in agreement with similar observations, made at Brisbane, and described by Brownlie *et al.* (1973a). Most of these echoes were observed within 15° of the zenith although on occasions echoes as far out as 28° from the zenith were observed. There appeared to be no anisotropy in the azimuth of the direction of arrival of the observed echoes when averaged over a long period of time. These results, when considered in conjunction with the computer simulation results, confirm that even random looking diffraction patterns are produced by the interference between discretely reflected rays. This has important consequences as far as the estimates of the "scales" of ionospheric irregularities are concerned. The results support the idea that the irregularities have "scales" of the order of 10 km or

so rather than of the order of a few hundred metres as suggested by the application of diffraction theory.

A comparison of the diffraction pattern structures observed in 1968/1969 (mostly summer) with those observed in 1973 (mostly winter) shows an increase in the number of patterns having a random structure. This is thought to be a seasonal effect but further work is required to confirm or reject this suggestion.

On occasions the movements of the reflection points (as observed with the focussed image display) and the structure of the diffraction pattern are both consistent with the theory that internal atmospheric gravity waves are responsible for at least some ionospheric irregularities. This suggestion was first discussed in detail by Hines (1960) although Martyn (1950) had earlier considered that wave motions might be responsible for travelling disturbances in the F region.

Most of the work described in this thesis could usefully be continued. In particular a more detailed study of reflections from sporadic E layers should be undertaken. However a different recording procedure should be considered. If film records with durations of say 30 minutes taken at two hourly intervals are made instead of the shorter more frequently recorded 5 minute records, then the results could be used not only for the statistical survey but they would also be of sufficient duration to show several cycles of any shorter period wave motions that may be present, i.e. records similar

to those described in chapter 7 might be obtained. These would be useful because, with a sufficient number of such records, it may be possible to identify sources of gravity waves particularly if these (the sources) lie in the troposphere. For example, it has been suggested that cold fronts may be a source of energy and an examination of the appropriate weather maps would be of interest.

When the image-forming system becomes operational on 6 MHz it will be possible to make daytime observations of reflections from the F region. In addition a 6 MHz system will make the study of reflections from spread F structures practicable because, although night time observations of the F region can be made using a probing frequency of 2 MHz the reflection level has so far been below that at which the spread F structures are present. Observations at 6 MHz would overcome this difficulty, and the system should be of use in studying, at least, the middle latitude variety of this phenomenon. Studies of spread F using a variety of techniques have already been made (see for reviews Wright, 1959; Clemesha, 1964 ; Herman, 1966 and others). It seems to be generally agreed that the spreading of the ionogram trace is caused by the presence of patches of field aligned irregularities. Measurements of the angular spectra will reveal:

(1) Whether the reflections from these irregularities are specular or otherwise. (To date most workers appear to support a specular reflection model (Herman 1966, Brownlie *et al.* 1973a)).

(2) Whether there is any anisotropy with respect to the directions of arrival of the reflected waves.

(3) Whether there is ever any true "range spreading" i.e. whether echoes from a given direction or neighbouring directions are spread in range.

A second transmitter (to operate at 6 MHz) is under construction and will be installed at a site (Willunga) some 70 km south of the Buckland Park array. The (group) range of echoes reflected from travelling ionospheric disturbances will be measured, and the angle of arrival will be determined at the same time using the image-forming system. Thus the variations in the height of the reflecting level, as a function of time, can be studied without the need to make assumptions about the position of the ionospheric reflection points. This will enable a more accurate determination of the distortion of the reflecting layer caused by the travelling ionospheric disturbance to be made.

In principle it should be a fairly simple matter to measure the phase of any echo from any one of the 89 directions which are sampled by the system. One possible method would be to use as a phase reference the intermediate frequency of a signal which has travelled a fixed distance. The intermediate frequency signal produced by the ground pulse would be a suitable signal. The phase of any echo could then be measured relative to this signal and this would enable the measurement of small changes in the range of an echo. Such information

might prove useful in studying the movement of meteor trails, as well as the movement of other reflecting surfaces. Recent theoretical (Brownlie *et al.* 1973c) and experimental work (Brownlie *et al.* 1973b) has shown that, from a knowledge of the angle(s) of arrival and the rate(s) of change of phase angle(s) of reflected signal(s), it is possible to determine the dispersion relation of the waves which might be producing a given reflecting structure. Information of this type is useful because it can be compared with the theoretically predicted dispersion relation for internal atmospheric gravity waves and the role that these waves play in the production of travelling ionospheric disturbances can be assessed. Initial results reported by Brownlie *et al.* (1973b) are in agreement with the theory that atmospheric gravity waves are responsible for the distortion of the ionospheric reflecting layer in the F region, at least on some occasions. The modifications to the image-forming system to enable these types of measurements to be made would involve the construction of 89 phase measuring and recording devices and would thus be an expensive project. However the measurement of the phase of echoes from a few selected directions (i.e. the measurement of the phases of the signals appearing on a few selected transducers in the image plane) could provide useful information.

Several other techniques for the measurement and recording of quantities of geophysical interest are available at Buckland Park. These include a micro-barograph, a system for measuring changes in the total electron content of the ionosphere in a given direction (using

the Faraday rotation method) and a system for measuring the changes in phase of signals incident on the array (Vincent 1972). Data from these instruments will help in the interpretation of information obtained from the image-forming system.

Finally, the use of the image-forming system for low frequency radio astronomy remains to be explored. The approaching minimum of solar activity, when ionospheric electron densities can be expected to reach their lowest values, should be an ideal time to initiate such observations.

APPENDIX 1

THE VOLTAGE CONTROLLED ATTENUATORS

A1.1 COMMENTS

The design for this circuit is based on a Hewlett-Packard application note, (No. 912).

The principle of operation is best illustrated by considering first fig. A1.1. This is a circuit diagram of a conventional π attenuator which can be made to attenuate an input signal by any desired amount by varying the values of R_1, R_2 and R_3. Further, if the values of R_1, R_2 and R_3 are chosen such that

$$R_1 = R_o \left\{ \frac{N^2-1}{2N} \right\} \qquad \text{and}$$

$$R_2 = R_3 = R_o \left\{ \frac{N+1}{N-1} \right\},$$

then the input impedance to the circuit will have a value R_o and the input signal will be attenuated by a factor 1/N. The same design considerations also apply to the attenuator depicted in Fig. A1.2.

The PIN diodes (H-P 5082-3080's) may be thought of as current controlled resistors at least as far as r.f. signals (greater than 1 MHz) are concerned. For example with a forward bias current of 100 mA the diodes appear to have a resistance (to r.f. signals) of less than 1 ohm. With zero bias current this resistance is in excess of 10 κ ohms. Now if the diodes are used to replace the resistors in

VOLTAGE CONTROLLED ATTENUATOR CIRCUIT DIAGRAM

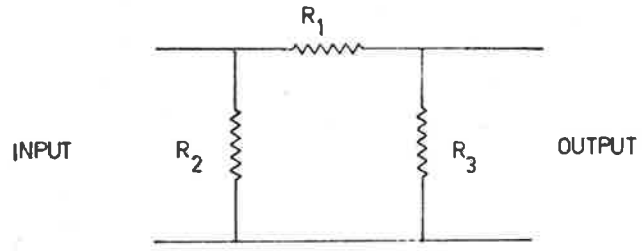

FIGURE A1·1

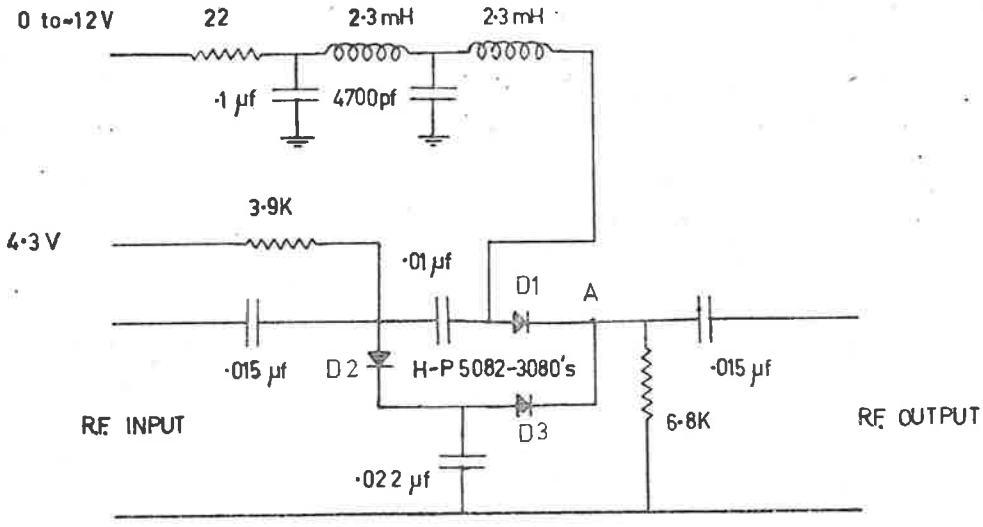

FIGURE A1·2

a π attenuator then it is possible, using the circuit shown in fig. A1.2, to construct a voltage/current controlled attenuator which when properly loaded has a constant input impedance and can attenuate in the range (approximately) -1 to -36 db.

A qualitative understanding of this circuit can be obtained by considering the following argument. As the variable voltage (0 to $\sim$ 12V) is increased so the current through the diode D1 increases. This will cause the r.f. resistance of this diode (D1) to decrease. Because of the increased direct current the potential at A will rise and the current through D1 and D2 will therefore decrease, thus increasing the r.f. resistance of D1 and D2. It can be seen that increasing the variable voltage from 0 towards 12V will result in a decrease in the overall attenuation of the circuit. The most important feature of this circuit, for image-forming applications, is that the phase shift of the attenuated signal is small of the order of 5^{o} or less at 2 MHz.

APPENDIX 2

THE R.F. STAGE OF THE RECEIVERS

A2.1 COMMENTS

Fig. A2.1 is a circuit diagram of the receiver used in the image-forming experiment.

The important points concerning this circuit are:

(1) The receiver is phase stable provided it is operated at fixed gain, i.e. the (A.G.C.) voltage at pin 12 is not changed.

(2) The bandwidth of the first two and the last tuned stages are broad and the overall bandwidth (28 kHz) is determined by the mechanical filter.

(3) All 89 receivers use the same local oscillator.

(4) The I.F. output (pin 11) provides the input to the transducer driver circuits.

(5) Only one stage (i.e. 2 or 6 MHz) can be operated at any one time.

Other comments relevant to this circuit may be found in section 3.6.

Circuit diagram of R.F. card of receivers

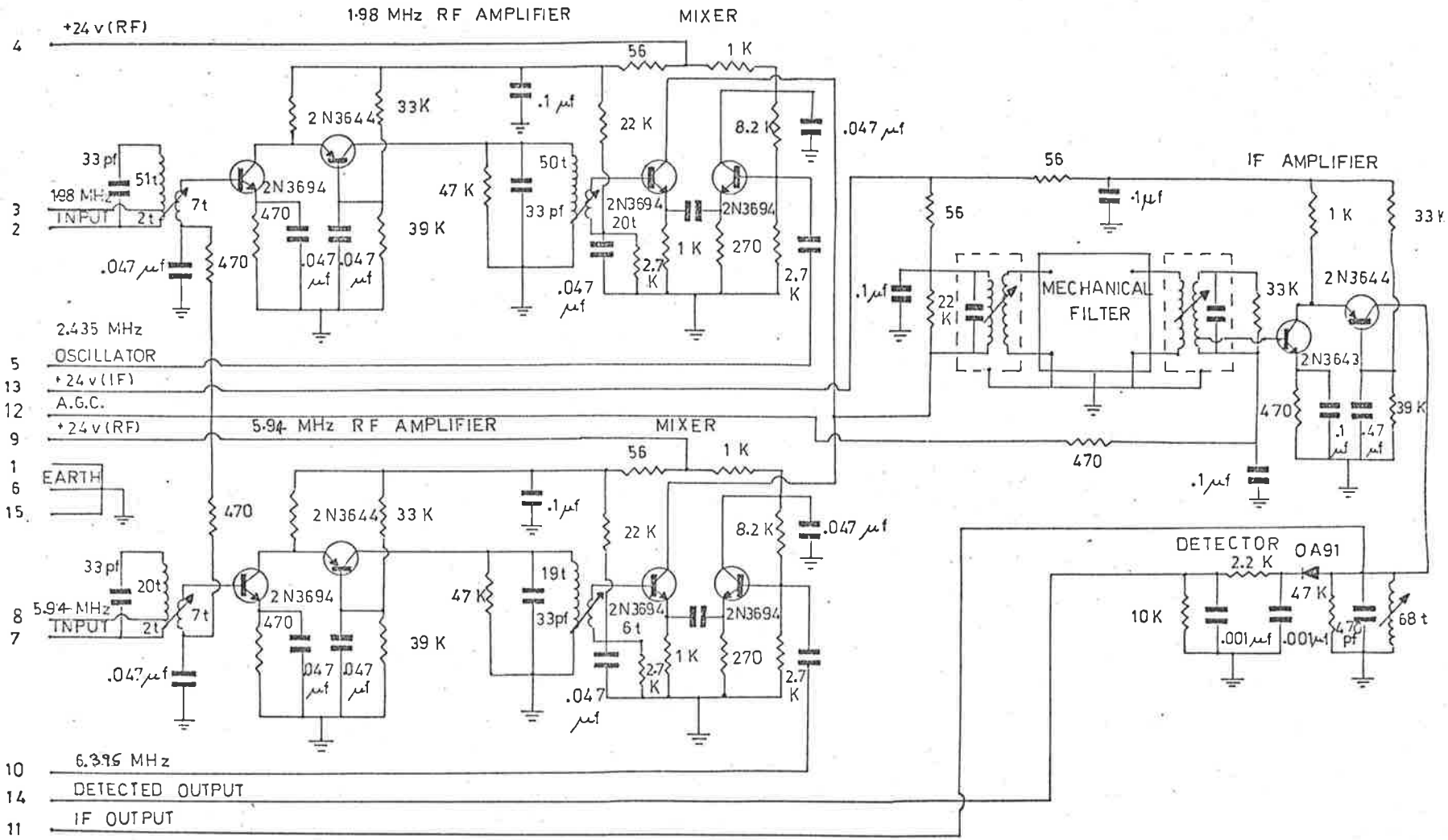

FIGURE A2·1

APPENDIX 3

THE LOCAL OSCILLATOR

A3.1 COMMENTS

Figures 3.1, 3.2, and 3.3 are diagrams of various stages of this circuit.

The unit can operate either in a continuous or a pulsed mode. When operated in a pulsed mode it may be triggered either from the mains, or alternatively, from externally generated positive or negative triggers.

The advantage of pulsed operation is that it is then possible to select the desired ionospheric echo and suppress the ground pulse or other unwanted signals that may be present. This greatly simplifies the task of selecting the correct acoustic signal, because as has already been explained, each input pulse into the tank gives rise to several pulses being received by the transducers in the receiving array. The first signal received is the wanted one and the others are reflections from the sides of the tank.

Note the capacitor 56/103 pf shown in fig. A3.3 can be changed to allow operation on either 2.435 MHz or 6.395 MHz.

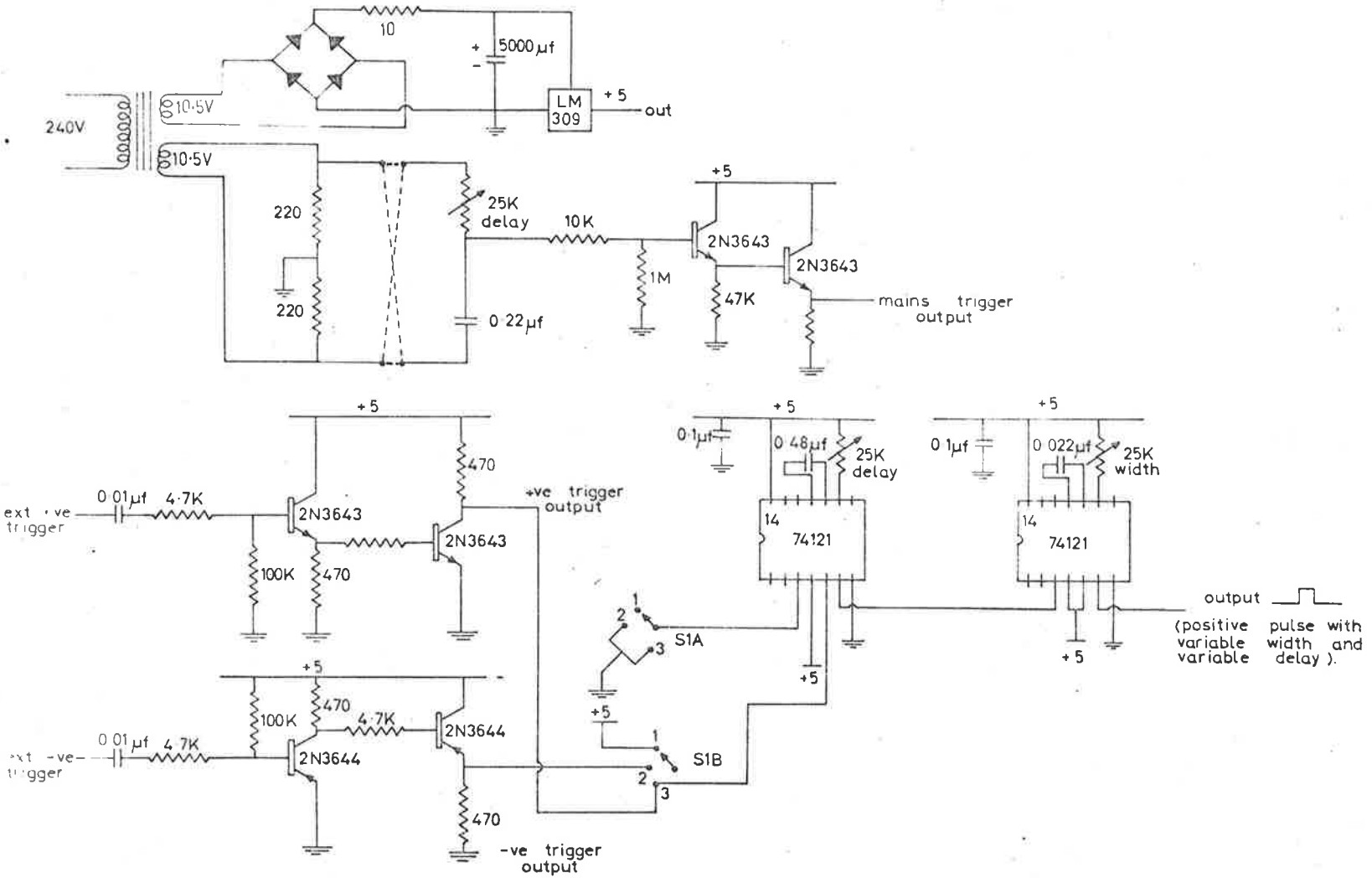

FIG. A 3.1 PULSE PRODUCING CIRCUIT FOR PULSED LOCAL OSCILLATOR

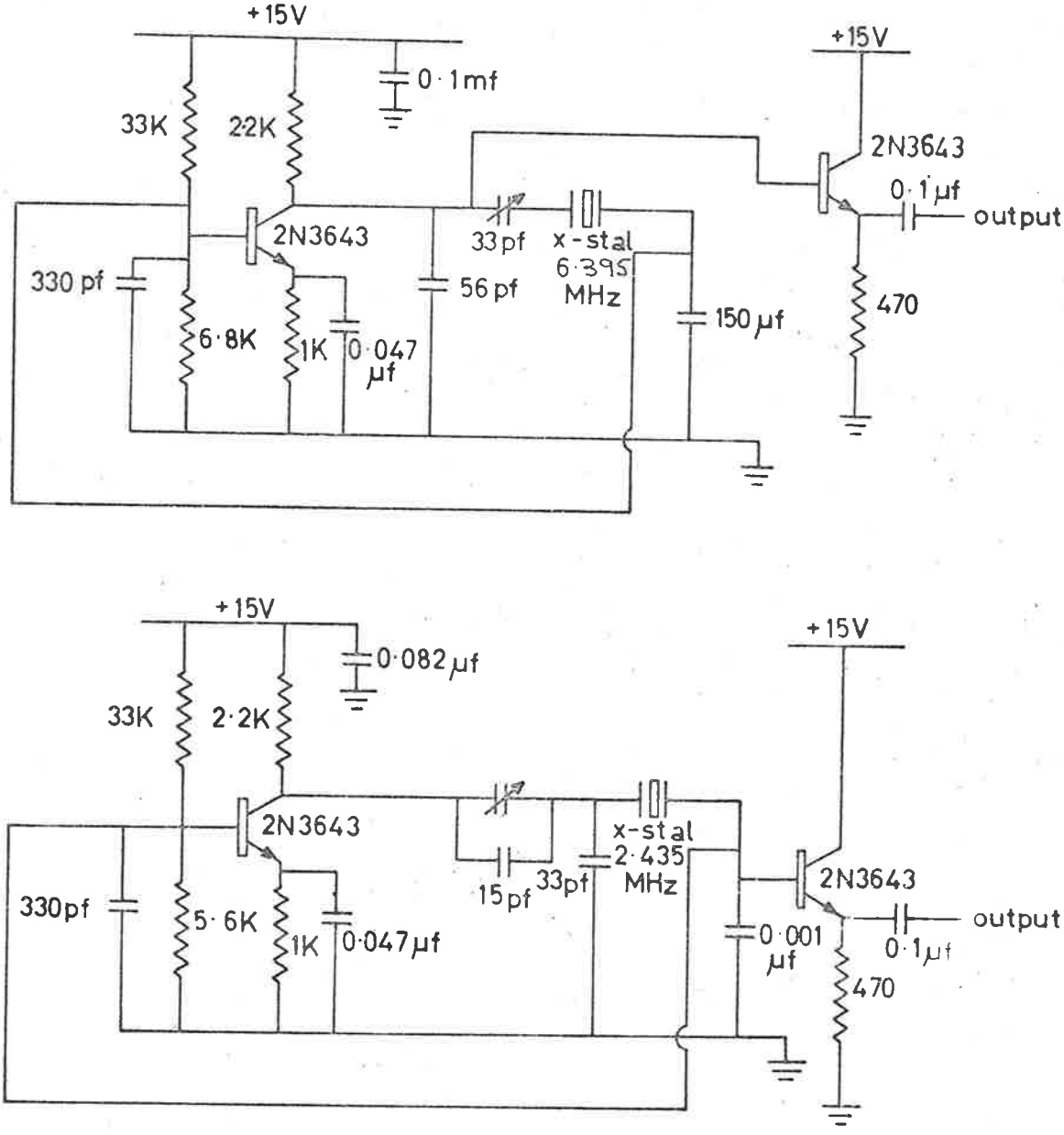

FIG. A 3·2 LOCAL OSCILLATORS (FOR 2MHz AND 6MHz SYSTEMS).

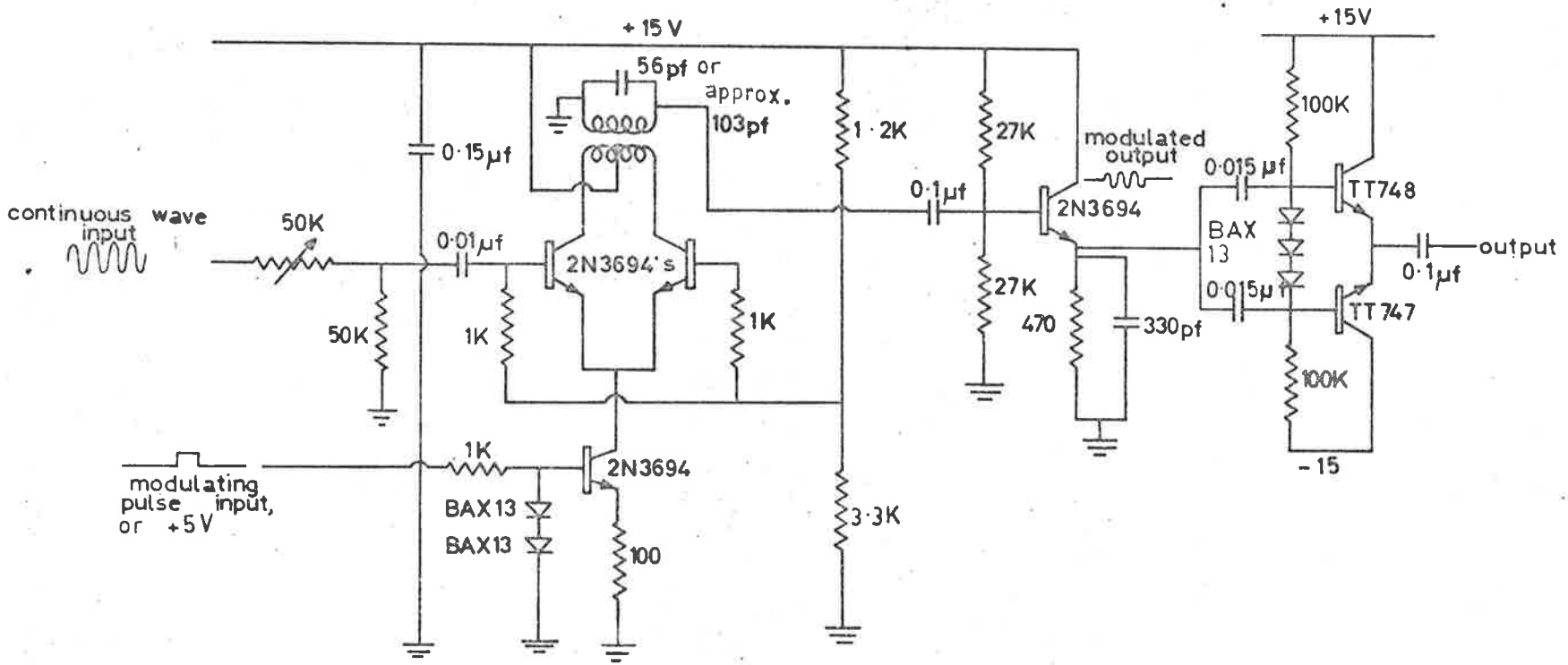

FIG. A3·3 PULSE MODULATING CIRCUIT FOR LOCAL OSCILLATOR.

APPENDIX 4

THE POST-DETECTOR CIRCUITS

A4.1 COMMENTS

There are two sets of 89 circuits of this type. The first set is used to process the 89 detected outputs from the receivers and the second set is used to process the 89 amplified and detected outputs from the transducers.

The circuit (see fig. A4.1) performed several functions which are listed below.

(1) Part of the circuit acted as a peak rectifier producing a d.c. voltage the amplitude of which varied with the amplitude of the input pulse (ionospheric echo or acoustic signal). This output (available on pin 8) was then used as the input to the 100 channel digitiser. A similar voltage was available for driving the light emitting diodes (L.E.D., see pin 13).

(2) Also produced was a slowly varying d.c. voltage which was used to control the attenuating circuits (see A1). This was available from pin 15. The similar but attenuated output from pin 9 was not used in the image-forming experiment.

(3) The inputs labelled strobe, clear and sample (see pins 4, 12, 14 respectively) were part of the gating system.

Circuit diagram of post-detector amplifier.

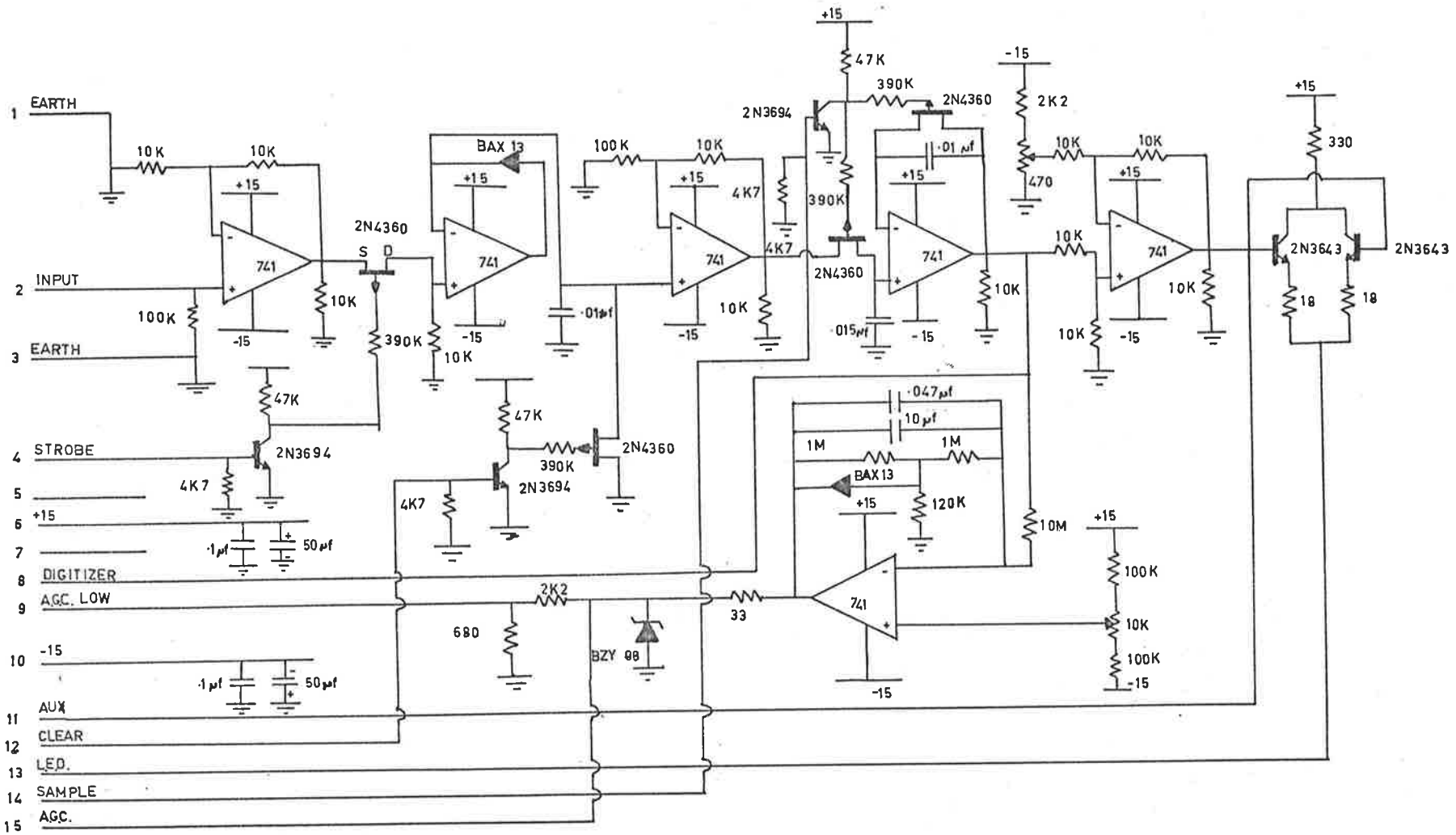

FIGURE A4-1

APPENDIX 5

THE TRANSDUCER DRIVING CIRCUITS

A5.1 COMMENTS

The input to this circuit comes from the I.F. outputs of the receivers. The circuit has a high input impedance which is necessary to avoid loading the receivers. The series tuned circuit formed by the inductor and the crystal has a broad resonance peak (in excess of 100 kHz to the half power points). The Q of the circuit is approximately 4. This results in amplification of the voltage appearing across the transducers and this allows more acoustic power to be emitted.

The method is one of the many which are commonly used to drive piezo-electric transducers and it was chosen for its simplicity, efficiency and cheapness.

TRANSDUCER DRIVER CIRCUIT DIAGRAM

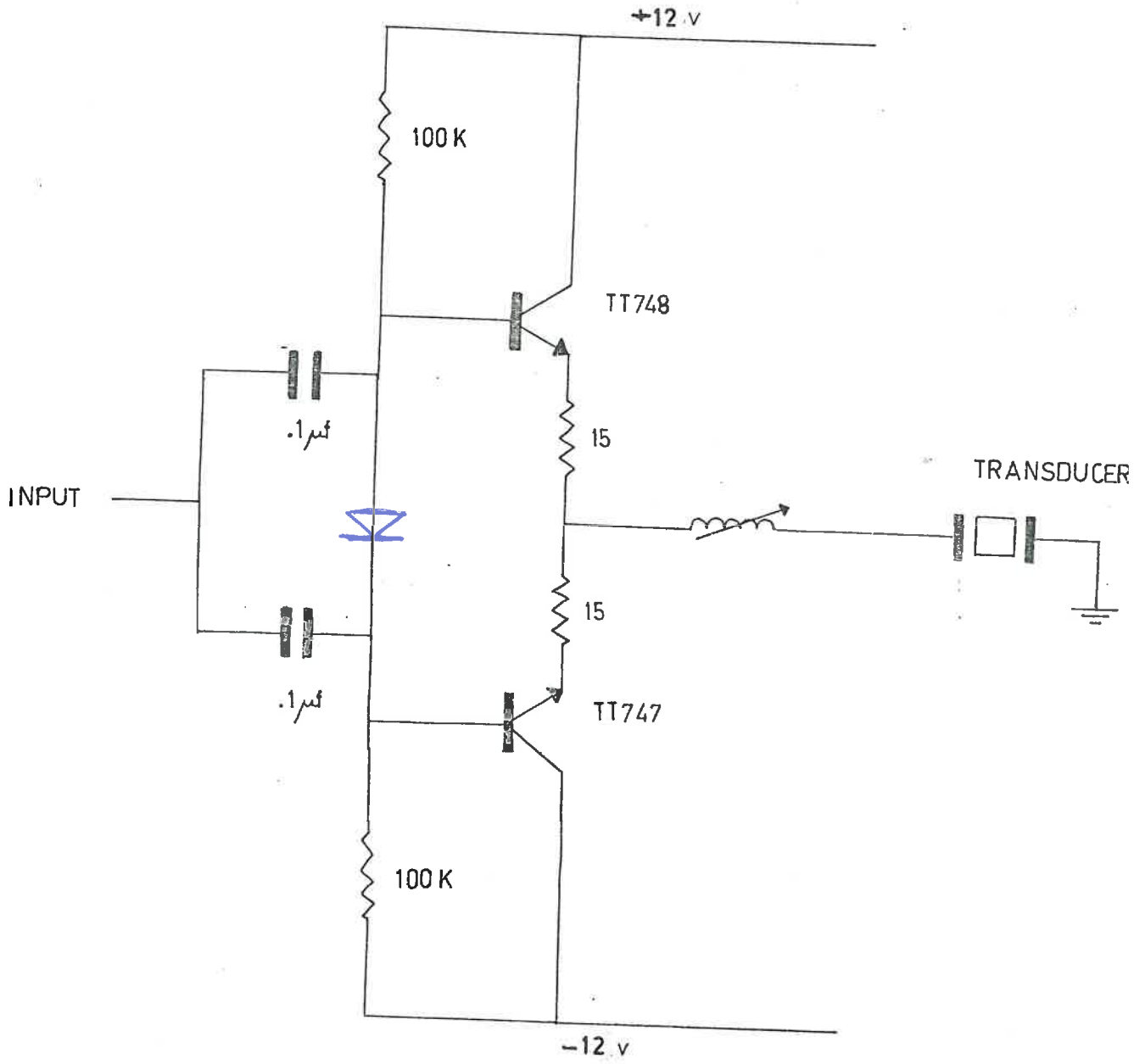

FIGURE A 5.1

APPENDIX 6

THE AMPLIFYING AND DETECTING CIRCUITS

A6.1 COMMENTS

This circuit (see fig. A6.1) is used to amplify and detect the signals appearing across the transducers in the receiving array. The first stage of the circuit consists of a tuned amplifier with a very high input impedance which is required to avoid loading the transducers. The second stage is a low level detecting circuit in which an (702) operational amplifier is effectively used to decrease the threshold of the detecting diode. This system is then able to detect very low level signals; of the order of 5 mV.
The final stage is simply an amplifier and buffer. The output signals are used as the inputs for one of the sets of 89 post-detector circuits.

The gain of the circuit can be varied by changing the value of the damping resistor (shown as 22K ohm in fig. A6.1) in the tuned circuit of the first stage. This of course alters the bandwidth of the amplifier but in practice the overall system bandwidth is determined by the bandwidth of the mechanical filters used by the receivers.

It was found necessary that these circuits should have a variable gain because the transducer efficiencies were found to vary from one transducer to another.

AMPLIFIER AND DETECTOR CIRCUIT DIAGRAM

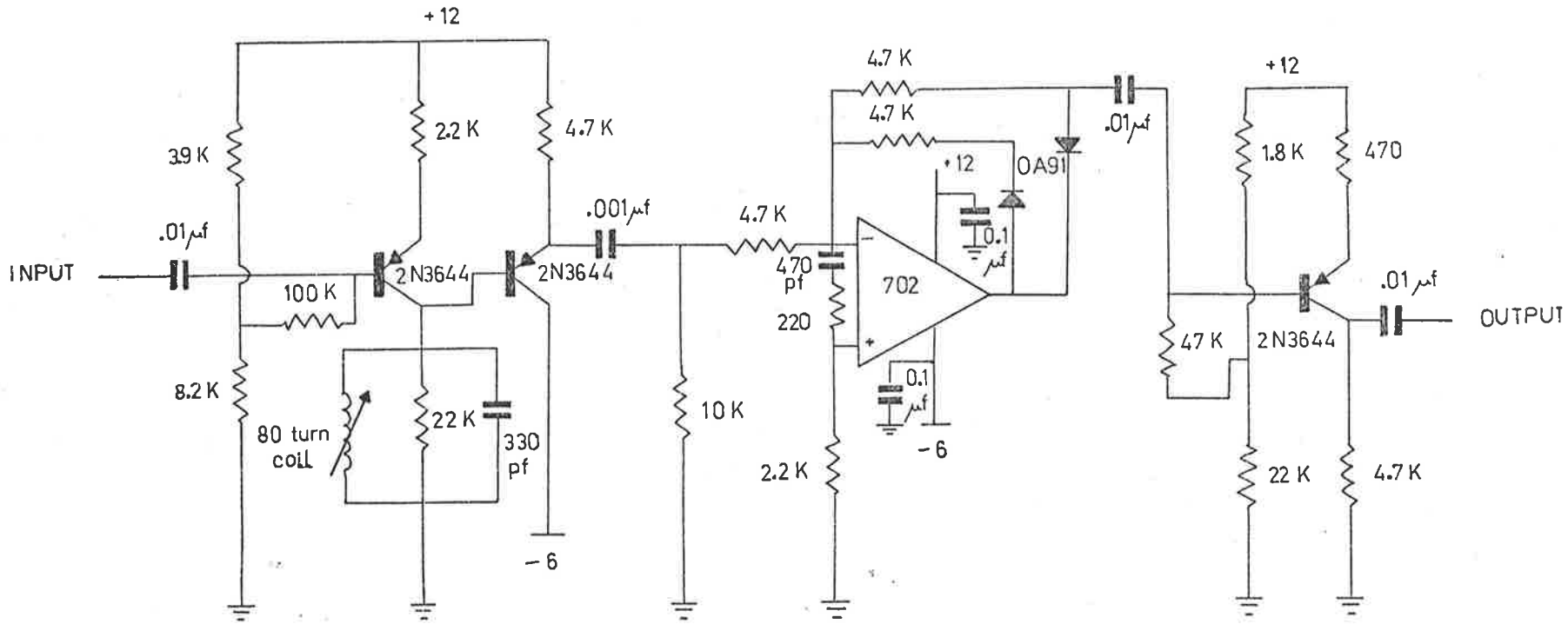

FIGURE A 6.1

BIBLIOGRAPHY

1a. Afraimovich, E. L. (see ref. 116)

1. Aimette, A., Arm, M. and Lambert, L. (1963) Quarterly progress report P-1/199 Columbia University Electronics Research Laboratories

"Electro-Optical signal processing techniques for phased array antennas"

2. Aimette, A., Arm, M. and Brown, D. (1964a) Quarterly progress report P-2/199 Columbia University Electronics Research Laboratories

"Electro-Optical signal processing techniques for phased array antennas"

3. Aimette, A., Arm, M. and Wyman, N. (1964b) Quarterly progress report P-3/199 Columbia University Electronics Research Laboratories

"Electro-Optical signal processing techniques for phased array antennas"

4. Aimette, A., Arm, M. and Wyman, N. (1964c) Quarterly progress report P-4/199 Columbia University Electronics Research Laboratories

"Electro-Optical signal processing techniques for phased array antennas"

5. Aimette, A., Arm, M., Bernstein, S., Krusos, G., Minkoff, J. and Wyman, N. (1966) Quarterly progress report P-6/321 Columbia University Electronics Research Laboratories

"Electro-Optical signal processing techniques for phased array antennas"

6. Allen, J. L. (1962) Microwave J. 5, 67

"Array radars a survey of their potential and their limitations"

7. Appleton, E. V. and Barnett, M. A. F. (1925) Proc. Roy. Soc. (London) A 109, 621

"On some direct evidence for downward atmospheric reflection of electric rays"

8. Arm, M., Aimette, A., Lambert, L. and Wyman, N. (1964) Quarterly progress report P-1/321 Columbia University Electronics Research Laboratories

"Electro-Optical signal processing techniques for phased array antennas"

9. Arm, M., Aimette, A. and Lambert, L. (1965a) Quarterly progress report P-2/321 Columbia University Electronics Research Laboratories

"Electro-Optical signal processing techniques for phased array antennas"

10. Arm, M., Aimette, A. and Bernstein, S. (1965b) Quarterly progress report P-5/321 Columbia University Electronics Research Laboratories

"Electro-Optical signal processing techniques for phased array antennas"

11. Arm, M., Bernstein, S., Minkoff, J. and Wyman, N. (1966a) Quarterly progress report P-7/321 Columbia University Electronics Research Laboratories

"Electro-Optical signal processing techniques for phased array antennas"

12. Arm, M., Bernstein, S., Minkoff, J. and Wyman, N. (1966b) Quarterly progress report P-8/321 Columbia University Electronics Research Laboratories

"Electro-Optical signal processing techniques for phased array antennas"

13. Austin, G. L. (1967) Amer. J. Phys. 35, 869

"Nature of radio waves reflected from an undulating surface"

14. Barrick, D. E. (1968) IEEE. Trans. on antennas and propagation AP-16, 449

"Rough surface scattering based on the specular point theory"

See also Correction: (1969)

15. Barrick, D.E. (1969) IEEE. Trans. on antennas and propagation AP-17, 81

"Correction to Rough surface scattering based on the specular point theory "

16. Booker, H. G. and Clemmow, M. A. (1950) Proc. Inst. Elect. Engrs. 97, 11

"The concept of an angular spectrum of plane waves, and its relation to that of polar diagram and aperture distribution"

17. Booker, H. G., Ratcliffe, J.A. and Shinn, D.H. (1950) Phil. Trans. Roy. Soc. (London) A 242, 579

"Diffraction from an irregular screen with applications to ionospheric problems"

18. Born, M. and Wolf, E. (1959) "Principles of Optics" Pergamon Press Chapter 12

19. Braccesi, A. and Ceccarelli, M. (1962) Nuovo Cimento 23, 208

"The Italian cross radio telescope. I. Design of the antennas"

20. Bracewell, R. N. (1961a) IRE. Trans. antennas and propagation AP-9, 22

"The Stanford microwave spectroheliograph antenna, a microsteradian pencil beam interferometer"

21. Bracewell, R.N. (1961b) IRE. Trans. on antennas and propagation AP-9, 49

"Tolerance theory of large antennas"

22. Bramley, E. N. (1951) Proc. IEE. 98, 18

"Diversity effects in spaced-aerial reception of ionospheric waves"

23. Bramley, E. N. (1953) Proc. Roy. Soc. (London) A 220, 39

"Direction-finding studies of large-scale ionospheric irregularities"

24. Briet, G. and Tuve, M. A. (1925) Terr. Mag. 30, 15

"Note on a radio method of estimating the height of the conducting layer"

25. Briet, G. and Tuve, M. A. (1926) Phys. Rev. 28, 554

"A test of the existence of the conducting layer"

26. Briggs, B. H. and Phillips, G. J. (1950) Proc. Phys. Soc. (London) B 63, 907

"A study of the horizontal irregularities of the ionosphere"

27. Briggs, B. H., Phillips, G. J. and Shinn, D. H. (1950) Proc. Phys. Soc. (London) B 63, 106

"Analysis of observations on spaced receivers of the fading of radio signals"

28. Briggs, B. H., Elford, W. G., Felgate, D. G., Golley, M. G., Rossiter, D. E. and Smith, J. W. (1969) Nature (London) 223, 1321

"Buckland Park aerial array"

29. Briggs, B. H. (1972) Geofysiske Publikasjoner 29, 121

"Recent work on ionospheric irregularities and drifts"

30. Briggs, B. H. and Holmes, N. E. (1973) Nature (Physical Science) 243, 111

"Ionospheric observations using an ultrasonic image-forming technique"

31. Brownlie, G. D., Dryburgh, L. G. and Whitehead, J. D. (1973a) Nature (Physical Science) 243, 112

"Pencil beam radar for ionospheric research"

32. Brownlie, G. D., Dryburgh, L. G. and Whitehead, J.D. (1973b) Nature (Physical Science) 244, 123

"Measurement of the dispersion of waves in the ionosphere"

33. Brownlie, G. D., Dryburgh, L. G. and Whitehead, J. D. (1973c) J. Atmosph. Terr. Phys. (in the press)

34. Burtynk, N., McLeish, C. W. and Wolfe, J. L. (1964) IEEE. Trans. on antennas and propagation AP-12, 243

"Wide aperture sampling linear array for direction finding"

35. Chinnick, J. H. (1972) M.Sc. Thesis (Electrical Engineering) Queen's University Ontario

"An optical processor for an antenna array"

36. Christiansen, W. N., Erickson, W. C. and Hogböm, J. A. (1963) Proc. Instn. Radio Engrs. Australia 24, 219

"The Benelux cross antenna project"

37. Clemesha, B. R. (1964) J. Atmosph. Terr. Phys. 26, 91

"An investigation of the irregularities in the F-region associated with equatorial type spread-F"

38. Cook, B. D. and Werchan, R. E. (1971) Ultrasonics 9, 101

"Mapping ultrasonic fields with cholesteric liquid crystals"

39. Cook, R. L. (1972) IEEE. Trans. on sonics and ultrasonics SU-19, 444

"Experimental investigation of acoustic imaging sensors"

40. Cottony, H. V. and Wilson, A. C. (1961) Journal of Research of the National Bureau of Standards- D Radio Propagation 65D, 101

"A high-resolution rapid scan antenna"

41. Ditchburn, R. W. (1963) "Light" Blackie and Son Limited Chapter 6

42. Eckart, C. (1960) "Hydrodynamics of oceans and atmospheres" Pergamon Press Oxford

43. Eckersley, T. L. and Farmer, F. T. (1945) Proc. Roy. Soc. (London) 184, 196

"Short period fluctuations in the characteristics of wireless echoes from the ionosphere"

44. Einaudi, F and Hines, C. O. (1970) Can. J. Phys. 48, 1458

"WKB approximation in application to acoustic-gravity waves"

45. Elliot, R. S. (1958) IRE. Trans. on antennas and propagation AP-6, 114

"Mechanical and electrical tolerances for two-dimensional scanning antenna arrays"

46. Felgate, D. G. (1969) Ph.D. Thesis University of Adelaide

"Studies of ionospheric drifts using a large aerial array"

47. Felgate, D. G. and Golley, M. G. (1971) J. Atmosph. Terr. Phys. 33, 1353

"Ionospheric irregularities and movements observed with a large aerial array"

48. Gossard, E. E. (1967) J. Geophys. Res. 72, 1563

"The apparent movement of the spectral components in fading records of ionospherically reflected radio waves"

49. Gossard, E. E. and Paulson, M. R. (1968) J. Atmosph. Terr. Phys. 30, 1795

"Measurement of off-path ionospheric irregularities deduced from short-path VLF measurements"

50. Guha, D. and Geller, M. A. J. Atmosph. Terr. Phys. (1973) 35, 1853

"Computer simulation studies of a spaced-receiver drift experiment"

51. Hamilton, P. A. (1968) Proc. IREE. (Aust.) 29, 56

"An electronic phasing system for aerial arrays"

52. Harnischmacher, E. (1963) "Winds and turbulence in the stratosphere, mesosphere and ionosphere" edited by K. Rawer, North Holland Publishing Co., Amsterdam p277

53. Harrold, S. O. (1969) Ultrasonics 7, 95

"Solid state ultrasonic camera"

54. Haslett, R. W. G. (1966) Radio Electronic Engr. 31, 161

"An ultrasonic to electronic image converter tube for operation at 1.20 Mc/s"

55. Haubert, A. and Doyen, G. (1966) Ann. Geophys. 22, 338

"Un perfectionnement des dispositifs de mesure des vents et de la diffraction des ondes radioélectriques dans l'ionosphère"

56. Herman, J. R. (1966) Rev. Geophys. 4, 255

"Spread F and ionospheric F-region irregularities"

57. Hines, C. O. (1960) Can. J. Phys. 38, 1441

"Internal atmospheric gravity waves at atmospheric heights"

58. Hines, C. O. (1965) "Physics of the earth's upper atmosphere" edited by Hines, C. O. Paghis, I., Hartz, T. R., Fejer, J. A. and Prentice-Hall, N. J.

59. Hueter, T. F. and Bolt, R. H. (1955) "Sonics" John Wiley and Sons, Inc., New York Chapter 4

60. Jacobs, J. E. (1968a) IEEE. Trans. on sonics and ultrasonics SU-15, 146

"Ultrasound image converter systems utilizing electron-scanning techniques"

61. Jacobs, J. E. (1968b) Transactions of the New York Academy of Sciences' Series 2, 30, 444

"Present status of ultrasound image converter systems"

62. Jasik, H. (1961) "Antenna Engineering Handbook" McGraw-Hill New York Chapter 15

63. Kalachov, P. D. (1963) Proc. Instn. Radio Engrs. (Aust.) 24, 237

"Some radiotelescopes in the USSR."

64 Kelleher, R. F. (1966) J. Atmosph. Terr. Phys. 28, 213

"Some statistical properties of the ground diffraction patterns of vertically reflected radio waves"

65. Kraus, J. D. "Radio Astronomy" McGraw-Hill New York Chapter 6

66. Krautkrämer, J. (1950) Arch. elekt. Übertragung 4, 133

"Motion effects in the rapid amplitude variations of ionospheric echoes"

67. Lambert, L. and Arm, M. (1963) Technical report T-1/199 Columbia University Electronics Research Laboratories

"The theory and physical constraints of an Electro-Optical signal processor"

68. Lambert, L. B. (1965a) Technical report T-1/321 Columbia University Electronics Research Laboratories

"Electro-Optical signal processors for array antennas"

69. Lambert, L. B. (1965b) Thesis, Columbia University Electronics Researc Laboratories

"Electro-Optical signal processor for phased array antennas"

70. Lambert, L. B., Arm, M. and Aimette, A. (1965) Proc. Symp. Opt. Electro-Optical Information Processing edited by Tippet, J. T. 715, (MIT press)

"Electro-Optical processor for phased array antennas"

71. Landmark, B. (1957) J. Atmosph. Terr. Phys. 10, 288

"The fading of radio waves reflected from the E layer"

72. Large, M. I. and Frater, R. H. (1969) Proc. IREE. (Aust.) 30, 227

"The beam forming system for the Molongolo radio telescope"

73. Li, T. (1959) IRE. Trans. on antennas and propagation AP-7, 223

"A study of spherical reflectors as wide-angle scanning antennas"

74. Lindner, B. C. (1972) Ph.D. Thesis University of Adelaide

"Radio studies of the lower ionosphere"

75. Longuet-Higgins, M. S. (1960a) J. Opt. Soc. Amer. 50, 838

"Reflection and refraction at a random moving surface. 1. Pattern and paths of specular points"

76. Longuet-Higgins, M. S. (1960b) J. Opt. Soc. Amer. 50, 845

"Reflection and refraction at a random moving surface. 2. Number of specular points in a Gaussian surface"

77. Longuet-Higgins, M. S. (1960c) J. Opt. Soc. Amer. 50, 851

"Reflection and refraction at a random moving surface. 3. Frequency of twinkling in a Gaussian surface"

78. MacDougall, J. W. (1966) J. Atmosph. Phys. 28, 1093

"The interpretation of ionospheric drift measurements"

79. Martyn, D. F. (1950) Proc. Roy. Soc. (London) A 201, 216

"Cellular atmospheric waves in the ionosphere and troposphere"

80. McGee, C. R. (1969) Ph.D. Thesis University of Adelaide

"On the nature of movements in the ionosphere"

81. McLean, D. J. and Wild, J. P. (1961) Aust. J. Phys. 14, 489

"System for simultaneous image formation with radio telescopes"

82. McLean, D. J. (1967) Proc. Astron. Soc. Aust. 1, 33

"The formation of simultaneous radio astronomical images and spectra by electro-optic methods"

83. McLean, D. J., Lambert, L. B. and Stark, H. (1967) Proc. IREE. (Aust.) 28, 375

"An Electro-Optical processor for the radioheliograph"

84. Midgley, J. E. and Liemohn, H. B. (1966) J. Geophys. Res. 71, 3729

"Gravity waves in a realistic atmosphere"

85. Mills, B. Y. and Little, A. G. (1953) Aust. J. Phys. 6, 273

"A high-resolution aerial system of a new type"

86. Mills, B. Y. (1963) Proc. IRE. (Aust.) 24, 132

"Cross type radio telescopes"

87. Mitra, S. N. (1949) Proc. Inst. Elect. Engrs. 96, Pt. 3, 441

"A radio method of measuring winds in the ionosphere"

88. Monro, P. E. (1962) Aust. J. Phys. 15, 387

"A study of phase fading of ionospheric reflections"

89. Morris, D. W., Mitchell, G., May, E. J. P., Hughes, C. J., and Dalgleish, D. I. (1963) Proc. IEE. 110 , 1569

"An experimental multiple-direction universally steerable aerial system for h.f. reception"

90. Munro, G. H. (1953) Proc. Roy. Soc. (London) A 219, 447

"Reflexions from irregularities in the ionosphere"

91. Parthasarathy, R. (1971) Annual Report Geophysical Institute Universit of Alaska

"Radiowave Camera"

92. Parthasarathy, R. (1972) Annual Report Geophysical Institute Universit of Alaska

"Radiowave Camera"

93. Pawsey, J. L. (1935) Proc. Camb. Phil. Soc. 31, 125

"Further investigations of the amplitude variations of downcoming wireless waves"

94. Pfister, W. (1971) J. Atmosph. Phys. 33, 999

"The wave-like nature of inhomogeneities in the E-region"

95. Phillips, G. J. and Spencer, M. (1955) Proc. Phys. Soc. (London) B 68, 481

95. Continued.

"The effects of anisometric amplitude patterns in the measurement of ionospheric drifts"

96. Pitteway, M. L. V. and Hines, C. O. (1963) Can. J. Phys. 41, 1935

"The viscous damping of atmospheric gravity waves"

97. Pohlman, R. (1937) Zeits. f. Physik, 107, 497

"Directive effect of sound field on non-spherical particles"

98. Ratcliffe, J. A. and Pawsey, J. L. (1933) Proc. Camb. Phil. Soc. 29, 301

"A study of the intensity variations of downcoming wireless waves"

99. Ratcliffe, J. A. (1956) Rep. Prog. Phys. 19, 188

"Some aspects of diffraction theory and their application to the ionosphere"

100. Rayleigh, J. W. S. (1879) Phil. Mag. 8, 477

"On the accuracy required in optical surfaces"

101. Rishbeth, H. and Garriot, O. K. (1969) "Introduction to ionospheric physics" Academic press New York and London Chapter 1

102. Rosenberg, L. D. (1955) Akust. Zh. 1, 99

"Review of methods for rendering ultrasonic fields visible"

103. Rudge, A. W. and Withers, M. J. (1971) Proc. Inst. Elec. Engrs. 118, 857

"New technique for beam steering with fixed-parabolic reflectors"

103. Ruze, J. (1952) Nuovo Cimento 9, 364

"The effect of aperture errors on antenna radiation pattern"

104. Singleton, R. C. (1969) IEEE. Trans. on audio and acoustics AU-17 93

"An algorithm for computing the mixed radix fast Fourier transform"

105. Skolnik, M. I. (1962) "Introduction to radar system" McGraw-Hill Co., Inc., New York Chapter 7

106. Sky and Telescope (1961) 22, 326

"Two giant radio telescopes"

107. Smythe, C. N., Poynton, F. Y., and Sayers, J. F. (1963) Proc. IEE. 110, 16

"The ultrasound image camera"

108. Tolstoy, I. (1963) Rev. Mod. Phys. 35, 207

"The theory of waves in stratified fluids including the effects of gravity and rotation"

109. Trott, G. W. (1966) Report on the main project for the degree of B.E. University of Adelaide

"The Buckland Park aerial problem"

110. Vincent, R. A. (1967) Ph.D. Thesis University of Canterbury

"Lower ionospheric irregularities"

111. Vincent, R. A. (1972) J. Atmosph. Terr. Phys. 34, 1881

"Ionospheric irregularities"

112. Vogt, G. (1962) IRE. Trans. on Antennas and Propagation AP-10, 193

"An electronic method for steering the beam and polarization of H.F. antennas"

113. Wild, J. P. (1967) Proc. IREE. (Aust.) 28, 279

"The Culgoora radioheliograph 1- specification and general design"

114. Willard, G. W. (1949) J. Acoust. Soc. Amer. 21, 360

"Focussing ultrasonic radiators"

115. Wright, R. W. H. (1959) J. Geophys. Res. 64, 2203

"Geomorphology of spread-F and characteristics of equatorial spread-F"

116. Afraimovich, E. L., Kalikman, A. D. and Korolev, V. A. (1972) Acad. Sci. Kazakh USSR. Geomagn. and Aeron. 21, 31

"Ray approximation and phase methods"